ALTERATION OF BRG1- OR BRM-ASSOCIATED FACTORS (BAFS), COMPONENTS OF SWI/SNF CHROMATIN REMODELING COMPLEX, AFFECTS PREIMPLANTATION PORCINE EMBRYO DEVELOPMENT

by

Yu-Chun Tseng

A Dissertation

Submitted to the Faculty of Purdue University

In Partial Fulfillment of the Requirements for the degree of

Doctor of Philosophy

Department of Animal Sciences

West Lafayette, Indiana

May 2021

THE PURDUE UNIVERSITY GRADUATE SCHOOL
STATEMENT OF COMMITTEE APPROVAL

Dr. Ryan Cabot, Chair

Department of Animal Sciences

Dr. Emily Dykhuizen

Department of Medicinal Chemistry and Molecular Pharmacology

Dr. Luiz Brito

Department of Animal Sciences

Dr. Shihuan Kuang

Department of Animal Sciences

Dr. Zoltan Machaty

Department of Animal Sciences

Approved by:

Dr. Zoltan Machaty

This dissertation is dedicated to my mother who encouraged me to pursue my dreams and finish my dissertation.

ACKNOWLEDGMENTS

The author wishes to thank the Indiana Packers Corporation (Delphi, IN, USA) for providing the porcine ovaries, Purdue Animal Sciences Research and Education Center (ASREC) for preparing porcine semen used in the study, and Purdue Meats Laboratory for porcine reproductive tracts collection. It is also important for the facilities of the Bindley Bioscience Center, a core facility of the NIH-funded Indiana Clinical and Translational Sciences Institute to allow us using the confocal microscope. Assistance and advices from committee members, Dr. Cabot, Dr. Dykhuizen, Dr. Brito, Dr. Kuang and Dr. Machaty are greatly appreciated. Mental and physical supports from Dr. Birgit Cabot and from our lab members, Hayly M. Goebel, Jennifer S. Crodian, and Sarah M. Innis are important to complete this study. Research wise, helps from faculty in Purdue Animal Sciences Department are necessary for me to finish my program.

TABLE OF CONTENTS

LIST OF TABLES

LIST OF FIGURES

ABSTRACT

Mammalian embryos undergo a dramatic amount of epigenetic remodeling during the first week of development to establish the correct epigenetic status to support the developmental program. SWI/SNF chromatin remodeling complexes are multi-subunits complexes and utilize energy from ATP hydrolysis to modify chromatin structure non-covalently. The collection of subunits determines the identity of a given SWI/SNF chromatin-remodeling complex, directs its activity, and dictate where that complex will act. The aims of this study were to 1) determine the requirement of SNF5, a SWI/SNF core subunit found in BAF and PBAF complexes during preimplantation porcine embryo development, 2) determine the requirement of BRD7, a PBAF complex-specific subunit during preimplantation porcine embryo development, and 3) investigate the role of CDH1, a downstream gene regulated by ARID1A, another subunit found exclusively in BAF complexes, in cleavage stage porcine embryos. Our results indicate that the differential requirement for each subunit during early embryo development. Depletion of different subunits results in embryo arrest at distinct developmental stage. Together, our data suggest the SWI/SNF chromatin remodeling complexes are necessary for proper porcine embryo development and this requirement is associated with the composition of the complex.

CHAPTER 1. LITERATURE REVIEW

Gene expression during embryo development in mammals is precisely regulated. Many important events need to be accomplished to achieve sexual reproduction successfully in an organism, including sex determination, gamete formation, fertilization, and embryogenesis. Dynamic changes in gene expression during early embryo development are controlled by several mechanisms and epigenetic modification is one of them. Epigenetic modification alters gene expression without a change in DNA sequence. Epigenetic modifications can be categorized into two forms, either covalent or non-covalent. One common covalent modification is histone methylation. Enzymes known as methyltransferases transfer methyl groups to histone proteins, which alter chromatin structure to either activate or repress transcription. Chromatin remodelers are employed to restructure the chromatin non-covalently. The SWI/SNF (SWItch/Sucrose Non-Fermentable) family of chromatin remodeling complexes are evolutionarily conserved in eukaryotes. These complexes have been shown to regulate expression of genes involved in cell cycle progression and cell differentiation. This literature review will cover key aspects of mammalian embryogenesis and several epigenetic modifications that regulate gene expression.

1.1 Sex determination and sex differentiation

In many animals, including both birds and mammals, sex is determined genetically by heterozygous or homozygous chromosome combinations. In placental mammals, a gene known as Sex determining Region of the Y-chromosome (*SRY*), located at the distal region of the short arm on the Y chromosome, determines sex (McLaren, 1991). *SRY* encodes a High Mobility Group (HMG) protein, which acts as transcription factor that activates a testis-forming pathway in most mammals (Harley and Goodfellow, 1994). There is no morphological difference in the gonads between genetic male and female embryos until the 6th week of embryonic age in humans. Undifferentiated gonads of XX and XY embryos are morphologically identical and have the potential to differentiate into either ovaries or testes. This period is known as the indifferent stage, or bipotential stage, of gonad development (Rahilly, 1984). Expression of the SRY-box 9 (*SOX9*) gene in bipotential gonads is upregulated by *SRY* in XY embryos and down-regulated in the gonads found in XX embryos. The expression of Fibroblast Growth Factor 9 (*FGF9*) is also increased in

XY gonads. *FGF9* inactivates the female Wingless related integration site 4 (*WNT4*) signaling pathway and the reduction of *WNT4* is required to maintain high level of *SOX9* (Sinclair *et al*., 1990). *SRY* and high levels of *SOX9* initiate pre-Sertoli cell differentiation and these cells direct subsequent events. Differentiation of Sertoli cells leads to the enclosure of the primordial germ cells (PGCs) inside testis cords. In mice, expression of *Sry* begins at embryonic day 10.5 and lasts for two days. The expression of *SRY* is critical and needs to be at a certain level to initiate male sex determination. Delayed or altered *SRY* expression leads to XY sex reversal, which is a male embryo developing female external genitalia, lacks sperm production, and retains Müllerian duct structures (Bullejos and Koopman, 2006).

After the testis begins to differentiate from the bipotential gonad, Leydig cells and Sertoli cells, the two supporting cell types in the testis, differentiate and begin to generate important regulatory molecules that direct sexual differentiation (Gao *et al*., 2006). Testosterone produced from Leydig cells promotes differentiation of the Wolffian ducts into the male tubular reproductive tract (including the epididymis, vas deferens, seminal vesicles) (Jost, 1947). Meanwhile, anti-Müllerian hormone (AMH) produced by Sertoli cells represses the differentiation of the Müllerian duct system into the female tubular reproductive tract (including the oviducts, uterus, cervix and cranial vagina) (Jost, 1953). Without AMH and testosterone, the Wolffian duct system regresses and the Müllerian duct system differentiates in that above-mentioned portions of the female tubular reproductive tract (Kobayashi and Behringer, 2003).

1.2 Formation of gametes

The origin of the germ cell lineage can be traced back to embryogenesis in mammals. The primordial germ cells (PGCs), which originate from a pluripotential population of cells in the proximal epiblast, were first identified in 1954 (Lawson and Hage, 1994). The PGCs begin to migrate from the yolk sac at embryonic day 7.5 in mice and can be identified by expression of B-lymphocyte-induced maturation protein 1 (*Blimp1*) / Pr domain containing protein 1 (*Prdm1*) and *Stella* (also known as *Dppa3* or *Pgc7*; Vincent *et al*., 2005). During migration, PGCs begin to exhibit polarized morphology and cytoplasmic extensions and pass through the hindgut and arrive at the indifferent gonad at embryonic day 12 (Hahnel and Eddy, 1986). Several signaling molecules are known to serve critical roles during PGC migration, including bone morphogenic

proteins 4 and 8 (BMP4 and BMP8, respectively) and interfering induced transmembrane protein 1 (IFITM1) from the extraembryonic ectoderm and visceral endoderm (Lawson *et al*., 1999). These genes regulate epiblast cells and promote the expression of PGC-specific genes, such as *Stella*, and represses the expression of somatic cell genes such as *Hox* gene family (Saitou *et al*., 2002). *WNT* signaling pathway is also reported to affect PGC fate through posttranscriptional interaction on BMP signaling molecules.

In mouse, PGCs are directed to the indifferent gonad by the c-kit receptor, a transmembrane protein found on the PGCs. C-kit receptor binds to kit ligand, which is expressed in somatic cells and this leads to the migration of the PGCs to the indifferent gonad (Matsui *et al*., 1990). In addition, kit ligand and c-kit activate the proliferation of PGCs during migration (Keshet *et al*., 1991). E-cadherin and the extracellular matrix molecule, integrin β1, are also reported to be involved in PGCs migration and colonization but the true mechanism is still unclear (Soto-Suazo and Zorn, 2005). Once PGCs arrive at the indifferent gonad, male germ cells divide mitotically for several rounds and then enter a quiescent state where they are known as gonocytes while female germ cells proliferate and differentiate into oogonia and initiate meiosis. These cells arrest at meiosis I and are referred to as primary oocytes. (McLaren, 2003).

1.3 Spermatogenesis

Spermatogenesis refers to the process of the development of the male gametes within the testes and male reproductive tract. The first phase of spermatogenesis takes place within the seminiferous tubules of the testes and is referred to as spermatocytogenesis. PGCs divide and become type A_1 spermatogonia after they arrive at the bipotential gonad. Morphologically, A_1 spermatogonia are smaller than the PGCs and possess oval nuclei containing chromatin associated with the nuclear membrane (Buehr, 1997).

A_1 spermatogonia are stem cells. After maturation, A_1 spermatogonia are able to renew themselves and also differentiate into a second cell type, the type A_2 spermatogonia.
Followed by several divisions, through A_2 to A_4, the A_4 spermatogonia are committed and differentiate into the type B spermatogonia. Type B spermatogonia continue mitotic division and differentiate into primary spermatocytes. The primary spermatocytes start meiotic division. Once

the first division of meiosis is completed; the secondary spermatocytes are produced. The secondary spermatocytes finish the second meiotic division and become spermatids. The initiation of spermatogenesis during puberty is reported to be regulated by the BMP8B protein secreted from the spermatogonia (Zhao *et al*., 1996).

The maturation of spermatids into mature spermatozoa is called spermiogenesis. During this polarization process, symmetric spermatids with oval nuclei and a large Golgi apparatus with proacrosomal granules migrate toward one end (Leblond and Clermont, 1952). Protamines are small arginine-rich proteins. During spermiogenesis, the nucleosomes are restructured, and the histone proteins are replaced by protamines. Protamines are arginine-rich proteins. The arginine-rich domain binds to the phosphate backbone of DNA and form a more compact ring-shaped structure. This process briefly shutdown transcription in the nucleus (Balhorn, 2007).

After nuclear condensation and acrosome formation, the mitochondria migrate to the neck section of the sperm and the microtubules elongate from the distal centriole, which become the future axoneme. The axoneme is a core of microtubules with a unique "9+2" structure in which two central microtubules are surrounded by nine pairs of outer microtubules. The axoneme forms the majority of the tail section of spermatozoa. The remaining cytoplasm and organelles, or residual bodies, are removed by Sertoli cells (Fawcett and Phillips, 1969). Spermatogenesis ends with the fully formed, non-motile spermatozoa released from the Sertoli cells. The spermatozoa are transported from the lumen of the seminiferous tubule to the epididymis, where maturation of the spermatozoa occurs. The maturation process takes few weeks depending on species. The epididymal tubule is highly organized and segmented (Orgebin-Crist and Jahad, 1979). The microenvironment in each segment is unique due to different compartments of luminal fluid which is controlled by androgens. The true mechanism for the maturation is still unclear but studies have reported that microRNA, proteins and lipids in the luminal fluid are key (Cornwall, 2009). Sperm can be stored in the cauda epididymis for 10-74 days (depending on species and the frequency of ejaculation) and the final maturation is completed in the female reproductive tract.

1.4 Oogenesis

Oogenesis refers to the formation of the oocyte. Unlike spermatogenesis in males, oogenesis is initiated during fetal development. In addition, spermatogenesis is essentially generating a motile nucleus, but the gamete resulted from oogenesis includes all the materials required to support the development of a preimplantation embryo. For humans and domestic animals, PGCs initiate rapid mitosis for a period (species dependent) to generate a few thousand cells after colonizing the bipotential gonad. There are approximately 18,000 germ cells in the murine ovary at E15 (McLaren *et al*., 2009). A portion of the PGC population dies during this period, while the surviving cells upregulate a set of genes and undergo differentiation into oogonia. The mesonephros, the second transient kidney, appeared in human embryo around 3.5 weeks old, secretes retinoic acid. The retinoic acid induces *Stra8* expression in the PGCs. As a result, PGCs stop proliferation and differentiate into oogonia then enter meiosis (Tam and Snow, 1981).

All primary oocytes within the ovary arrest uniformly at the diplotene stage of prophase I of the first meiotic division (Vermeiden and Zeilmaker, 1974). Each individual primary oocyte is contained within an ovarian structure called a follicle. The meiotic arrest is unique to oogenesis and is controlled by four major factors, including anaphase promoting complex (APC), M-phase promoting factor (MPF), cytostatic factor (CSF), and cAMP (Vermeiden and Zeilmaker, 1974). The MPF is a heterodimer composed of cdk1/p34 and cyclin B. In the primary oocyte, cyclin B accumulates and binds to cdk1. This leads to low activity of MPF and maintains the meiotic arrest in the primary oocyte. In addition, cAMP supplied from cumulus cells inhibits the activation (dephosphorylation of cdk1) of MPF in the oocytes (Byskov *et al*., 1997).

1.5 Folliculogenesis

During ovarian development, germ cells are enclosed within epithelial structures called "ovigerous cords" made by granulosa cell precursors and lined by a basement membrane. Ovigerous cords fragment into primordial follicles, which contain a primary oocyte arrested in each follicle, surrounded by a flattened layer of somatic pre-granulosa cells (Channing *et al*., 1980). Folliculogenesis is the development of ovarian follicles. Cells in ovarian follicles are responsible for secreting paracrine factors and supporting maturation of oocyte.

Folliculogenesis starts with primordial follicle and and progresses through the four following stages, including primary, secondary, tertiary (antral), and, finally, the pre-ovulatory (Graafian) follicle stages (Lintern-Moore *et al*., 1974). As the folliculogeneis progresses, the pre-granulosa cells develop into granulosa cells and theca cells differentiate from the interfollicular stroma in response to proteins secreted from growing follicles. Granulosa cells surround the oocyte and respond to follicle stimulating hormone (FSH) and produce estrogen. Theca cell, compares to granulosa cell, respond to luteinizing hormone (LH) and produce both androgens and progesterone (Macklon and Fauser, 1999).

Before puberty, primordial follicles develop into primary follicles and it is characterized by the transformation of the flattened granulosa cells into cubic shape. The zona pellucida is formed during the primary follicle stage. Proliferation of granulosa cells increased and the zona pellucida is completely formed during the secondary stage. Theca cells also appear at the secondary stage and are separated from granulosa cells by the basement membrane. Androstenedione, one of the critical hormones produced by theca cells is converted 17β-estradiol by the enzyme aromatase found in granulosa cells. Granulosa cells also produce 17β-estradiol, a necessary hormone for folliculogenesis. The last stage of folliculogenesis involves development of antral follicles or tertiary follicles. The growth of the follicle is hormone dependent. FSH receptors on granulosa cells are expressed and the theca cells express receptors for LH. Without appropriate balanced LH and FSH, follicles undergo atresia (DiZerega and Hodgen, 1981). During the tertiary stage, granulosa cells start to secret follicular fluid which expands the size of the follicle.

Gonadotropin-releasing hormone (GnRH) is released from hypothalamus and stimulates the secretion of FSH and LH from anterior pituitary gland. The slowly increased FSH and LH continue the growth of follicles until the estrogen produced by granulosa cells are enough to activate the surge center in hypothalamus to release the surgical GnRH and ultimately leads to a surge of LH from the anterior pituitary. The surge of LH triggers ovulation. The primary oocytes within periovulatory follicles resume meiosis in response to the LH surge. The secondary oocyte is arrested at the metaphase II stage until fertilization (Macklon and Fauser, 1998). It is generally agreed that the number of oocytes in females is fixed after differentiation of oogonia into primary oocytes during fetal development; no additional primary oocytes can be created after birth.

However, some studies have suggested that a stem cell population exists in the ovary that is able to renew the pool of primary oocytes (Leitch, *et al*., 2013).

The zona pellucida is a transparent layer, composed of glycoproteins, surrounding the plasma membrane of oocytes. The zona pellucida is responsible for species-specific fertilization, prevention of polyspermy, and acrosome reaction that allows successful adhesion and penetration of the sperm. The major glycoproteins are known as sperm-binding proteins, ZP1, ZP2, and ZP3 (Bleil and Wassarman, 1980). The ZP1 is the homodimeric filament crosslinker connected to ZP2 and ZP3. ZP2 and ZP3 are proposed to function as species-specific receptors for spermatozoa (Hinsch *et al*., 1999).

Folliculogenesis is precisely controlled by cytokines and hormones, especially the TGF-β family. TGF-β family hormones support follicle development during early stages. BMP-15 and Growth differentiation factor 9 (GDF-9) are two major TGF-β family cytokines secreted by oocytes. GDF-9 mRNA can be found in oocytes across all stages. It is reported in mouse study that depletion of *Gdf9* in oocytes blocks folliculogenesis at the primary stage (Dong *et al*., 1996; Günesdogan and Surani, 2016) and Bmp15 null mice are sub-fertile with ovulation defects and the embryo development competency is compromised (Yan *et al*., 2001). In human, polycystic ovarian syndrome (PCOS) is related to misregulated GDF-9, and Bmp15 mutation can cause premature ovarian failure (Di Pasquale *et al*., 2006; Teixeira Filho *et al*., 2002).

1.6 Ovulation

At ovulation, the LH surge induces the secretion of hyaluronic acid from cumulus cells. The gap junctions connecting cumulus cells and the oocyte are broken, which leads to a reduction of cAMP in the oocyte. Dephosphorylation of Cdk1 activates MPF and the oocyte resumes the cell cycle into metaphase I (Tunquist and Maller, 2003). When the primary oocyte divides, the germinal vesicle breaks down, and the metaphase spindle migrates to the periphery of the oocyte. At telophase, one of the two daughter cells have nearly no cytoplasm, while the other one retains the vast majority of the cellular constituents. The smaller cell is called the first polar body and the larger cellis the secondary oocyte.

The oocyte completes meiosis I and enters meiosis II after ovulation. MPF accumulates again (cdk1 binds to cyclin B) and CSF (including several protein kinases, such as MAPK, MAPK kinase and p90rsk) inhibits APC from binding MPF, thus slowing the rate of cyclin B destruction and the oocytes arrests at metaphase II (Abrieu *et al*., 2001).

1.7 Fertilization

Fertilization is the fusion of haploid gametes to form a genetically unique individual.
The Ca^{2+} oscilation during fertilization activates calmodulin-dependent protein kinase II (CaMKII) and this leads to the activation of APC which induces cyclin B ubiquitination and targeted for degradation. MPF is then inactivated and meiosis is resumed (Kosako *et al*., 1994). During the second division of meiosis, a similar unequal cytokinesis takes place. Most of the cytoplasm is saved in the mature oocyte and a second polar body receiving only a haploid nucleus is protruded. This resulting a single haploid oocyte rather than splitting the cell contents into four cells.

Sperm must undergo the process of capacitation in order to have the ability to penetrate and fertilize the oocyte (Austin, 1952). Capacitation consists of a series of biochemical and physiological modifications to the sperm cell that take place in the female reproductive tract. The movement of the sperm tail becomes vigorous and asymmetric when sperm enter the female reproductive tract. This hyperactivated motility (HAM) is triggered by the zinc ion in the female tract and benefit the fertilization (Allouche-Fitoussi *et al*., 2018). An efflux of cholesterol from sperm plasma membrane results in the increasing fluidity and permeability of membrane to bicarbonate and calcium ions. The increasing of bicarbonate and calcium ions activate protein kinase A (PKA) through the bicarbonate-calcium ion dependent soluble adenylyl cyclase. Overall, capacitation gives sperm the ability to produce HAM, the chemotactic response, and enable the sperm to undergo the acrosome reaction once it encounters an oocyte (Bedford, 1970; Lishko and Kirichok, 2010; Ickowicz *et al*., 2012).

The true molecules that are responsible for sperm and zona pellucida binding is still unknown, but it is suggested that a receptor on the surface of the sperm cap binds to ZP3 and triggers the acrosome reaction. The receptors on sperm membrane activate adenylyl cyclase which leads to increasing in cAMP and activates protein kinase A (PKA). PKA then activates calcium channels

on outer acrosomal membrane. Calcium ions, from the interior of the acrosome are released to the cytosol. A rise of pH and cAMP levels within the sperm head cause exocytosis of the acrosome contents (Breitbart and Spungin, 1997). The acrosome reaction involves an opening of the acrosomal cap and leads to an influx of calcium ions from environment to peri-acrosomal space. The zona pellucida is then digested by acrosin, a serine proteinase (Austin, 1975). After the sperm through the acrosome reaction, ZP2 acts as a receptor binding sperm and facilitates penetration of the zona pellucida to allow fusion of the sperm with the oocyte membrane (Bleil and Wassarman, 1986).

Interaction between the plasma membranes of the sperm and oocyte requires several proteins but the precise mechanisms remain unresolved. It has been suggested that members of the disintegrin and metalloprotease proteins family (ADAMs), including ADAM1, 2, and 3 are responsible for sperm-oocyte fusion (Chen *et al*., 1999). The ADAM proteins on the sperm membrane interact with integrins on oocyte membrane. In mouse, the fertilin β (ADAM2) protein binds the α6β1 integrin receptor on the oocyte plasma membrane (Evans *et al*., 1997). Evidence suggests the sperm membrane protein, IZUMO1 interact with the folate receptor 4 (FOLR4) and the protein JUNO on oocyte membrane (Wassarman, 2014). IZUMO1 has been reported to contribute significantly to the fusion process, although this molecule does not appear to possess any fusogenic domain (Inoue, 2005). Other studies have suggested SPESPs (sperm equatorial segment proteins) partner with IZUMO1 and JUNO to accomplish the fusion process (Ellerman *et al*., 2009).

Fusion of sperm and oocyte cell membranes lead to a local increase in cytosolic calcium ion concentration; this change in calcium concentration triggers a process known as the cortical reaction to prevent polyspermy. The cortical reaction involves the release of cortical granules into the perivitelline space; the contents of the cortical granules modify the zona pellucida and prevent polyspermy. The initial increase of calcium ion also leads to a series of calcium oscillations which activate the fertilized oocyte to resume meiosis (Allen and Griffin, 1958).

Upon membrane fusion, a sperm-specific phospholipase called PLZ-zeta hydrolyzes the phospholipid phosphatidylinositol 4,5-bisphosphate (PIP2) into diacylglycerol (DAG) and inositol 1,4,5-trisphosphate (IP3) which triggers calcium oscillations in the oocyte. This increased

intracellular concentration of calcium leads to the exocytosis of cortical granules from the oocyte. The content in the cortical granules is release to zona pellucida and modifies the ECM into a barrier to prevent polyspermy (Jaffe *et al*., 198).

Calcium ions also act as a secondary messenger that upregulates the calcium/calmodulin-dependent protein kinase II (CaMKII) pathway and leads to the activation of anaphase-promoting complex/cyclosome (APC/C). MPF (cdc2 and cyclin B complex) is targeted by the APC to ubiquitination and results in inactivation of metaphase promoting factor (MPF). The fertilized zygote finishes the meiosis and results in the extrusion of the second polar body (Lorca *et al*., 1993).

1.8 Blocks to polyspermy

Polyspermy results when an oocyte is fertilized by multiple sperm. Polyspermy gives abnormal numbers of chromosomes, disrupts mitotic division and ultimately leads to embryo death (Snook *et al*., 2011). Mammalian embryos have developed two strategies to prevent this lethal situation, , known as the fast and slow blocks to polyspermy. In sea urchin, the fast block to polyspermy involves an induced electrical charge change across the oocyte membrane, which is referred to depolarization, at the second that the sperm and oocyte fuse together (Jaffe, 1976). The slow block to polyspermy is referred to the modification of zona pellucida by cortical reaction (Abbott and Ducibella, 2001).

1.9 Preimplantation embryo development

In most mammals, the fertilization takes place in the oviduct and the embryo moves through the oviduct to the uterus preparing for implantation in the next few days. Thus, this period is referred to as preimplantation development. After fertilization, the zygote undergoes a series of cell divisions to proliferate; this is referred to as cleavage development. During cleavage development, the embryo increases the total cell number but not the total cytoplasmic volume. The cell division is asynchronous and accompanied by complete cytokinesis and this is referred to holoblastic cleavage.

The cell cycle of the embryo is divided into two major phases: interphase and the mitotic (M) phase. Interphase includes three different phases: gap 1 (G1) phase, synthesis (S) phase, and gap 2 (G2) phase. There are two distinct processes in the M phase: karyokinesis, where the chromosomes separate and cytokinesis, where the cytoplasm divides into two daughter cells. The cell cycle is under tight regulation by proteins and mechanisms, such as cyclins, c-Myc gene, MPF, APC/C and cyclin-dependent kinases (Cdk) (Sorensen and Wassarman, 1976). The first mitotic cell cycle is longer than somatic cells and the time is species dependent (Wright and Longo, 1988). Studies show that the G2 and S phases are elongated in the first cell cycle because of transformation of maternal and paternal derived chromatin into nuclei (Howlett and Bolton, 1985). The second and third cell division cycles have been observed with shorten G1 phase and S phase. They start almost immediately after the previous mitosis is completed (Bolton *et al*., 1984). The initiation of DNA synthesis can occur either in the pronuclear stage (during migration) or after the formation of the zygote nucleus.

In most mammals, the pronuclei never fuse together. Instead, the nuclear envelopes breakdown after migration and the chromatin condenses into chromosomes and the first mitosis starts. At pronuclear stage, the proximal sperm centriole can be identified in the ooplasm and the maternal centrosome appears. The sperm aster, a structured microtubule, surrounds the centriole and directs the female pronucleus migration towards the male pronucleus. The embryo enters cleavage stage and undergoes mitosis (Longo, 1976). In sea urchin, the sperm centriole acts as a microtubule organizing center and integrates with oocyte microtubules to form an aster. These microtubules guide the two pronuclei migrate toward each other and the pronuclei eventually fusion together to form the diploid zygote nucleus (Hamaguchi and Hiramoto, 1980; Bestor and Schatten, 1981).

The first important event during cleavage development is called maternal-to-zygotic transition (MZT) and zygotic genome activation (ZGA) because the zygotic genome needs to be reprogrammed to a totipotent state. The maternal mRNAs and proteins loaded into the oocyte during oogenesis direct the first mitotic divisions and the zygotic genome is transcriptionally quiescent (Flach *et al*., 1982; Gurdon, 1962). Global demethylation of zygotic genome before ZGA also contributes to the transcriptional silence of the zygote (Gao *et al*., 2014). However, in order to continue developing beyond this point, the zygotic genome must be activated. The precise

mechanism that initiates this transition is not entirely clear, but studies show it relates to the nuclear to cytoplasmic ratio in blastomeres of the embryo (Schulz and Harrison, 2019). Degradation of maternal mRNA is regulated by RNA-binding protein complexes. These complexes recognize sequences present within maternal RNAs and target them to degradation by cleavage, deadenylation, and decapping (Yartseva and Giraldez, 2015). ZGA has been considered a landmark during preimplantation embryo development. Epigenetic marks, including DNA methylation and histone modifications, are remodeled on a global scale to activate the zygotic genome (Schulz and Harrison, 2019).

Compaction is the first cell differentiation event during embryo development. The significance of this event is that the blastomeres undergo a morphological change. Once the cleavage stage embryo reaches the morula stage, proteins on the cell membrane of the blastomeres start to polarize and cell adhesion molecules (CAM) bind to the cytoskeleton. The outer blastomeres begin to flatten and result in a compact and separates the blastomeres into a group of inner cells and a group of outer cells. The outer cells develop distinct apical and basolateral membrane domains due to asymmetrical organelles localization. Tight junction complexes form between adjacent outer cells in the morula, these cells join to each other by cadherins and catenins (Shirayoshi, 1983). In outer cells, the tight junction complexes function as a seal to limit movement of extracellular molecules. The active transport mechanisms accumulate sodium ions against their concentration gradients by the sodium pump that has been localized to the basolateral side of the trophectoderm. Water follows the sodium gradient to create a fluid filled the extracellular space called a blastocoel (Lo and Gilula, 1979). At this point, the embryo is said to be at the blastocyst stage.

As the blastocyst stage embryo expands, the zona pellucida becomes thinner; the embryo secrets a trypsin-like protease from trophoblast to digest zona (Sawada *et al*., 1990). Blastomeres differentiate into two types: the outer cells differentiate into the trophectoderm (TE) and inner cells turn into the inner cell mass (ICM). The ICM will grow into the fetus (and part of the placenta, for example, blood vessels) and the TE is destined only to contribute to extra-embryonic tissues.

1.10 Epigenetic modifications

Epigenetics has been used to describe many biological processes which change our genetic materials, including DNA and chromatin. Chromatin is a complex made by chromosomal DNA associated with histone proteins. The basic unit, nucleosome, is composed of 147 bp of DNA wrapped around an octomeric core of histone proteins. The octomeric histone complex contains two dimers of histone proteins H4 and H3, surrounded on either side by a dimer of histone proteins H2A and H2B. The N-terminal region of histone proteins H3 and H4 extend from nucleosomes and are referred to as histone tails. Double-stranded DNA, about 38-53 bp long, connects two nucleosome cores with histone H1 (Kornberg, 1974). The histone protein is lysine and arginine rich. The negatively charged DNA is tightly associated with histone proteins. To accomplish the transcription machinery, the chromatin must be unwound, and the DNA needs to be dissociated from histone proteins. Epigenetic modifications modify both DNA and histone tails so affect the accessibility of transcriptional proteins, therefore regulate gene expression (Bird, 1986).

The modification of chromatin structure can be covalent or non-covalent, including histone methylation, histone acetylation, DNA methylation, and chromatin remodeling. This modification can be heritable or inheritable. In addition, there are post-transcriptional modifications. Examples of post-transcriptional regulation include non-coding RNAs, micro RNAs (miRNA), and riboswitches. Epigenetic modifications are necessary for transcriptional regulation, for example, maternal DNA methylation imprints and the maintenance of chromosome stability during embryogenesis.

1.11 DNA methylation

DNA methylation is a common epigenetic modification that cells use to down-regulate transcription. DNA methylation is important for numerous events, including genomic imprinting, X-chromosome inactivation, embryo development, and chromosome stability (McGhee and Ginder, 1979). About 45% of the mammalian genome contains transposable elements that are silenced by DNA methylation (Schulz *et al.*, 2006). A family of enzymes called DNA methyltransferases transfer methyl groups, to the cytosine bases, which are then converted to 5-methylcytosine (Evans and Evans, 1970). The 5-methylcytosines paired with guanine (or CpG

sites) result in two methylated cytosines sitting in a diagonal direction to each other on opposing DNA strands.

The CpG sites are critical and about 70% of gene promoters reside in CpG islands (Bird *et al*., 1985). CpG islands have been evolutionarily conserved to promote gene expression because of the loose nucleosome structure (Tazi and Bird, 1990). A region of genome with a GC base composition greater than 50% and a CpG observed/expected ratio of more than 0.6 within a 700 bp strand of DNA are called CpG islands (Gardiner-Garden and Frommer, 1987). Methylation on CpG islands can prevent transcription factors from binding and also recruits methyl-binding proteins, thus silencing gene expression (Mohn *et al*., 2013). DNA methylation is dynamic during embryo development. In the mouse embryo, the global DNA demethylation can be observed in the paternal pronucleus right after fertilization and DNA methylation increases to silence of genes related to pluripotency during differentiation stages (Krakauer and Mira, 2000).

1.12 Histone methylation

Histone proteins are integral components of chromatin structure. The methylation of histone proteins involves the attachment of methyl groups to residues by histone methyltransferases; the methylation occurs primarily on lysine, arginine, and histidine residues. Depending on the degree of methylation, the result can be activation or repression of a gene. Lysine methylation on histone proteins can occur in either mono, di, or tri-methylation states. Methylation at the lysine 4, lysine 36, and lysine 79 resides of histone protein H3 (H3K4, H3K36, H3K79, respectively) is associated with active transcription, while methylation at the lysine 9 and lysine 27 residues of histone protein H3 (H3K9 and H3K27, respectively) is associated with transcriptional repression (Barski *et al*., 2007). Methylation at arginine is much more complex than lysine methylation as the impact on gene expression is still unclear. Dimethylation of the arginine 9 residue of histone protein H3 (H3R8me2), as well as dimethylation of the arginine 3 residue of histone protein H3 (H4R3me2) are considered to methylation marks of transcription repression (Majumder *et al*., 2010).

There are positive and negative upstream regulators that control the degree of histone methylation. The catalytic domain of histone lysine methyltransferases is the SET domain, but DOT1, a methyltransferase that acts H3K79 does not have a SET domain (Feng *et al*., 2002). Histone

methylation was considered to be a permanent epigenetic mark until the discovery of a histone H3K4 demethylase, Lysine Specific Demethylase 1 (LSD1) (Thakur, 19). The regulation of histone methylation depends on the turnover rate of the methyl group and recruiting histone methyltransferases to the destination. A specific DNA sequence is identified that enhances Polycomb Group (PcG) Response Elements (PREs) to direct the Polycomb repressive complex 2 (PRC2), which is responsible for H3K27 trimethylation, to its destination (Chan *et al*., 1994). Long non-coding RNAs (lncRNAs) and microRNAs are also reported to bind to certain methyltransferases and demethylases and direct the enzymes to specific loci (Pandey *et al*., 2008). Histone methylation dynamics are critical in many biological processes, including cell cycle regulation, DNA damage, cell proliferation and differentiation.

1.13 Histone acetylation

Histone acetylation and histone deacetylation involve the addition and removal, respectively, of acetyl groups on lysine residues found on histone proteins. These modifications are carried out by a families of enzymes called histone acetyltransferases (HATs) and histone deacetylases (HDACs), respectfully (Chen *et al*., 2001). Histone acetylation alters nucleosome structure and enables chromatin to become less condense, thereby promoting conditions that favor transcription. Nucleosome structure is held by the positive charges on the H4 histones and the negative charge on the H2A. Acetylation of the histone tails changes the charge and disrupts this association. This ends up with weaker binding of the nucleosomal components. As a result, the transcription factors can have better access to the promoter region and initiate transcription more frequently. The unwound chromatin structure also facilitates the elongation process during transcription (Studitsky *et al*., 1997).

1.14 Non-covalent epigenetic modifications/ chromatin remodeling

DNA methylation, histone methylation and histone acetylation are considered covalent modifications. Non-covalent modification of chromatin involves the process as known as chromatin remodeling, which is the restructuring of nucleosome spacing. This remodeling employs ATP-dependent chromatin remodeling complexes to alter the positions of nucleosomes and render DNA (Hamiche *et al*., 1999). These complexes are large, multi-subunit complexes and require the

energy from ATP hydrolysis to complete their job (Wang, *et al*., 1996). The core ATPase subunits in these complexes belong to the SNF2 protein. Based on the composition, the complexes can been classified into four major subfamilies, which are SWI/SNF (switch/sucrose non-fermentable), CHD (chromodomain helicase DNA-binding), ISWI (imitation SWI), and INO80 (and SWR superfamily) (Chen and Dent, 2013; Eisen *et al*., 1995). The overall structure of these complexes is a single ATPase core associated with multiple subunits. The ATPase core subunit hydrolyzes ATP and other associated subunits and guide the complex to specific loci. The subunits in a given complex can be varied in the number, ranging from two in some ISWI complexes to 12 in the SWI/SNF complexes (Kingston and Narlikar, 1999). Different combination of associated subunits, together, provide unique biological function to the complex (Wu *et al*., 2009). Research suggests that additional chromatin remodeling complexes can be recruited by other chromatin remodelers and some transcriptional activators (Struhl, 1999; Yudkovsky *et al*., 1999).

1.15 SWI/SNF chromatin remodeling complexes

The SWI/SNF (SWItch/Sucrose Non-Fermentable) family of chromatin remodeling complexes are evolutionarily conserved in eukaryotes from yeast to humans. They were discovered in yeast by identifying mutations in genes that regulate the mating-type switching (SWI) and sucrose fermentation (Sucrose Non-Fermenting - SNF) (Neigeborn and Carlson, 1984). These complexes have a helicase-SANT–associated (HSA) domain, which is an actin binding domain, and a bromo domain that interacts with acetylated lysins (Workman and Kingston, 1998). BRM and BRG1 are ATPases that can serve as the catalytic subunit of SWI/SNF complexes. A series of BRG1-associated factors (BAFs) assemble with either BRM or BRG1 to create a functional SWI/SNF chromatin-remodeling complex. The collection of BAFs that associate with a catalytic subunit determine the identity of a given SWI/SNF chromatin-remodeling complex, determine its activity, and dictate where that complex will act (Smith *et al*., 2003). BRG1 appears to regulate zygotic genome activation in mammalian embryos (Bultman *et al.,* 2006). Maternal BRG1 is required to successfully program gene expression patterns in both mouse and pig embryo (Bultman *et al.,* 2006; Magnani and Cabot, 2009). Alteration of BRG1 levels results in decreased methylation on the lysine 4 residue of histone protein H3 (H3K4), which leads to abnormal embryo development and changes the expression levels of other chromatin remodeling proteins (Bultman *et al.,* 2000; Glanzner *et al.,* 2017).

In addition to the ATPase, SWI/SNF related, matrix associated, actin dependent regulator of chromatin, subfamily B, member 1 (SMARCB1; also referred to as sucrose non-fermenting 5, SNF5), BRG1 associated factor 155 (BAF155, also known as SMARCC1), and BRG1 associated factor 170 (BAF170, also known as SMARCC2) are considered core subunits of SWI/SNF complexes. Between nine and fifteen additional BAFs interact with this core set to make distinct SWI/SNF complexes. SWI/SNF complexes can be categorized as BAF complexes, which contain either AT-Rich Interaction Domain 1A (ARID1A, also known as BAF250a) or AT-Rich Interaction Domain 1B (ARID1B, also known as BAF250b), and polybromo-associated BAF (PBAF) complexes, which contain PBRM1 and AT-Rich Interaction Domain 2 (ARID2, also known as BAF200) (Clapier and Cairns, 2009). A third SWI/SNF complex has been identified and is named GBAF (glioma tumor suppressor candidate region gene 1 [GLTSCR1] BAF) which is considered as non-canonical BAF. GBAF lacks the conserved core subunit SNF5, which stimulates chromatin remodeling activity and genomic targeting of BAF and PBAF (Alpsoy and Dykhuizen, 2018).

1.16 BRG1- or BRM-associated factors (BAFs)

BAF155 and BAF170 are structural subunits and required for full ATPase and remodeling functions (Phelan *et al.*, 1999). SNF5, BAF57, BAF53, and actin can also be found in all canonical SWI/SNF complexes (BAF and PBAF). ARID2, BAF45D, and BRD7 are only identified in PBAF while ARID1, BCL7, and BCL11 belong to BAF. The critical roles of several BAFs have been characterized during early embryo development. BRG1 appears to regulate zygotic genome activation (ZGA) in mammalian embryos and has been shown to affect porcine embryo development (Bultman *et al.,* 2000; Magnani and Cabot, 2009; Glanzner *et al.,* 2017). BAF155 is reported to regulate the expression of pluripotency marker Nanog, and other genes associated with cellular differentiation in mouse embryos during cleavage development (Schaniel *et al.*, 2009). SNF5 depletion in mouse embryos results in early developmental arrest where embryos fail to finish implantation (Klochendler-Yeivin *et al.,* 2000). During human pluripotent cell differentiation, SNF5 changes the SWI/SNF complex occupancy at regulatory sites of POU5F1 target genes, repressing POU5F1 activated genes and activating POU5F1 repressed genes (You *et al.,* 2013). Except core BAFs, the expression level and profile of other subunits leading to distinct SWI/SNF complexes are unique to cell type. (Ho and Crabtree, 2010). ARID1A is highly

expressed in embryonic stem cells. In mice, ARID1A is required for complete development of the germ layers, given that Arid1a depletion in mouse embryos results in developmental arrest at the blastocyst stage (Gao *et al*., 2008). In porcine embryo, *ARID1A* knockdown significantly decrease the development competence (Tseng *et al*., 2018). ARID2 and BRD7 also play critical roles in development and the cause embryonic lethality in null mice (Kaeser *et al*., 2008; Xu *et al*., 2012). Studies also indicate that the composition of BAFs have time-dependent effect and suggest a dynamic requirement for the BAF complex in the regulation of pluripotency (Panamarova *et al*., 2016). This could be controlled through changes in BAF complex stoichiometry or through mobilization dynamics of existing subunits.

1.17 BAF, PBAF and GBAF

BAF155, BAF170 and SNF5 have been considered as core subunits for all SWI/SNF chromatin remodeling complexes. A new category of SWI/SNF family has been identified in 2018. The GBAF complex, unlike BAF and PBAF complexes, has two BAF155 (BAF155 dimer), GLTSCR1, GLTSCR1L and BRD9 (Alpsoy and Dykhuizen, 2018). The relation and interaction between BAF, PBAF and GBAF are still unclear. Studies suggests that losing SNF5 leads to an increase in BRD9 and ultimately increases GBAF formation. The Domain of unknown function 3512 (DUF3512) of BRD9 is critical for SWI/SNF integrity in the absence of SNF5 (Wang *et al*., 2019). It is also reported that GBAF is not essential for general cellular viability, but mouse knockout data suggests that lacking GLTSCR1L leads to embryonic lethality (Dickinson *et al*., 2016). Studies have suggested that the functional similarity between canonical BAF and GBAF. Both BAF and GBAF has been suggested to regulate pluripotency factors, such as NANOG in embryonic stem cells (Ho *et al*., 2009; Gatchalian *et al*., 2018). GBAF potentially binds to H3K27ac and is considered as an enhancer-associated chromatin remodeler which regulates activity of enhancers (Jefimov *et al*., 2018). This new discovered SWI/SNF subfamily, GBAF, indicates there are more investigations required to reveal the network of SWI/SNF chromatin remodeling complexes and BAFs

1.18 *In vitro* embryo production

Assisted reproduction technologies (ARTs), such as intracytoplasmic sperm injection (ICSI), cryopreservation of gametes, and *in vitro* fertilization (IVF), are used in animals to improve

reproductive efficiency and to generate models for embryo studies. In pig**,** Motlik and Fulka first matured porcine oocytes to the MII *in vitro* in 1974 (Motlk and Fulka, 1974). The first IVF in the swine industry was performed by Iritani and colleagues in 1978 (Iritani *et al*., 1978). Frozen semen was used to performed *in vitro* fertilization in 1988 (Nagai *et al*., 1988). Next year, the *in vitro* produced porcine embryo was able to develop into blastocyst (Mattioli *et al*., 1989). The first piglet produced by transferring *in vitro* produced 2-cell embryos to a recipient was reported by Yoshida *et al*., in 1993 (Yoshida *et al*., 1993). ARTs are also used in humans to address infertility. According to the CDC's Fertility Clinics Report in 2017, there were 68,908 live births and 78,052 live born infants in the U.S. through ART and the main type of ART is IVF. The Market Analysis Report predicts the global ART market is expected to reach USD 45 billion by 2025 due to aging population, chronic diseases, and same-sex marriage.

Although *in vitro* embryo production has been practiced worldwide in both animal and humans, there are still concerns regarding to the embryo health. Several studies from different species have indicate that embryos produced *in vitro* have reduced developmental potential compared with *in vivo* produced embryos (Sirard and Blondin, 1996; Kikuchi *et al*., 1999; Zhu *et al*., 2018). Several factors can affect the *in vitro* embryo production efficiency and contribute to the existing differences between *in vivo* and *in vitro* produced embryos. The micro condition during *in vitro* manipulation has been suggested to alter the epigenetic states of *in vitro* produced embryos and leads to potential diseases, for example the large offspring syndrome in cattle and sheep; Beckwith-Wiedemann syndrome (BWS) and Silver-Russell syndrome (SRS) in human (Chen *et al*., 2013; Hattori *et al*., 2019). It is important to identify the consequences of *in vitro* manipulation so the current *in vitro* embryo production procedure can be improved.

1.19 References

Abbott AL, Ducibella T. 2001. Calcium and the control of mammalian cortical granule exocytosis. Front Biosci 6:D792-D806.

Abrieu A, Doree M, Fisher D. 2001. The interplay between cyclin-B-Cdc2 kinase (MPF) and MAP kinase during maturation of oocytes. J Cell Sci 114:257–267.

Albini S, Coutinho TP, Dall'Agnese A, Malecova B, Cenciarelli C, Felsani A, Caruso M, Bultman SJ, Puri PL. 2015. Brahma is required for cell cycle arrest and late muscle gene expression during skeletal myogenesis. EMBO Rep 16:1037–1050.

Alfageme CR, Zweidler A, Mahovald A, Cohen LH. 1974. Histones of Drosophila embryos Electrophoretic isolation and structural studies. J Biol Chem 249:3729-3736.

Allen RD, Griffin JL. 1958. The time sequence of early events in the fertilization of sea urchin eggs. I. The latent period and the cortical reaction. Exp Cell Res 15(1):163-73.

Allouche-Fitoussi D, Bakhshi D, Breitbart H. 2018. Signaling pathways involved in human sperm hyperactivated motility stimulated by Zn^{2+}. Mol Reprod Dev 85(6):543-556.

Alpsoy A, Dykhuizen EC. 2018. Glioma tumor suppressor candidate region gene 1 (GLTSCR1) and its paralog GLTSCR1-like form SWI/SNF chromatin remodeling subcomplexes. J Biol Chem 293:3892–3903.

Austin C. 1952. The 'Capacitation' of the Mammalian Sperm. Nature 170:326.

Austin CR. 1975. Membrane fusion events in fertilization. J Reprod Fertil 44(1):155–166.

Balhorn R. 2007. The protamine family of sperm nuclear proteins. Genome biology 8(9):227.

Barski A, Cuddapah S, Cui K, Roh TY, Schones DE, Wang Z, Wei G, Chepelev I, Zhao K. 2007. High-resolution profiling of histone methylations in the human genome. Cell 129(4):823-837.

Bedford JM. 1970. Sperm Capacitation and Fertilization in Mammals. Biology of Reproduction 2:128–158.

Bestor TH, Schatten G. 1981. Anti-tubulin immunofluorescence microscopy of microtubules present during the pronuclear movement of sea urchin fertilization. Dev Biol 88(1):80-91.

Bird AP. 1986. CpG-rich islands and the function of DNA methylation. Nature 321:209–213.

Bleil JD, Wassarman PM. 1980. Synthesis of zona pellucida proteins by denuded and follicle-enclosed mouse oocytes during culture in vitro. Proc Natl Acad Sci U S A 77(2):1029-1033.

Bleil JD, Wassarman PM. 1986. Autoradiographic visualization of the mouse egg's sperm receptor bound to sperm. J Cell Biol 102(4):1363-1371.

Bolton VN, Oades PJ, Johnson MH. 1984. The relationship between cleavage, DNA replication, and gene expression in the mouse 2-cell embryo. J Embryol Exp Morphol 79:139–163.

Breitbart H, Spungin B. 1997. The biochemistry of the acrosome reaction. Mol Hum Reprod 3(3):195-202.

Buehr M. 1997. The primordial germ cells of mammals: some current perspectives. Exp Cell Res 232:194–207.

Bullejos M, Koopman P. 2004. Germ cells enter meiosis in a rostro-caudal wave during development of the mouse ovary. Mol Reprod Dev 68(4):422-428.

Bultman S, Gebuhr T, Yee D, La Mantia C, Nicholson J, Gilliam A, Randazzo F, Metzger D, Chambon P, Crabtree G, Magnuson T. 2000. A Brg1 null mutation in the mouse reveals functional differences among mammalian SWI/SNF complexes. Mol Cell 6:1287–1295

Bultman S, Gebuhr T, Pan H, Svoboda P, Schultz R, Magnuson T. 2006. Maternal BRG1 regulates zygotic genome activation in the mouse. Genes Dev 20:1744–1754.

Byskov AG, Yding AC, Hossaini A, Guoliang X. 1997. Cumulus cells of oocyte-cumulus complexes secrete a meiosis-activating substance when stimulated with FSH. Mol Reprod Dev 46:296–305.

Cedar H, Razin A. 1990. DNA methylation and development. Biochim. Biophys Acta 1049:1–8.

Chan CS, Rastelli L, Pirrotta V. 1994. A Polycomb response element in the Ubx gene that determines an epigenetically inherited state of repression. EMBO J 13(11):2553-2564.

Chang H, Brown CW, Matzuk MM. 2002. Genetic analysis of the mammalian transforming growth factor-beta superfamily. Endocr Rev 23(6):787-823.

Channing CP, Schaerf FW, Anderson LD, Tsafriri A. 1980. Ovarian follicular and luteal physiology. Int Rev Physiol 22:117–201.

Chen MS, Tung KS, Coonrod SA, Takahashi Y, Bigler D, Chang A, Yamashita Y, Kincade PW, Herr JC, White JM. 1999. Role of the integrin-associated protein CD9 in binding between sperm ADAM 2 and the egg integrin α6β1: Implications for murine fertilization. Proc. Natl Acad Sci USA 96:11830–11835.

Chen H, Tini M, Evans RM. 2001. HATs on and beyond chromatin. Curr Opin Cell Biol 13(2):218-224.

Chen T, Dent SY. 2014. Chromatin modifiers and remodellers: regulators of cellular differentiation. Nat Rev Genet 15(2):93-106.

Chen Z, Robbins KM, Wells KD, Rivera RM. 2013. Large offspring syndrome: a bovine model for the human loss-of-imprinting overgrowth syndrome Beckwith-Wiedemann. Epigenetics 8(6):591-601.

Chi TH, Wan M, Lee PP, Akashi K, Metzger D, Chambon P, Wilson CB, Crabtree GR. 2003. Sequential roles of Brg, the ATPase subunit of BAF chromatin remodeling complexes. Thymocyte Development Immunity 19:169–182.

Clapier CR, Cairns BR. 2009. The biology of chromatin remodeling complexes. Annu Rev Biochem 78:273–304.

Cornwall GA. 2009. New insights into epididymal biology and function. Hum Reprod Update 15(2):213-227.

Côté J, Quinn J, Workman JL, Peterson CL. 1994. Stimulation of GAL4 derivative binding to nucleosomal DNA by the yeast SWI/SNF complex. Science 265:53–60.

Dandekar P, Talbot P. 1992. Perivitelline space of mammalian oocytes: extracellular matrix of unfertilized oocytes and formation of a cortical granule envelope following fertilization. Mol Reprod Dev 31(2):135–143.

Dickinson ME, Flenniken AM, Ji X, Teboul L, Wong MD, White JK, Meehan TF, Weninger WJ, Westerberg H, Adissu H, Baker CN, Bower L, Brown JM, Caddle LB, Chiani F. 2016. High-throughput discovery of novel developmental phenotypes. Nature 537:508–514.

Di Pasquale E, Rossetti R, Marozzi A, Bodega B, Borgato S, Cavallo L, Einaudi S, Radetti G, Russo G, Sacco M, Wasniewska M, Cole T, Beck-Peccoz P, Nelson LM, Persani L. 1976. Identification of new variants of human BMP15 gene in a large cohort of women with premature ovarian failure. J Clin Endocrinol Metab 91(5):1976-1979.

DiZerega GS, Hodgen GD. 1981. Folliculogenesis in the primate ovarian cycle. Endocr Rev 2:27-49.

Dong J, Albertini DF, Nishimori K, Kumar TR, Lu N, Matzuk MM. 1996. Growth differentiation factor-9 is required during early ovarian folliculogenesis. Nature 383(6600):531-535.

Eisen A, Reynolds GT. 1985. Sources and sinks for the calcium release during fertilization of single sea urchin eggs. J Cell Biol 100:1522–1527.

Eisen JA, Sweder KS, Hanawalt PC. 1995. Evolution of the SNF2 family of proteins: subfamilies with distinct sequences and functions. Nucleic Acids Res 23(14):2715-2723.

Ellerman DA, Pei J, Gupta S, Snell WJ, Myles D, Primakoff P. 2009. Izumo is part of a multiprotein family whose members form large complexes on mammalian sperm. Mol Reprod Dev 76(12):1188-1199.

Evans HH, Evans TE. 1970. Methylation of the deoxyribonucleic acid of Physarum polycephalum at various periods during the mitotic cycle. J Biol Chem 245(23):6436-6441.

Evans JP, Kopf GS, Schultz RM. 1997. Characterization of the binding of recombinant mouse sperm fertilin β subunit to mouse eggs. Dev Biol 187:79-83.

Feng Q, Wang H, Ng HH, Erdjument-Bromage H, Tempst P, Struhl K, Zhang Y. 2002. Methylation of H3-lysine 79 is mediated by a new family of HMTases without a SET domain. Curr Biol 12(12):1052-1058.

Fawcett DW, Phillips DM. 1969. The fine structure and development of the mammalian spermatozoon. Anat Rec 165:153-184.

Flach G, Johnson MH, Braude PR, Taylor RA, Bolton VN. 1982. The transition from maternal to embryonic control in the 2-cell mouse embryo. The EMBO journal 1:681–686.

Gao F, Maiti S, Alam N, Zhang Z, Deng JM, Behringer RR, *et al*., 2006. The Wilms tumor gene, Wt1, is required for Sox9 expression and maintenance of tubular architecture in the developing testis. Proc Natl Acad Sci USA 103(32):11987–11992.

Gardiner-Garden M, Frommer M. 1987. CpG islands in vertebrate genomes. J Mol Biol 196(2):261-82.

Gatchalian J, Malik S, Ho J, Lee DS, Kelso TWR, Shokhirev MN, Dixon JR, Hargreaves DC. 2018. A non-canonical BRD9-containing BAF chromatin remodeling complex regulates naïve pluripotency in mouse embryonic stem cells. Nat Commun 9:5139.

Glanzner WG, Wachter A, Coutinho AR, Albornoz MS, Duggavathi R, GonÇAlves PB, Bordignon V. 2017. Altered expression of BRG1 and histone demethylases, and aberrant H3K4 methylation in less developmentally competent embryos at the time of embryonic genome activation. Mol Reprod Dev 84(1):19-29.

Gonzales-Cope M, Sidoli S, Bhanu NV, Won KJ, Garcia BA. 2016. Histone H4 acetylation and the epigenetic reader Brd4 are critical regulators of pluripotency in embryonic stem cells. BMC Genomics 17-95.

Gould M, Luis Stephano J. 1987. Fertilization events. Nature 328:766–767.

Gurdon JB. 1962. The developmental capacity of nuclei taken from intestinal epithelium cells of feeding tadpoles. J Embryol Exp Morphol:622-640.

Günesdogan U, Surani MA. 2016. Developmental Competence for Primordial Germ Cell Fate. Curr Top Dev Biol 117:471-496.

Griffin CT, Brennan J, Magnuson T. 2008. The chromatin-remodeling enzyme BRG1 plays an essential role in primitive erythropoiesis and vascular development. Development 135:493–500.

Hahnel AC, Eddy EM. 1986. Cell surface markers of mouse primordial germ cells defined by two monoclonal antibodies. Gamete Res 15:25–34.

Hamaguchi M, Hiramoto Y. 1980. Fertilization process in the heart-urchin, Clypeaster japonicus, observed with a differential interference microscope. Dev. Growth Differ 22:517– 530.

Hamiche A, Sandaltzopoulos R, Gdula DA, Wu C. 1999. ATP-dependent histone octamer sliding mediated by the chromatin remodeling complex NURF. Cell 97(7):833-842.

Harley VR, Goodfellow PN. 1994. The biochemical role of SRY in sex determination. Mol Reprod Dev 39(2):184-193.

Hauser C, Schuettengruber B, Bartl S, Lagger G, Seiser C. 2002. Activation of the mouse histone deacetylase 1 gene by cooperative histone phosphorylation and acetylation. Mol Cell Biol 22:7820-7830.

Hattori H, Hiura H, Kitamura A, Miyauchi N, Kobayashi N, Takahashi S, Okae H, Kyono K, Kagami M, Ogata T, Arima T. 2019. Association of four imprinting disorders and ART. Clin Epigenetics 11(1):21.

Hinsch E, Orhninger S, Schill WB, Hinsch KD. 1999. Species specificity of human and murine anti-ZP3 synthetic peptide antisera and use of the antibodies for localization and identification of ZP3 or ZPC domains of functional significance. Hum Reprod 14:419–28.

Ho L, Ronan JL, Wu J, Staahl BT, Chen L, Kuo A, Lessard J, Nesvizhskii A, Ranish J, Crabtree GR. 2009. An embryonic stem cell chromatin remodeling complex, esBAF, is essential for embryonic stem cell self-renewal and pluripotency. PNAS 106:5181-5186.

Ho L, Crabtree GR. 2010. Chromatin remodelling during development. Nature 463:474–484.

Holliday R, Pugh JE. 1975. DNA modification mechanisms and gene activity during development. Science 187:226–232.

Howlett SK. 1986. A set of proteins showing cell cycle dependent modification in the early mouse embryo. Cell 45:387–396.

Ickowicz D, Finkelstein M, Breitbart H. 2012. Mechanism of sperm capacitation and the acrosome reaction: role of protein kinases. Asian J Androl 14:816–821.

Iritani A, Niwa K, Imai H. 1978. Sperm penetration *in vitro* of pig follicular oocytes matured in culture. J Reprod Fertil 54(2):379-383.

Jaffe LA, Gould-Somero M, Holland LZ. 1982. Studies of the mechanism of the electrical polyspermy block using voltage clamp during cross-species fertilization. J Cell Biol 92(3):616-621.

Jefimov K, Alcaraz N, Kloet S, Varv S, Aastedatter Sakya S, Dalager Vaagenso C, Vermeulen M, Aasland R, Andersson R. 2018. The GBAF chromatin remodeling complex binds H3K27ac and mediates enhancer transcription. bioRxiv doi: https://doi.org/10.1101/445148, 17 October 2018, preprint: not peer reviewed.

Jost A. 1947The Age Factor in the Castration of Male Rabbit Fetuses. Proceedings of the Society for Experimental Biology and Medicine 66(2):302-303.

Jost A. 1953. Degeneration of the extremities of the rat fetus induced by adrenaline. C R Hebd Seances Acad Sci 236(15):1510-1512.

Keshet E, Lyman SD, Williams DE, Anderson DM, Jenkins NA, Copeland NG, Parada LF. 1991. Embryonic RNA expression patterns of the c-kit receptor and its cognate ligand suggest multiple functional roles in mouse development. EMBO J 10:2425–2435.

Kikuchi K, Kashiwazaki N, Noguchi J, Shimada A, Takahashi R, Hirabayashi M, Shino M, Ueda M, Kaneko H. 1999. Developmental competence, after transfer to recipients, of porcine oocytes matured, fertilized, and cultured in vitro. Biol Reprod 60(2):336-340.

Kingston RE, Narlikar GJ. 1999. ATP-dependent remodeling and acetylation as regulators of chromatin fluidity. Genes Dev 13(18):2339-2352.

Klochendler-Yeivin A, Fiette L, Barra J, Muchardt C, Babinet C, Yaniv M. 2000. The murine SNF5/INI1 chromatin remodeling factor is essential for embryonic development and tumor suppression. EMBO Rep 1(6):500–506.

Kobayashi A, Behringer RR. 2003. Developmental genetics of the female reproductive tract in mammals. Nat Rev Genet 4:969–980.

Kornberg RD. 1974. Chromatin structure:a repeating unit of histones and DNA. Science 184(4139):868-871.

Kosako H, Gotoh Y, Nishida E. 1994. Requirement for the MAP kinase kinase/MAP kinase cascade in Xenopus oocyte maturation. EMBO J 13:2131–2138.

Krakauer DC, Mira A. 2000. Mitochondria and the death of oocytes. Nature 403:501-501.

Lawson KA, HageWJ. 1994. Germline development. J. Goode (Ed.), CIBA Foundation Symposium, vol. 182, Wiley, Chichester pp. 68-91.

Lawson KA, Dunn NR, Roelen, BA, Zeinstra LM., Davis AM, Wright CV, Korving JP, Hogan B. L. 1999. Bmp4 is required for the generation of primordial germ cells in the mouse embryo. Genes & development 13(4):424–436.

Leblond CP, Clermont Y. 1952. Spermiogenesis of rat, mouse, hamster and guinea pig as revealed by the “Periodic acid-fuchsin sulfurous acid” technique. Am J Anat 90:167-215.

Lee MT, Bonneau AR, Giraldez AJ. 2014. Zygotic genome activation during the maternal-to-zygotic transition. Annual Review of Cell and Developmental Biology 30:581–613.

Leitch HG, Tang WW, Surani MA. 2013. Primordial germ-cell development and epigenetic reprogramming in mammals. Curr Top Dev Biol 104:149 – 187.

Li E. 2002. Chromatin modification and epigenetic reprogramming in mammalian development. Nat Rev Genet 3:662–673.

Lintern-Moore S, Peters H, Moore GP, Faber M. 1974. Follicular development in the infant human ovary. J Reprod Fertil 39(1):53-64.

Liu X, Wang C, Liu W, Li J, Li C, Kou X, Chen J, Zhao Y, Gao H, Wang H, Zhang Y, Gao Y, Gao S. 2016. Distinct features of H3K4me3 and H3K27me3 chromatin domains in pre-implantation embryos. Nature 537:558–562.

Lishko PV, Kirichok Y. 2010. The role of Hv1 and CatSper channels in sperm activation. J Physiol 588:4667–4672.

Lo CW, Gilula NB. 1979. Gap junctional communication in the preimplantation mouse embryo. Cell 18:399–409.

Longo FJ. 1976. Sperm aster in rabbit zygotes: its structure and function. J Cell Biol 69(3):539-547

Longo FJ, Lynn JW, McCulloh DH, Chambers EL. 1986. Correlative ultrastructural and electrophysiological studies of sperm-egg interactions of the sea urchin, Lytechinus variegatus. Dev Biol 118:155–166.

Lorca T, Cruzalegui FH, Fesquet D, Cavadore JC, Mery J, Means A, Doree M. 1993. Calmodulin-dependent protein kinase II mediates inactivation of MPF and CSF upon fertilization of Xenopus eggs. Nature 366:270–273.

Luthardt FW, Donahue RP. 1973. Pronuclear DNA synthesis in mouse eggs. An autoradiographic study. Exp Cell Res 82:143–151.

Ma PP, Schultz RM. 2008. Histone deacetylase 1 (HDAC1) regulates histone acetylation, development, and gene expression in preimplantation mouse embryos. Dev Biol 319(1): 110–120.

Macklon NS, Fauser BC. 1998. Follicle development during the normal menstrual cycle. Maturitas 30(2):181-188.

Macklon NS, Fauser BC. 1999. Aspects of ovarian follicle development throughout life. Horm Res 52(4):161-170.

Majumder S, Alinari L, Roy S, Miller T, Datta J, Sif S, Baiocchi R, Jacob ST. 2010. Methylation of histone H3 and H4 by PRMT5 regulates ribosomal RNA gene transcription. Journal of cellular biochemistry 109(3):553–563.

Matsui Y, Zsebo KM, Hogan BLM. 1990. Embryonic expression of a hematopoietic growth factor encoded by the Sl locus and the ligand for c-kit. Nature 347:666–669.

Mattioli M, Bacci ML, Galeati G, Seren E. 1989. Developmental competence of pig oocytes matured and fertilized *in vitro*. Theriogenology 31:1201-1207.

McCulloh DH, Chambers EL. 1992. Fusion of membranes during fertilization. J Gen Physiol 99:137–175.

McGhee JD, Ginder GD. 1979. Specific DNA methylation sites in the vicinity of the chicken beta-globin genes. Nature 280(5721):419-420.

McLaren A. 2003. Primordial germ cells in the mouse. Developmental Biology 262(1):1–15.

Moore L, Le T, Fan G. 2013. DNA Methylation and Its Basic Function. Neuropsychopharmacol 38:23–38.

Morrish BC, Sinclair AH. 2002. Vertebrate sex determination: many means to an end. Reproduction 124:447–457.

Motlì J, Fulka J. 1974. Fertilization of pig follicular oocytes cultivated *in vitro*. J Reprod Fertil 36(1):235-237.

Murray K. 1964. The occurrence of e-N-methyllysine in histones. Biochemistry 3:10–15.

Nagai T, Takahashi T, Masuda T, Shioya Y, Kuwayama M, Fukushima M, Iwasaki S, Hamada A. 1988. *In vitro* fertilization of frozen boar spermatozoa. J Reprod Fertil 84:585-591.

Neigeborn L, Carlson M. 1984. Genes affecting the regulation of SUC2 gene expression by glucose repression in Saccharomyces cerevisiae. Genetics 108(4):845-858.

O'Rahilly R, Müller F. 1984. Embryonic length and cerebral landmarks in staged human embryos. Anat Rec 209(2):265-271.

Orgebin-Crist MC, Jahad N. 1979. The maturation of rabbit epididymal spermatozoa in organ culture: stimulation by epididymal cytoplasmic extracts. Biol Reprod 21(2):511-515.

Ozil JP. 1998. Role of calcium oscillations in mammalian egg activation: experimental approach. Biophys Chem 72(1–2):141–152.

Pacchierotti F, Spano M. 2015. Environmental Impact on DNA Methylation in the Germline: State of the Art and Gaps of Knowledge. Biomed Res Int 2015:123484.

Panamarova M, Cox A, Wicher KB, Butler R, Bulgakova N, Jeon S, Rosen B, Seong RH, Skarnes W, Crabtree G. 2016. The BAF chromatin remodelling complex is an epigenetic regulator of lineage specification in the early mouse embryo. Development 143:1271-1283.

Pandey P, Brors B, Srivastava PK, Bott A, Boehn SN, Groene HJ, Gretz N. 2008. Microarray-based approach identifies microRNAs and their target functional patterns in polycystic kidney disease. BMC Genomics 9:624.

Pereda J, Zorn T, Soto-Suazo M. 2006. Migration of human and mouse primordial germ cells and colonization of the developing ovary: an ultrastructural and cytochemical study. Microsc Res Tech 69(6):386-395.

Pfister NT. 2015. Mutant p53 cooperates with the SWI/SNF chromatin remodeling complex to regulate VEGFR2 in breast cancer cells. Genes Dev 29:1298–1315.

Phelan ML, Sif S, Narlikar GJ, Kingston RE. 1999. Reconstitution of a core chromatin remodeling complex from SWI/SNF subunits. Mol Cell 3:247–253.

Reyes JC, Barra J, Muchardt C, Camus A, Babinet C, Yaniv M. 1998. Altered control of cellular proliferation in the absence of mammalian brahma (SNF2α). EMBO Journal 17:6979-6991.

Sawada H, Yamazaki K, Hoshi M. 1990. Trypsin-like hatching protease from mouse embryos: evidence for the presence in culture medium and its enzymatic properties. J Exp Zool 254:83–87.

Saitou M, Barton S. Surani M. 2002. A molecular program for the specification of germ cell fate in mice. Nature 418:293–300.

Schaniel C, Ang YS, Ratnakumar K, Cormier C, James T, Bernstein E, Lemischka IR, Paddison PJ. 2009. Smarcc1/Baf155 couples self-renewal gene repression with changes in chromatin structure in mouse embryonic stem cells. Stem Cells 27:2979–2991.

Schulz WA, Hatina J. 2006. Epigenetics of prostate cancer: beyond DNA methylation. J Cell Mol Med 10(1):100-125.

Schulz KN, Harrison MM. 2019. Mechanisms regulating zygotic genome activation. Nat Rev Genet 20(4):221-234.

Shirayoshi Y, Okada TS, Takeichi M. 1983. The calcium-dependent cell-cell adhesion system regulates inner cell mass formation and cell surface polarization in early mouse development. Cell 35:631–638.

Sirard M, Blondin P. 1996. Oocyte maturation and IVF in cattle. Anim Reprod Sci 42:417-426.

Smith CL, Horowitz-Scherer R, Flanagan JF, Woodcock CL, Peterson CL. 2003. Structural analysis of the yeast SWI/SNF chromatin remodeling complex. Nat Struct Biol 10(2):141-145.

Snook RR, Hosken DJ, Karr TL. 2011. The biology and evolution of polyspermy: insights from cellular and functional studies of sperm and centrosomal behavior in the fertilized egg. Reproduction 142(6):779-792.

Sorensen RA, Wassarman PM. 1976. Relationship between growth and meiotic maturation of the mouse oocyte. Dev Biol 50:531–536.

Struhl K. 1999. Fundamentally different logic of gene regulation in eukaryotes and prokaryotes. Cell 98(1):1-4.

Studitsky VM, Kassavetis GA, Geiduschek EP, Felsenfeld G. 1997. Mechanism of transcription through the nucleosome by eukaryotic RNA polymerase. Science 278(5345):1960-1963.

Tachibana M, Sugimoto K, Nozaki M, Ueda J, Ohta T, Ohki M, Fukuda M, Takeda N, Niida H, Kato H, Shinkai Y. 2002. G9a histone methyltransferase plays a dominant role in euchromatic histone H3 lysine 9 methylation and is essential for early embryogenesis. Genes Dev 16(14): 1779–1791.

Tam PPL, Snow MHL. 1981. Proliferation and migration of primordial germ cells during compensatory growth in mouse embryos. Journal of Embryology and Experimental Morphology. 64:133–147.

Tazi J, Bird A. 1990. Alternative chromatin structure at CpG islands. Cell 60(6):909-920.

Teixeira Filho FL, Baracat EC, Lee TH, Suh CS, Matsui M, Chang RJ, Shimasaki S, Erickson GF. 2002. Aberrant expression of growth differentiation factor-9 in oocytes of women with polycystic ovary syndrome. J Clin Endocrinol Metab 87(3):1337-1344.

Terasaki M, Sardet C. 1991. Demonstration of calcium uptake and release by sea urchin egg cortical endoplasmic reticulum. J Cell Biol 115:1031–1037.

Thakur MK. 1983. Covalent modifications of chromosomal proteins during aging. Arch Gerontol Geriatr 2(1-2):1-10.

Tunquist BJ, Maller JL. 2003. Under arrest: cytostatic factor (CSF)-mediated metaphase arrest in vertebrate eggs. Genes Dev 17:683–710.

Vermeiden JP, Zeilmaker GH. 1974. Relationship between maturation division, ovulation and leuteinization in the female rat. Endocrinology 95(2):341-351.

Vincent SD, Dunn NR, Sciammas R, Shapiro-Shalef M, Davis MM, Calame K, Bikoff EK, Robertson EJ. 2005. The zinc finger transcriptional repressor Blimp1/Prdm1 is dispensable for early axis formation but is required for specification of primordial germ cells in the mouse. Development 132(6):1315-1325.

Wang W, Xue Y, Zhou S, Kuo A, Cairns BR, Crabtree GR. 1996. Diversity and specialization of mammalian SWI/SNF complexes. Genes Dev 10(17):2117-2130.

Wang FC, Kou ZH, Zhang Y, Gao SR. 2007. Dynamic Reprogramming of Histone Acetylation and Methylation in the First Cell Cycle of Cloned Mouse Embryos, Biol Reprod 77:1007–1016.

Wang J, Gu H, Lin H, Chi T. 2012. Essential roles of the chromatin remodeling factor BRG1 in spermatogenesis in mice. Biol Reprod 86:186.

Wang X, Haswell JR, Roberts CW. 2014. Molecular pathways: SWI/SNF (BAF) complexes are frequently mutated in cancer—mechanisms and potential therapeutic insights. Clin Cancer Res 20:21–27.

Wang X, Wang S, Troisi EC, Howard TP, Haswell JR, Wolf BK, Hawk WH, Ramos P, Oberlick EM, Tzvetkov EP, Ross A, Vazquez F, Hahn WC, Park PJ, Roberts CWM. 2019. BRD9 defines a SWI/SNF sub-complex and constitutes a specific vulnerability in malignant rhabdoid tumors. Nat Commun 10(1):1881.

Wassarman PM. 2014. Sperm protein finds its mate. Nature 508:466–467.

Workman JL, Kingston RE. 1998. Alteration of nucleosome structure as a mechanism of transcriptional regulation. Annu Rev Biochem 67:545–579.

Wright SJ, Longo FJ. 1988. Sperm nuclear enlargement in fertilized hamster eggs is related to meiotic maturation of the maternal chromatin. J Exp Zool 247:155–165.

Wutz A, Smrzka OW, Schweifer N, Schellander K, Wagner EF, Barlow DP. 1997. Imprinted expression of the Igf2r gene depends on an intronic CpG island. Nature 389(6652):745-749.

Xu F, Flowers S, Moran E. 2012. Essential role of ARID2 protein-containing SWI/SNF complex in tissue-specific gene expression. J Biol Chem 287:5033–5041.

Yartseva V, Giraldez AJ. 2015. The Maternal-to-Zygotic Transition During Vertebrate Development: A Model for Reprogramming. Curr Top Dev Biol 113:191-232.

Yoshida M. 1993. Birth of piglets derived from *in vitro* fertilization of pig oocytes matured *in vitro*. Theriogenology 39:1303 – 1311.

Yudkovsky N, Logie C, Hahn S, Peterson CL. 1999. Recruitment of the SWI/SNF chromatin remodeling complex by transcriptional activators. Genes Dev 13(18):2369-2374.

Zhao GQ, Deng K, Labosky PA, Liaw L, Hogan BL. 1996. The gene encoding bone morphogenetic protein 8B is required for the initiation and maintenance of spermatogenesis in the mouse. Genes Dev 10(13):1657-1669.

Zhao JG, Hao YH, Ross JW, Spate LD, Walters EM, Melissa S, Rieke S, Murphy CN, Prather RS. 2010. Histone Deacetylase Inhibitors Improve *In vitro* and *In vivo* Developmental Competence of Somatic Cell Nuclear Transfer Porcine Embryos. Cell Reprogram 12(1): 75–83.

Zhu J, Moawad AR, Wang CY, Li HF, Ren JY, Dai YF. 2018. Advances in in vitro production of sheep embryos. Int J Vet Sci Med 6(Suppl):S15-S26.

CHAPTER 2. INTRODUCTION

Embryogenesis requires a series of events to develop into a functional individual. These events are precisely governed by tremendous number of genes. One of the upstream regulator to control gene expression is through epigenetic modifications. Studies have indicated that *in vitro* manipulations during assisted reproductive techniques can potentially disrupt the epigenetic status therefore have profound impact on embryo developmental competence.

Epigenetic modifications can be done by several ways to establish the proper epigenetic status. DNA methylation, histone acetylation and histone methylation are considered as covalent modifications. Repositioning of nucleosomes by chromatin remodeling complexes is an example of a non-covalent epigenetic modification. SWI/SNF chromatin remodeling complexes are large, multi-subunits complexes built up by series of BRG1-associated factors (BAFs). The SWI/SNF chromatin remodeling complexes utilize energy from ATP hydrolysis to restructure nucleosomes therefore regulate gene expression. The SWI/SNF family is evolutionarily conserved, and the homologous proteins were subsequently identified in yeast, flies, plants, and mammals.

The significance of SWI/SNF chromatin remodeling complexes is the BAFs. The collection of BAFs provides unique function to a given SWI/SNF chromatin-remodeling complex and dictate where that complex will act. A SWI/SNF chromatin remodeling complex can be made by up to 16 subunits while other ATP-dependent chromatin remodeling complexes have much less subunits, for example, the ISWI complexes are built up by only 2-6 subunits. Several BAFs have been reported to regulate genes that participate in cell cycle and cell differentiation. Mutations in the genes encoding these BAFs lead to cancers in human and mice. Studies also have identified these BAFs are involved in embryogenesis and othe biological pathways.

In our previous work, we have localized the intracellular localization in both *in vitro* and *in vivo* produced porcine embryos. We have found BAFs are shuttle between different cellular compartment during preimplantation stage. This indicates the potential requirement of these subunits. We also knockdown *ARID1A,* one of the well-studied subunit in cancer research, in preimplantation porcine embryos and the result indicates that ARID1A is required for porcine

embryo to proceed beyond 4-cell stage. The aim of this dissertation is to identify the developmental requirements of selected BAFs and how these subunits dictate to their gene regulation functions. Our short-term goal is to identify the requirement of each BAFs during early embryo development and reveal their explicit roles in embryogenesis. The long-term goal is to compare the activities carried out by SWI/SNF chromatin remodeling complexes in embryo produced *in vitro* and *in vivo*. Ultimately, we can pinpoint the procedures that disrupt the epigenetic status during *in vitro* manipulations and improve our current protocols.

CHAPTER 3. SNF5, A SWI/SNF CHROMATIN REMODELING COMPLEX CORE SUBUNIT, IS REQUIRED FOR PORCINE EARLY STAGE EMBRYO DEVELOPMENT

3.1 Abstract

The objective of the experiments presented here was to determine the developmental requirements of a core subunit of classical switch/sucrose non-fermentable (SWI/SNF) chromatin remodeling complexes, SNF5 (SMARCB1/INI1/BAF47). SWI/SNF chromatin remodeling complexes are composed of multiple protein subunits; the unique collection of subunits determines the specific activities of a given SWI/SNF complex. We hypothesized that SNF5 depletion would lead to developmental arrest of porcine embryos and lead to changes in the abundance of transcripts that show dynamic changes in abundance during early cleavage. An RNA interference assay was used to determine the developmental requirements of SNF5 in porcine embryos and to determine the extent to which perturbation in *SNF5* levels impacted transcript abundance of genes known to display dynamic changes during cleavage development. Our findings indicate that SNF5 is required for early cleavage, and attenuation of *SNF5* levels results in aberrant expression of both *NANOG* and POU Class 5 Homeobox 1 (*POU5F1*, also referred to as *OCT4)*.

3.2 Introduction

Cell division and cell differentiation require precise and appropriate gene regulation to ensure embryo development occurs in a correct manner (Hochedlinger and Plath, 2009). Maternally inherited transcripts are replaced by mRNA synthesized by the embryo (Embryonic Genome Activation, EGA) during the 4-cell stage of embryo development in the pig (Davis, 1985). Approximately 5 days after fertilization, porcine embyros initiate the first differentiation event and form the cells of the Inner Cell Mass (ICM) and trophectoderm (TE) at the blastocyst stage of development. These two events require highly controlled gene regulation (Telford *et al*., 1990).

The structure of the genetic material in the mammalian embryos undergoes a series of rearrangements during the first week of development that impact transcription. Epigenetic remodeling impacts phenotype without changes in DNA sequences (Monk *et al*., 1987). Examples

of epigenetic marks include methylation and hydroxymethylation of DNA, methylation, acetylation, phosphorylation, and ubiquitination of histone proteins, and repositioning of nucleosomes (Clapier and Cairns, 2009; Fulka *et al*., 2006). The nucleosome is the basic functional unit of chromatin and consists 147 base pairs of DNA wrapped around an octomeric core of histone proteins (Teif and Rippe, 2009)

The switch/sucrose non-fermentable (SWI/SNF) family of chromatin remodeling complexes are composed of multiple protein subunits (Peterson *et al*., 1994); these complexes alter chromatin structure by using the energy from ATP hydrolysis to reposition nucleosomes and alter the accessibility of transcription machinery. Multiple SWI/SNF complexes have been characterized biochemically and their activities are dependent upon the collection of subunits that make up a given complex. All SWI/SNF complexes possess one of two ATPases as their catalytic subunit. These ATPases are either SWI/SNF related, matrix associated, actin dependent regulator of chromatin, subfamily A, member 4 (SMARCA4; also referred to as Brahma-related gene 1, BRG1) or SWI/SNF related, matrix associated, actin dependent regulator of chromatin, subfamily A, member 2 (SMARCA2; also referred to as Brahma, BRM).

In addition to the ATPase SNF5, BAF155, and BAF170 are considered core subunits of SWI/SNF complexes (Euskirchen *et al*., 2012). Additional subunits interact with this core set to make distinct SWI/SNF complexes (Nie *et al*., 2003; Fukumoto *et al*., 2018); discrete signature subunits are known to associate with particular SWI/SNF complexes. For instance, the BAF complexes contain either AT-rich interacting domain 1A (ARID1A; also known as BAF250A) or AT-rich interacting domain 1B (ARID1B; also known as BAF250B), while polybromo BAF (PBAF) complexes contain SMARCA4, AT-rich interaction domain 2 (ARID2), BAF180 (PBRM1) and bromodomain-containing protein 7 (BRD7). Most recently described is the GBAF complex; GBAF contains the proteins glioma tumor suppressor candidate region gene 1 (GLTSCR1), glioma tumor suppressor candidate region gene 1 like (GLTSCR1L), and BRD9 (Alpsoy and Dykhuizen, 2018). The GBAF complex is unique in that SNF5, thought to be a core subunit in all SWI/SNF complexes, is not present in GBAF. GBAF, PBAF, and BAF complexes have been shown to bind discrete loci within the genome (Gatchalian *et al*., 2018).

SMARCA4 appears to regulate zygotic genome activation in mammalian embryos (Bultman *et al*., 2006). Maternal SMARCA4 is required to successfully program gene expression patterns in both mouse and pig (Bultman *et al*., 2006; Singh *et al*., 2016; Glanzner *et al*., 2017). Alteration of SMARCA4 levels results in decreased methylation on the lysine 4 residue of histone protein H3 (H3K4), which leads to abnormal embryo development and changes the expression levels of other chromatin remodeling proteins (Bultman *et al*., 2006; Glanzner *et al*., 2017).

Several studies have indicated that mutations in genes that encode SWI/SNF subunits affect cell differentiation and cell cycle progression (Zhang *et al*., 2014).SNF5 has been reported to be involved in many cell cycle and cell differentiation regulation pathways, including sonic hedgehog pathways (Isakoff *et al*., 2005). Loss of SNF5 activity is associated with rhabdoid tumors, which are an aggressive pediatric malignancy that arises in the kidney, brain, and soft tissues (Roberts *et al*., 2000; Roberts *et al*., 2002; Roberts and Biegel, 2009).Recent studies have shown alteration of *SNF5* expression affects several SWI/SNF target genes and alters the affinity of SWI/SNF complexes to promoters (Kuwahara *et al*., 2013). Snf5 depletion in mouse embryos results in early developmental arrest where embryos fail to finish implantation (Klochendler-Yeivin *et al*., 2000).

During human pluripotent cell differentiation, SNF5 changes the SWI/SNF complex occupancy at regulatory sites of POU Class 5 Homeobox 1 (POU5F1, also referred to as OCT4*)* target genes, repressing POU5F1 activated genes and activating POU5F1 repressed genes (You *et al*., 2013). In the absence of POU5F1, cells of the epiblast and ES cells both revert to the trophoblast lineage; overexpression of POU5F1 causes early differentiation of ES cell into endoderm and mesoderm (Nichols *et al*., 1998; Niwa *et al*., 2000). Reduction of Nanog in embryos leads to differentiation of pluripotent cells into the extraembryonic endoderm lineage. The pluripotency gene *Nanog* is required after Pou5f1 during embryo development, but both Pou5F1 and Nanog are required to maintain pluripotency (Chambers *et al*., 2003; Mitsui *et al*., 2003). Previous work from our group revealed that *POU5F1* transcript levels increase at the 2-cell stage while *NANOG* and SRY-box 2 (*SOX2)* are activated at the 4-cell stage (Magnani and Cabot, 2008).

We have previously reported that SNF5 is in the nuclei of germinal vesicle (GV) stage porcine oocytes and in the nuclei of blastomeres of cleavage stage embryos (Cabot *et al*., 2017), suggesting SNF5-containing SWI/SNF complexes may interact with chromatin throughout early embryogenesis. According to the critical roles that SWI/SNF chromatin remodeling complexes serve, we hypothesize that SNF5 is required for cleavage development and impacts transcription during cleavage development in the porcine embryo.

To test our hypothesis, we first determined *SNF5* transcript abundance in porcine oocytes and cleavage stage embryos. We next performed an RNA interference-mediated knockdown assay to determine the developmental requirements of SNF5 in porcine embryos. Lastly, we determined how a discrete set of genes that regulate pluripotency (*NANOG, POU5F1,* and *SOX2*) were altered upon SNF5 depletion. While our results indicate that transcript levels of *SNF5* remain unchanged during progression from immature oocyte to the blastocyst stage of embryo development, loss of *SNF5* induces developmental arrest during early cleavage and leads to significant changes in transcript abundance of *NANOG* and *POU5F1*. Taken together, our work demonstrates that SNF5 serves a critical role in porcine embryogenesis.

3.3 Materials and Methods

Oocyte collection

Chemicals used in experiments were all obtained from Sigma Chemical Company (St. Louis, MO) unless stated otherwise. Prepubertal gilt (*Sus scrofa*) ovaries were collected from a local abattoir and transported to the laboratory in an insulated container filled with 37ºC saline. Antral follicles that were 3–5 mm in diameter were aspirated to acquire follicular fluid containing cumulus-oocyte-complexes (COCs). COCs were selected from the follicular fluid and resuspended in 4-(2-hydroxyethyl)-1-piperazineethanesulphonic acid (HEPES)-buffered medium containing 0.01% polyvinyl alcohol (PVA) (Abeydeera et al., 1998). COCs with multiple layers of intact cumulus cells were selected for the experiments. For germinal vesicle (GV)-stage oocytes used in PCR studies and microinjection assays, selected COCs were placed in 0.1% hyaluronidase in HEPES-buffered medium and vortexed for 8 minutes to remove cumulus cells.

In vitro maturation

COCs (90-120) were matured in 500 µl of tissue culture medium 199 containing 0.14% PVA, 10 ng/mL epidermal growth factor, 20 ng/mL insulin-like growth factor 1 (IGF1; Prospec Protein Specialists), 40 ng/mL fibroblast growth factor 2 (FGF2; PeproTech), 20 ng/mL leukaemia inhibitory factor (LIF; MilliporeSigma), 0.57 mM cysteine, 0.5 IU/ml FSH, and 0.5 IU/ml LH (Yuan *et al*.,, 2017). COCs were matured for 42-43 hours at 39°C and 5% CO_2 in air, 100% humidity (Abeydeera *et al*., 1998; Yuan *et al*., 2017). Matured COCs then were placed in 0.1% hyaluronidase in HEPES-buffered medium and vortexed for 4 minutes to remove cumulus cells.

In vitro fertilization and embryo culture

Matured and denuded oocytes were placed in a modified Tris-buffered medium (mTBM) (30 oocytes in 50 µl mTBM droplet) and fertilized following an established protocol (Abeydeera and Day, 1997). Semen used for fertilization was collected from a mature boar with proven fertility housed at Purdue's Animal Science Research and Educational Center, extended with a commercial semen extender (EnduraGuard Plus; Mofa Global, Verona, WI) and stored at 17.5°C for up to three days. Before fertilization, 1 mL of extended semen was mixed with 9 ml Dulbecco's phosphate buffered Saline (PBS) containing 1 mg/ml BSA and centrifuged at 1000xg, 25°C, for 4 minutes; washing was repeated a total of three times. The sperm pellet was resuspended in mTBM. 50 µl of sperm suspension were added to oocytes at a final concentration of 5×10^5 spermatozoa/ml; gametes were co-incubated for 5 hours at 39°C and 5% CO_2. Embryos were cultured in Porcine Zygote Medium 3 (PZM3), an embryo culture medium (Yoshioka *et al*., 2002), supplemented with 3 mg/ml fatty acid-free bovine serum albumin (BSA) at 39°C, 5% CO_2 and 100% humidity for 20 hours, 48 hours, and 7 days in order to collect pronuclear, 4-cell, and blastocyst stage embryos, respectively.

RNA isolation, reverse transcription

Dynabeads mRNA DIRECT Micro Kit was employed to isolate RNA from porcine oocytes and embryos (Invitrogen Corporation, Carlsbad, CA, USA) according to the manufacturer's protocol. Briefly, pools of 100-150 GV-stage porcine oocytes, 4-cell stage embryos, and blastocyst stage porcine embryos were washed in HEPES-buffered medium three times, placed in 100 µl DYNABEADS lysis buffer, and incubated for 10 minutes at room temperature. Lysed cells were

stored at -80°C until further processing. Upon thawing, mRNA was isolated using Dynabeads, cDNA was produced using the iScript kit (Bio-rad, Hercules, CA, USA) in a 20 µl reaction volume according to the manufacturer's protocol (Lonergan *et al*., 2003).

Quantitative PCR

Primers used to amplify *SNF5* in this experiment were designed from publicly available sequence data in GenBank (XM_001929437). Primer sequences for *POU5F1*, *NANOG*, and *SOX2* were previously reported (Magnani and Cabot, 2008). Oligonucleotide primer sets used in this experiment were as follow: *SNF5* forward: 5'- GGAGATTGCCATCCGGAACA; and reverse 5'- CCTCCTCCCAGAAGACAGGA, product size is 226 nucleotides; *NANOG* forward: 5'- CGAAGCATCCATCTCCAGCGAATC; and reverse 5'- CGAGGGTCTCAGCAGATGACATCTG; *POU5F1* forward: 5'- AGGTGTTCAGCCAAACG; and reverse 5'- CGAAGCATCCATCTCCAGCGAATC; *SOX2* forward: 5'- CTGCGAGCGCTGCAGATGAA; and reverse 5'- CCTCCGGGCAGTGTGTACTTATCCT. The *SNF5*, *POU5F1*, *NANOG*, and *SOX2* PCR products were cloned into pENTR^{TM}/SD/D-TOPO vector (Invitrogen, Carlsbad, CA, USA). The amplification efficiency of the primer sets was determined to validate our assay. Briefly, standard curves for *SNF5, POU5F1, NANOG*, and *SOX2* were generated by performing PCR on serial dilutions of known quantities of target template. These curves were used to determine the range of threshold cycles (Ct values) for which each primer set produced a linear amplification of the target amplicon. Transcript levels of *YWHAG* (Genbank accession number CO94522) were used to normalize template input; *YWHAG* is a housekeeping gene that has been previously shown to maintain stable transcript levels during cleavage development (Whitworth *et al*., 2005). The abundance of *SNF5, POU5F1*, *NANOG*, and *SOX2* was determined relative to a housekeeping gene, *YWHAG*. *YWHAG* primers were: forward: 5'-TCCATCACTGAGGAAAACTGCTAA; and reverse 5'- TTTTTCCAACTCCGTGTTTCTCTA, product size 130 nucleotides (Whitworth *et al*., 2005).

A PCR mastermix was prepared for each gene as follows: 10 µl of SybrGreen Master mix (Bio-Rad), 1µl of 5µM forward primer, 1µl of 5µM reverse primer and 3µl of each cDNA. For each replicate, cDNA from one pool of embryos or oocytes was used to amplify target gene and *YWHAG*; reactions for each biological replicate were performed within the same PCR run. Reactions for

each gene were run in duplicates and at least three biological replicates were performed. The CFX Connect Real-Time Detection system (Bio-Rad) and the following program were used: 5 minutes initial denaturation at 94°C, followed by 45 cycles of 5 seconds at 94°C, 30 seconds at 60°C, and 30 seconds at 72°C. Fluorescence data were collected during the extension step of each cycle; a melt curve was produced to identify individual PCR amplicons.

Quantification of transcript levels

The relative transcript levels of *SNF5, POU5F1*, *NANOG*, and *SOX2* were analyzed by the comparative threshold cycle (Ct) method as described previously (Magnani and Cabot, 2008). The Ct value, the point where the PCR product rises above background during the log-linear phase, was determined for each reaction. The change in Ct (△Ct) was obtained by subtracting the Ct value of *SNF5, POU5F1*, *NANOG*, and *SOX2* from the Ct of *YWHAG*. The GV stage △Ct was used as the calibrator and used subsequently to obtain △△Ct values. The transcript level of *SNF5* in this study was calculated assuming an amplification efficiency of two and using the equation $2^{-\triangle\triangle Ct}$. In our RNA interference assay, the △Ct value found in the non-injected group was used as the calibrator to obtain △△Ct values.

RNA interference

SNF5 siRNA used in this study was design by the BLOCK-iT™ RNAi Designer software (Invitrogen) based on the full-length porcine *SNF5* open reading frame (XM_001929437). Custom made Stealth™ double stranded RNAi nucleotides targeting porcine *SNF5 5* were 5'-CGUAUGUUCCGAGGUUCUCUGUACA and 5'- UGUACAGAGAACCUCGGAACAUACG. As a control, a scrambled version of nonsense Stealth™ siRNA nucleotides were 5'-CGUCUUGGAGCCUUGGUCUUUAACA and 5'- UGUUAAAGACCAAGGCUCCAAGACG. Duplex Stealth™ siRNA nucleotides were diluted in DEPC treated water and stored at –20°C. A final concentration of 1 μM siRNA was injected.

Microinjection

Sperm were removed from presumptive zygotes by vortexing embryos in 0.1% hyaluronidase in HEPES-buffered medium for 4 minutes after gamete co-incubation. Presumptive zygotes were

then divided into three groups in HEPES-buffered medium containing 3mg/ml BSA. The three groups were as follows: *SNF5* siRNA injected, nonsense siRNA injected, and non-injected controls. Injection pipettes were loaded with 5µl of 1µM siRNA; a Femtojet microinjector (Eppendorf, Hauppauge, NY, USA) was used to perform microinjection. Embryos that lysed immediately after microinjection were discarded and excluded from analysis. After injection, surviving embryos were placed in PZM3 embryo culture medium. Embryos were cultured for seven days to determine the impact on developmental capacity in the respective treatment groups. Following seven days of culture, embryos were stained with Hoechst 33342 (5 µg/ml) and examined on an epifluorescence microscope to count nuclei. To determine changes in SNF5 protein levels in each treatment group, embryos were fixed in 3.7% paraformaldehyde 20 hours after microinjection and processed to detect SNF5 immunocytochemically. For assessment of *NANOG, POU5F1,* and *SOX2* transcript abundance, embryos were removed after 20 hours of culture for RNA isolation.

α-Amanitin treatment

In vitro matured oocytes were denuded, fertilized, and assigned to one of two treatments: injection with SNF5 interfering RNAs (SNF5-siRNA) or non-injected. Following microinjection, each of these treatment groups was further subdivided such that embryos were cultured either in control embryos culture medium (PZM3) or in culture medium containing 20µM α-amanitin, in a 2x2 factorial arrangement of treatments. Embryos were cultured for 20 hours post microinjection (Anderson *et al*., 1999). Messenger RNA was isolated from all groups of embryos was subjected to reverse transcription as described above; qPCR was used to determine the transcript abundance of *POU5F1*. A subset of non-injected embryos was cultured until day 7 to control for the overall quality of the embryos produced in each experimental replicate; replicates for which non-injected, control embryos failed to form morphological blastocyst embryos were excluded from the analysis.

Effectiveness of interfering RNAs targeting SNF5

To determine the effectiveness of the interfering RNAs designed to knockdown *SNF5* transcripts, denuded GV-stage oocytes were assigned to one of three treatment groups: *SNF5* siRNA injected (*SNF5* siRNA), nonsense siRNA injected (control siRNA), and non-injected controls (non-injected). After microinjection, all oocytes in their respective treatment groups were placed in *in*

vitro maturation medium for 30 hours. Messenger RNA was then isolated from intact oocytes from each treatment and RT-PCR was performed to determine *SNF5* transcript abundance.

Immunocytochemical staining

Embryos from all treatment groups in the RNA-interference assay were fixed at 4°C for 1 hour in 3.7% paraformaldehyde 20 hours after microinjection. Fixed cells were washed three times in phosphate-buffered saline (PBS) containing 0.1% Tween-20 (PBST) for 15 minutes for each. Permeabilization was performed in 1% Triton X-100 in PBS for 1 hour; embryos were then incubated in blocking solution (0.1 M glycine, 1% goat serum, 0.01% Triton X-100, 1% powdered nonfat dry milk, 0.5% BSA and 0.02% sodium azide in PBS) overnight (12-18 hours) (Prather and Rickords, 1992). Embryos were incubated with primary antibody against SNF5 (Abcam, Cambridge, MA, USA, catalog number ab12167), diluted 1:500 in PBST at 4°C overnight. Following a series of three washes in PBST (15 minutes per wash), embryos were incubated with secondary antibody (goat-anti-rabbit-IgG, fluorescein isothiocyanate (FITC)-conjugated, 1:500; Sigma–Aldrich. St. Louis, MO) in PBST at 4°C overnight. Embryos were washed three times in PBST (15 minutes per wash), stained with Hoechst 33342 (5 µg/ml) for 20 minutes, and mounted on slides in Vectashield mounting medium (Vector Laboratories, Inc., Burlingame, CA, USA). Slides were sealed with nail polish and examined by confocal microscopy using an inverted Nikon A1R_MP microscope, including de-scanned detectors and laser lines at 408 nm (Hoechst 33342) and 488 nm (FITC). Controls used in each replicate of immunocytochemical staining included groups of embryos that were stained with secondary antibody alone (to control for non-specific binding of secondary antibody) and embryos incubated with no antibodies (to control for background fluorescence).

Statistical analysis

The relative expression of each gene was calculated from the average Ct values of each duplicate using the $2^{-\triangle\triangle Ct}$ method (Livak and Schmittgen, 2001). The $2^{-\triangle\triangle Ct}$ values were imported into Statistical Analysis Software (SAS, SAS Institute, Cary, NC, USA) The linear model was processed by SAS LR program and analyzed with two-way ANOVA using GLM procedures. The embryo stages and replicates were considered as the main factors; a p-value < 0.05 was considered significant. Average nuclei numbers from the *SNF5* knockdown experiment were compared using

a two-way ANOVA using GLM procedures to perform multiple comparison of main effect means; treatments and replicates were considered as the main factors. Data pertaining to the percentage of morphological blastocyst stage embryos in the *SNF5* knockdown experiment were subjected to arcsine transformation; transformed values were analyzed with one-way ANOVA and compared by using Tukey's multiple comparison test. A p-value less than 0.05 was considered significant.

3.4 Results

SNF5 transcript abundance does not differ between porcine oocytes and cleavage stage embryos

SNF5 transcript abundance was determined in porcine GV-stage oocytes and *in vitro* produced 4-cell and blastocyst stage embryos. No significant differences in transcript abundance of *SNF5* were detected between GV-stage oocytes, 4-cell stage embryos, or blastocyst stage embryos (Figure 1).

Efficiency of SNF5 knockdown by interfering RNAs

Messenger RNA was isolated from oocytes from each treatment group 30 hours after microinjection. Following cDNA production, PCR was performed to determine the relative transcript abundance of *SNF5* in each treatment group. Our results indicate *SNF5* transcript levels were dramatically reduced in the *SNF5* siRNA treatment compared to two control groups (*SNF5* siRNA vs control siRNA and non-injected, $p<0.05$; Figure 2).

Immunocytochemical staining was performed on pronuclear stage porcine embryos to evaluate the level of reduction of SNF5 protein. *In vitro* matured porcine oocytes were fertilized and presumptive zygotes were assigned to each treatment, cultured for 20 hours, and processed to determine the intracellular localization of SNF5. Our results show a dramatic reduction in fluorescence in the *SNF5* siRNA group compared to the two control groups (*SNF5* siRNA n=137 vs control siRNA and non-injected, n=164 and n=147, respectively; Figure 3).

In vitro embryo developmental potential is reduced following SNF5 knockdown

In vitro matured porcine oocytes were fertilized *in vitro* and presumptive zygotes were assigned to treatments; the number of nuclei was determined in each embryo in each treatment group following seven days of embryo culture. We found a significant reduction in the number of nuclei

in the embryos from the *SNF5* siRNA treatment as compared to controls (1.7 nuclei/embryo [*SNF5* siRNA] vs 7.6 nuclei/embryo [control siRNA] and 7.8 nuclei/embryo [non-injected], $p<0.05$; Table 1). Significantly fewer embryos in the *SNF5* siRNA treatment formed morphological blastocyst stage embryos as compared to controls (0.7% blastocysts for *SNF5* siRNA vs 16.7% and 16.4% blastocysts for control siRNA and non-injected, respectively, $p<0.05$; Table 1). Of the embryos that reached the blastocyst stage, we found a significant reduction in the number of nuclei in embryos from the *SNF5* siRNA treatment group as compared to the controls (21 nuclei/blastocyst [*SNF5* siRNA] vs 32 nuclei/blastocyst [control siRNA] and 31 nuclei/blastocyst [non-injected], $p<0.05$; Table 1).

NANOG and POU5F1 transcript levels change upon SNF5 knockdown

The abundance of *NANOG*, *SOX2* and *POU5F1* transcripts was measured to determine if a reduction in *SNF5* impacted their levels. Messenger RNA was isolated from the treatment groups 20 hours after microinjection to assess transcript abundance. While no significant change in *SOX2* transcript abundance was detected, we found *NANOG* and *POU5F1* transcripts increased significantly in the *SNF5* siRNA treatment as compared to controls (*SNF5* siRNA vs control siRNA and non-injected, $p<0.05$; Figure 4).

Increased POU5F1 transcript abundance upon SNF5 knockdown is dependent on de novo mRNA synthesis

Presumptive zygotes injected with *SNF5* siRNA were cultured in the presence or absence of α-amanitin to determine if the change in POU5F1 transcript abundance was due to *de novo* mRNA synthesis. We found a significant reduction in the *POU5F1* transcript abundance in the embryos treated with α-amanitin as compared to embryos culture in control medium (*SNF5* siRNA + α-amanitin vs *SNF5* siRNA-control medium, $p<0.05$; Figure 5).

Relative abundance of *POU5F1* transcript abundance is significantly decreased in porcine embryos injected with *SNF5* interfering RNAs cultured in the presence of 20μM α-amanitin (*SNF5* siRNA + α-amanitin), as compared to embryos injected with *SNF5* interfering RNAs cultured and cultured in control medium (a vs b, $p<0.05$). *POU5F1* transcript abundance between non-injected embryos cultured in either the presence or absence of α-amanitin did not differ significantly from

one another; however both groups possessed a significantly lower level of *POU5F1* transcripts as compared to *SNF5* siRNA cultured in control medium. Fold changes were calculated using the formula $2^{-\Delta\Delta Ct}$. ΔCt values were calculated by subtracting the Ct value for *POU5F1* from the Ct value for *YWHAG* in each treatment. The ΔCt value for the non-injected treatment group (without α-amanitin) was used as the calibrator to derive the ΔΔCt values. Depicted in this graph are $2^{-\Delta\Delta Ct}$ values. The results shown here are the average of three independent biological replicates; bars represent standard deviation. Different superscripts reflect statistical differences ($p<0.05$).

Table 1. Knockdown of SNF5 reduces porcine embryo developmental potential in vitro

Treatment	Number (%) of embryos at the blastocyst stage	Average nuclei number per embryo*	Average nuclei number per blastocyst	N
SNF5 siRNA	3 (0.7%)[a]	1.7[a]	21[a]	411
control siRNA	72 (16.7%)[b]	7.6[b]	32[b]	430
Non-injected	67 (16.4%)[b]	7.8[b]	31[b]	409

*All embryos were included in the analysis; degenerated embryos were considered as having zero nuclei for the purpose of determining nuclei number. Superscripts indicate differences at $p<0.05$.

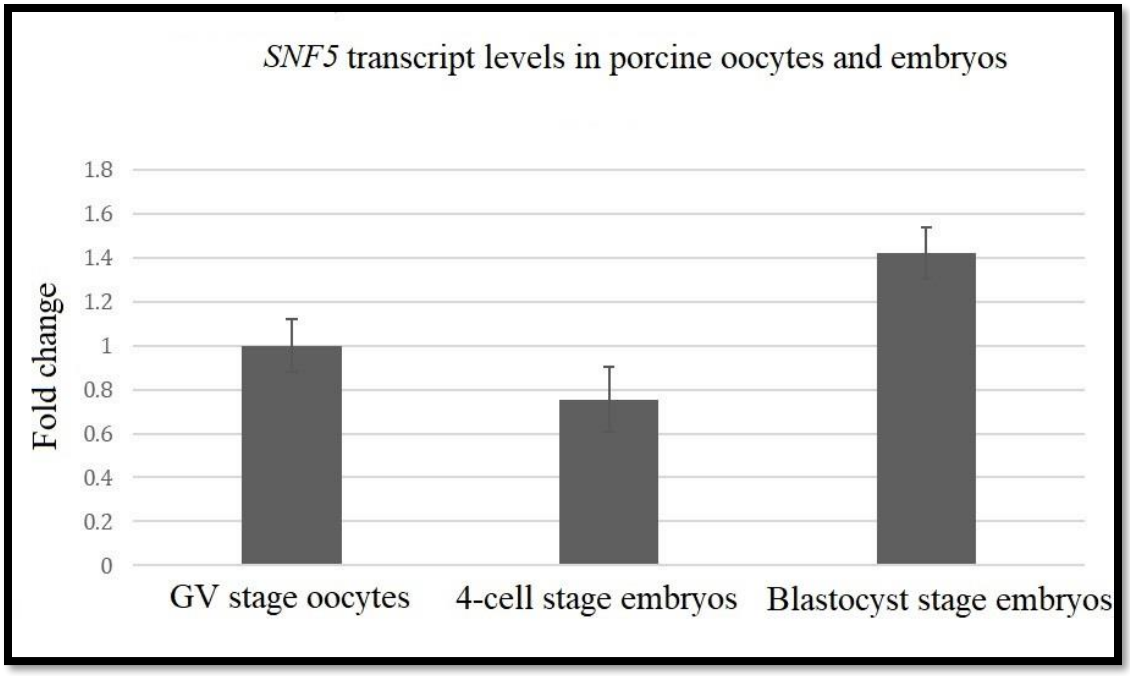

Figure 1. Relative abundance of *SNF5* transcript levels do not differ between porcine oocytes, 4-cell stage embryos, or blastocyst stage embryos. Fold differences were calculated using GV-stage oocytes as the calibrator. The results shown here are the average of three independent experimental replicates. Bars represent standard deviation.

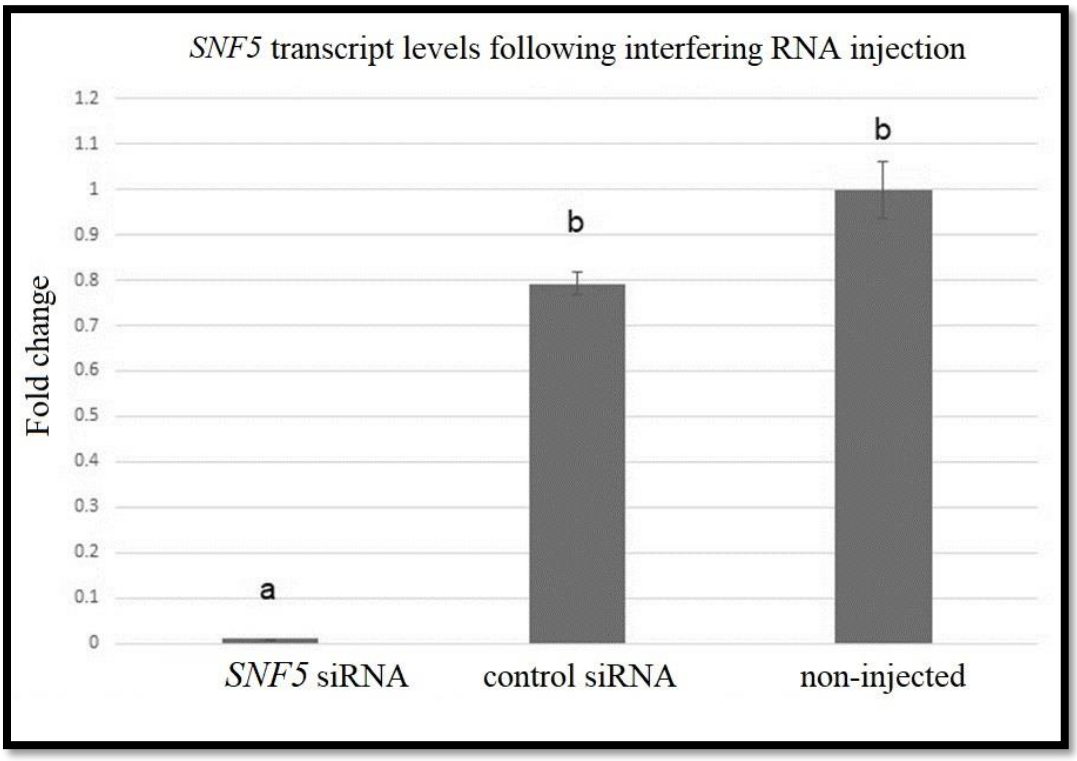

Figure 2. Validation of RNA interference-mediated knockdown of *SNF5* transcripts in porcine oocytes. Quantitative PCR results of GV-stage oocytes 30 hours after injection of interfering RNAs targeting *SNF5*. ΔCt values were calculated by subtracting the Ct value for *SNF5* from the Ct value for *YWHAG* in each treatment. The ΔCt value for the non-injected treatment group was used as the calibrator to derive the ΔΔCt values. Depicted in this graph are $2^{-\Delta\Delta Ct}$ values. The average of two independent experimental replicates is shown; error bars represent standard deviation. Different superscripts reflect statistical differences ($p<0.05$).

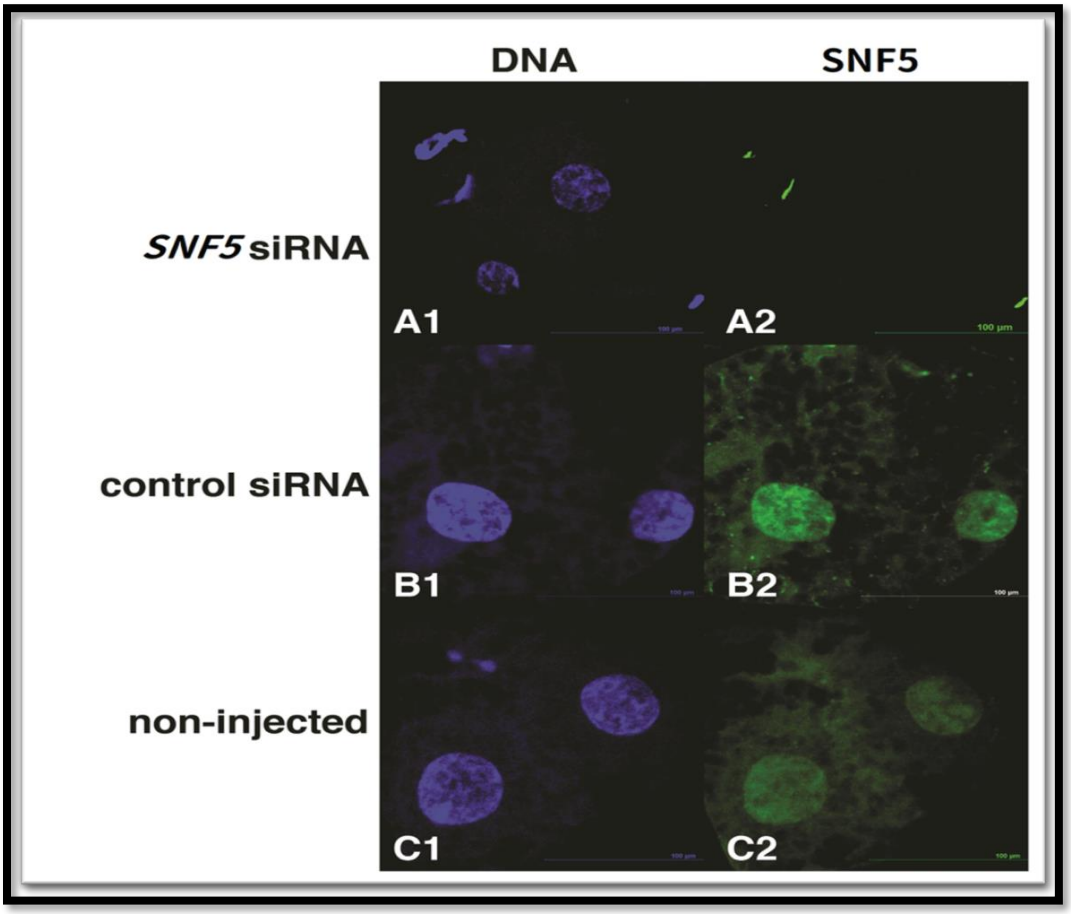

Figure 3. Representative images of pronuclear stage embryos 20 hours after SNF5 interfering RNA injection. Panels A contain representative images of a pronuclear stage embryo injected with *SNF5* interfering RNAs (*SNF5* siRNA); panels B contain representative images of a pronuclear stage embryo injected with control RNAs (control siRNA); panels C contain representative images of a pronuclear stage embryo from the non-injected control group (non-injected). DNA staining is shown in panels 1; panels 2 show the respective staining of SNF5.

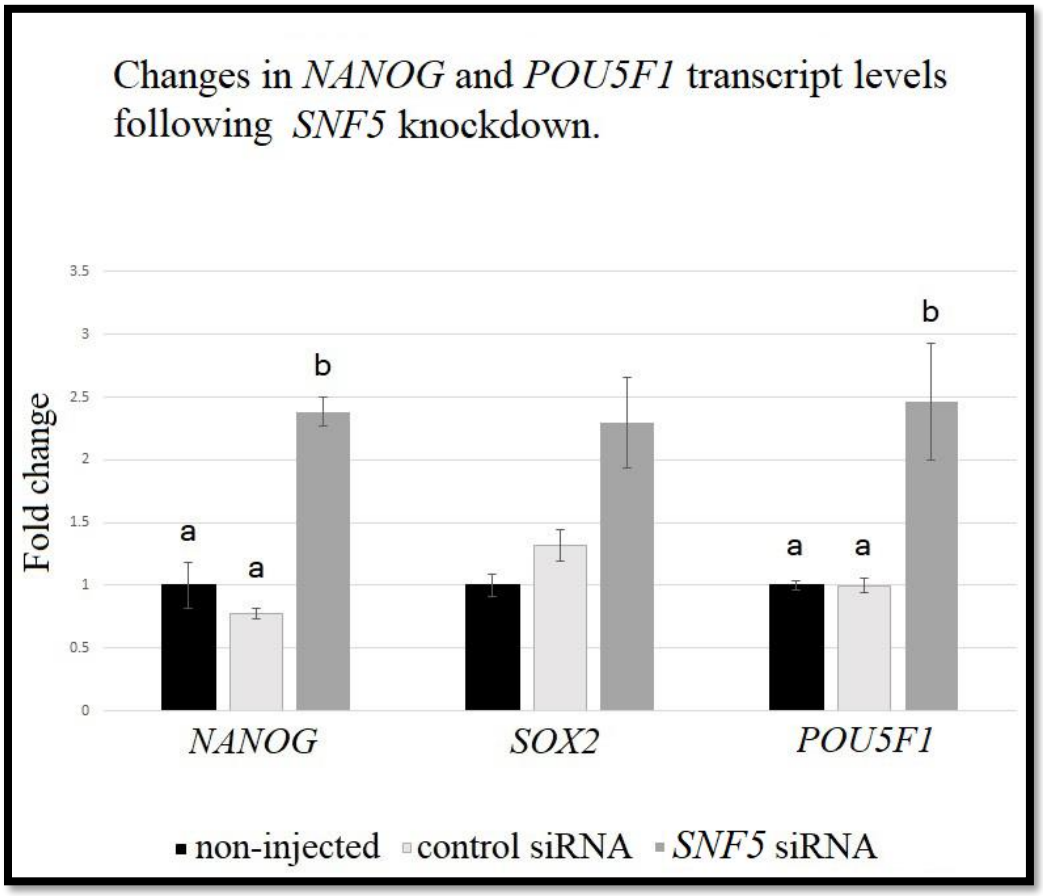

Figure 4. Relative abundance of *NANOG* and *POU5F1* is increased in porcine embryos 20 hours after injection of *SNF5* interfering RNAs (*SNF5* siRNA) as compared to controls (control siRNA and non-injected). Fold changes were calculated using the formula $2^{-\Delta\Delta Ct}$. ΔCt values were calculated by subtracting the Ct value for either *NANOG, POU5F1,* or *SOX2* from the Ct value for *YWHAG* in each treatment. The ΔCt value for the non-injected treatment group was used as the calibrator to derive the ΔΔCt values. Depicted in this graph are $2^{-\Delta\Delta Ct}$ values. The results shown here are the average of four independent biological replicates; bars represent standard deviation. Different superscripts reflect statistical differences ($p<0.05$).

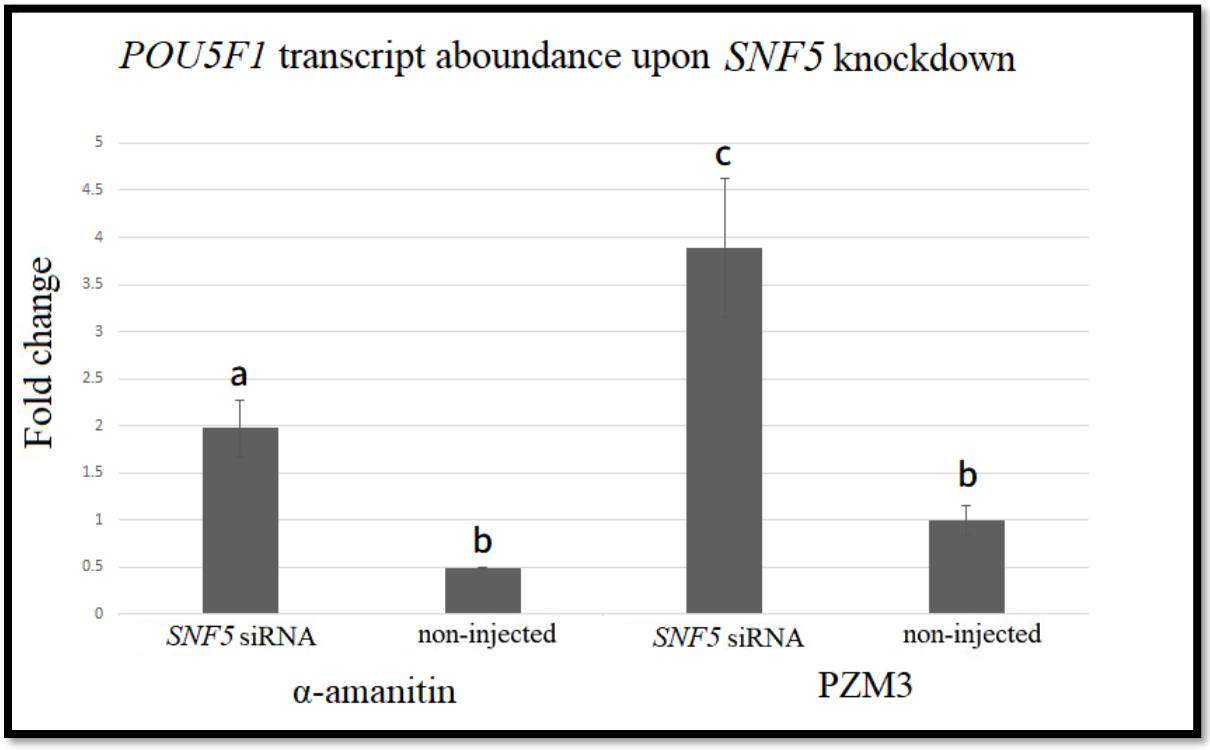

Figure 5. Relative abundance of *POU5F1* transcript abundance is significantly decreased in porcine embryos injected with *SNF5* interfering RNAs cultured in the presence of 20μM α-amanitin (*SNF5* siRNA + α-amanitin), as compared to embryos injected with *SNF5* interfering RNAs cultured and cultured in control medium (a vs b, $p<0.05$). *POU5F1* transcript abundance between non-injected embryos cultured in either the presence or absence of α-amanitin did not differ significantly from one another; however both groups possessed a significantly lower level of *POU5F1* transcripts as compared to *SNF5* siRNA cultured in control medium. Fold changes were calculated using the formula $2^{-\Delta\Delta Ct}$. ΔCt values were calculated by subtracting the Ct value for *POU5F1* from the Ct value for *YWHAG* in each treatment. The ΔCt value for the non-injected treatment group (without α-amanitin) was used as the calibrator to derive the ΔΔCt values. Depicted in this graph are $2^{-\Delta\Delta Ct}$ values. The results shown here are the average of three independent biological replicates; bars represent standard deviation. Different superscripts reflect statistical differences ($p<0.05$).

3.5 Discussion

Precise control over gene expression is central to ensuring successful embryo development. The experiments presented here were designed to examine the role of SNF5, a core subunit of the SWI/SNF chromatin remodeling complexes, in porcine oocytes and cleavage stage embryos. Based on previously published work in the mouse (Guidi *et al*., 2001; Klochendler-Yeivin *et al*., 2000), which showed that *SNF5* null embryos died between E3.5 and E5.5, we hypothesized that *SNF5* was required for cleavage development in the porcine embryo, and that alterations in SNF5 abundance would lead to changes in gene expression.

We found the transcript abundance of *SNF5* did not change significantly during the course of development from immature GV-stage oocyte to blastocyst stage embryo (Figure 1). This observation is not entirely unexpected. SNF5 is a core component of many SWI/SNF complexes, stable *SNF5* transcript levels during this timeframe likely reflect a global need for this SWI/SNF component during this developmental window. *SMARCA4* (*BRG1*) transcript levels have also been found to remain unchanged over the course of this same developmental timeframe (Magnani and Cabot, 2009). In contrast, transcripts encoding additional SWI/SNF subunits display significant changes in transcript abundance across this developmental timeframe. For instance, *ARID1A* transcripts are decreased 11-fold at the 4-cell stage of porcine embryo development (which coincides with timing of zygotic genome activation in the pig embryo) as compared to levels found in GV-stage oocytes. This decrease in *ARID1A* appears transient as levels in blastocyst stage embryos do not differ from those found in GV-stage oocytes (Tseng *et al*., 2017). In addition, transcripts encoding *SMARCA2* (*BRM*) have been shown to be significantly lower in blastocyst stage porcine embryos as compared to levels found in GV-stage oocytes (Magnani and Cabot, 2009).

Our RNAi-mediated knockdown experiments indicate that SNF5 plays a critical role in embryo development prior to zygotic genome activation. Not only did we find a significant reduction in cell number in *SNF5*-depleted embryos seven days after fertilization and a significant reduction in the proportion of *SNF5*-depleted embryos that formed morphological blastocyst stage embryos (Table 1), the vast majority of *SNF5*-depleted embryos ceased development prior to cleavage. Although the disruption in embryonic development appears to occur earlier in the porcine embryo

than what has been reported in *SNF5*-knockout mice (Guidi *et al*., 2000; Klochendler-Yeivin *et al*., 2000), it is important to keep in mind that the ablation approaches used in these studies differ. While the knockout mice will lack any zygotic *SNF5*, maternal stores of *SNF5* transcript may enable embryos to proceed to a later stage of development than the RNAi-mediated knockdown employed in our assay. *SNF5* transcripts are reported to be present in the murine oocyte and zygotic *SNF5* begins to be synthesized during the 4-cell stage in mice (Klochendler-Yeivin *et al*., 2000).

Depletion of SNF5 could lead to the changes in overall SWI/SNF complex stability *in vivo*. Work published by Sohn and colleagues (Sohn *et al*., 2007). has shown that depletion of a SWI/SNF scaffolding subunit, Swi3-related gene (Srg3), leads to rapid depletion of SNF5 and SMARCA4 protein. While not tested in our studies, the report by Sohn and colleagues indicate the half-life of SNF5 may be on the order of 1-2 hours (Sohn *et al*., 2007).

In an attempt to ascertain how depletion of *SNF5* at the pronuclear stage leads to an abrupt impact on development, we determined how transcript levels for *NANOG*, *SOX2*, and *POU5F1* differed 20 hours after treatment began. *SNF5* knockdown in murine ES cells has been shown to lead to an upregulation of *Pou5f1* expression (You *et al*., 2013). We found a 2-fold increase in the relative transcript abundance of both *NANOG* and *POU5F1* in the *SNF5*-depleted embryos as compared to controls (*SNF5* siRNA vs control siRNA and non-injected, $p<0.05$; Figure 4). The changes in *POU5F1* and *NANOG* transcript levels we identified are in line with what has been determined to occur with regard to Nanog and Pou5F1 protein levels in murine ES cells (You *et al*., 2013).

We next wanted to determine if the change in POU5F1 transcript abundance was due to a change in mRNA synthesis upon SNF5 knock-down. Presumptive zygotes were either injected with SNF5 interfering RNAs, or left non-injected. These two groups of embryos were then cultured in the presence or absence of the RNA polymerase II inhibitor, α-amanitin, in a 2 x 2 factorial treatment arrangement. *POU5F1* transcripts were found to be in lower abundance in SNF5-knockdown embryos treated with α-amanitin as compared to SNF5-knockdown embryos in control medium (Figure 5) This demonstrates that the increase in transcription observed in SNF5-knockdown embryos is due, in part, to *de novo* transcription at the pronuclear stage. The observation that

SNF5-knockdown embryos (both those cultured in the presence of α-amanitin or control medium) both had significantly higher transcript abundance of *POU5F1* transcripts as compared to the non-injected controls (Figure 5), we hypothesize a second mechanism contributes to the observed increase in *POU5F1* transcripts in pronuclear stage embryos upon SNF5 knockdown. Although not tested directly, it is possible the loss of SNF5 also alters transcript stability, or alters polyadenylation POU5F1 transcripts.

In their work, You and colleagues (You *et al*., 2013) revealed that *SNF5* interacts with promoter regions of *Pou5f1* and *Nanog* and that depletion of *SNF5* using an RNA interference approach resulted in increased *Pou5f1* and *Nanog* levels in comparison to controls. A major difference between the findings reported by You and colleagues and our present work is the timeline post-RNAi. In the murine ES cell model, Nanog and Pou5f1 levels were assessed at the protein level at least 72 hours post knockdown; our work examined transcript levels only 20 hours post-RNAi induction.

Reports that characterized the novel SWI/SNF complexes that lack SNF5 (e.g., the GBAF complex) have shown that ablation or alteration in the abundance of a given SWI/SNF subunit can impact the stoichiometry of SWI/SNF complexes (Alpsoy and Dykhuizen, 2018). BAF and GBAF complexes interact with different factors and localize to distinct genomic loci. Greater occupancy of POU5F1, SOX2, and NANOG has been found with BAF sites than with GBAF sites; there is also an enrichment in POU5F1, SOX2, NANOG motifs with BAF sites, as compared to GBAF sites (Gatchalian *et al*., 2018). Together, these findings suggest that depletion of SNF5 could also disrupt the stoichiometry of both BAF and PBAF complexes, thereby enabling the formation of excess non-canonical SWI/SNF complexes with unique binding properties that ultimately impact transcription.

In summary, the collective data presented here demonstrate that *SNF5* is required for porcine embryo development. These data further our understanding of the roles served by SWI/SNF chromatin remodeling complexes during porcine embryogenesis.

3.6 References

Abeydeera LR, Day BN. 1997. Fertilization and subsequent development *in vitro* of pig oocytes inseminated in a modified Tris-buffered medium with frozen–thawed ejaculated spermatozoa. Biol Reprod 57:729-734.

Abeydeera LR, Wang WH, Prather RS, Day BN. 1998. Maturation *in vitro* of pig oocytes in protein-free media: fertilization and subsequent embryo development *in vitro*. Biol Reprod 58: 1316-1320.

Alpsoy A, Dykhuizen EC. 2018. Glioma tumor suppressor candidate region gene 1 (GLTSCR1) and its paralog GLTSCR1-like form SWI/SNF chromatin remodeling subcomplexes. J Biol Chem 293:3892-3903.

Anderson JE, Matteri RL, Abeydeera LR, Day BN, Prather RS. 1999. Cyclin B1 transcript quantitation over the maternal to zygotic transition in both in vivo- and in vitro-derived 4-cell porcine embryos. Biol Reprod 61:1460-1467.

Bultman SJ, Gebuhr TC, Pan H, Svoboda P, Schultz RM, Magnuson T. 2006. Maternal BRG1 regulates zygotic genome activation in the mouse. Genes Dev 20:1744-1754.

Cabot B, Tseng YC, Crodian JS, Cabot RA. 2017. Differential expression of key subunits of SWI/SNF chromatin remodeling complexes in porcine embryos derived in vitro or in vivo. Mol Reprod Dev 84:1238-1249.

Chambers I, Colby D, Robertson M, Nichols J, Lee S, Tweedie S, Smith A. 2003. Functional expression cloning of Nanog, a pluripotency sustaining factor in embryonic stem cells. Cell 113: 643-655.

Clapier CR, Cairns BR. 2009. The biology of chromatin remodeling complexes Annu Rev Biochem 78:273-304.

Davis DL. 1985. Culture and storage of pig embryos. J Reprod Fertil Suppl 33:115-124.

Euskirchen G, Auerbach RK, Snyder M. 2012. SWI/SNF chromatin-remodeling factors: multiscale analyses and diverse functions. J Biol Chem 287:30897-30905.

Fukumoto T, Magno E, Zhang R. 2018. SWI/SNF Complexes in Ovarian Cancer: Mechanistic Insights and Therapeutic Implications. Mol Cancer Res 16:1819-1825.

Fulka J, Fulka H, Slavik T, Okada K. 2006. DNA methylation pattern in pig in vivo produced embryos. Histochem Cell Biol 126:213-217.

Gatchalian J, Malik S, Ho J, Lee DS, Kelso TWR, Shokhirev MN. 2018. A non-canonical BRD9-containing BAF chromatin remodeling comples regulates naïve pluripotency in mouse embryonic stem cells. Nat Commun 9:5139.

Glanzner WG, Wachter A, Coutinho ARS, Albornoz MS, Duggavathi R, GonÇAlves PB. 2017. Altered expression of BRG1 and histone demethylases, and aberrant H3K4 methylation in less developmentally competent embryos at the time of embryonic genome activation. Mol Reprod Dev 84:19-29.

Guidi CJ, Sands AT, Zambrowicz BP, Turner TK, Demers DA, Webster W, Smith TW. 2001. Disruption of Ini1 leads to peri-implantation lethality and tumorigenesis in mice. Mol Cell Biol 10:3598-3603.

Hochedlinger K, Plath K. 2009. Epigenetic reprogramming and induced pluripotency. Development 136:509-523.

Isakoff MS, Sansam CG, Tamayo P, Subramanian A, Evans JA, Fillmore CM. 2005. Inactivation of the Snf5 tumor suppressor stimulates cell cycle progression and cooperates with p53 loss in oncogenic transformation. Proc Natl Acad Sci USA 102:17745-17750.

Klochendler-Yeivin A, Fiette L, Barra J, Muchardt C, Babinet C, Yaniv M. 2000. The murine SNF5/INI1 chromatin remodeling factor is essential for embryonic development and tumor suppression. EMBO Rep 1:500-506.

Kumar BM, Jin HF, Kim JG, Ock SA, Hong Y, Balasubramanian S. 2007. Differential gene expression patterns in porcine nuclear transfer embryos reconstructed with fetal fibroblasts and mesenchymal stem cells. Dev Dyn 236:435-446.

Kuwahara Y, Wei D, Durand J, Weissman BE. 2013. SNF5 reexpression in malignant rhabdoid tumors regulates transcription of target genes by recruitment of SWI/SNF complexes and RNAPII to the transcription start site of their promoters. Mol Cancer Res 11:251-260.

Lonergan P, Rizos D, Gutierrez-Adan A, Fair T, Boland MP. 2003. Effect of culture environment on embryo quality and gene expression-experience from animal studies. Reprod Biomed Online 7:657-663.

Magnani L, Cabot RA. 2008. In vitro and in vivo derived porcine embryos possess similar, but not identical, patterns of Oct4, Nanog and Sox2 mRNA expression during cleavage development. Mol Reprod Dev 75:1726-1735.

Magnani L, Cabot RA. 2009. Manipulation of SMARCA2 and SMARCA4 transcript levels in porcine embryos differentially alters development and expression of SMARCA1, SOX2, NANOG, and EIF1. Reproduction 137:23-33.

Mitsui K, Tokuzawa Y, Itoh H, Segawa K, Murakami M, Takahashi K. 2003. The homeoprotein Nanog is required for maintenance of pluripotency in mouse epiblast and ES cells. Cell 113:631-642.

Monk M, Boubelik M, Lehnert S. 1987. Temporal and regional changes in DNA methylation in the embryonic, extraembryonic and germ cell lineages during mouse embryo development. Development 99:371-382.

Nichols J, Zevnik B, Anastassiadis K, Niwa H, Klewe-Nebenius D, Chambers I. 1998. Formation of pluripotent stem cells in the mammalian embryo depends on the POU transcription factor Oct4. Cell 95:379-391.

Nie Z, Yan Z, Chen EH, Sechi S, Ling C. 2003. Novel SWI/SNF chromatin-remodeling complexes contain a mixed-lineage leukemia chromosomal translocation partner. Mol Cell Biol 23:2942–2952.

Niwa H, Miyazaki J, Smith AG. 2000. Quantitative expression of Oct-3/4 defines differentiation, dedifferentiation or self-renewal of ES cells. Nat Genet 24:372 -376.

Peterson CL, Dingwall A, Scott MP. 1994. Five SWI/SNF gene products are components of a large multisubunit complex required for transcriptional enhancement.
Proc Natl Acad Sci USA 91:2905-2908.

Prather RS, Rickords LF. 1992. Developmental regulation of a snRNP core protein epitope during pig embryogenesis and after nuclear transfer for cloning. Mol Reprod Dev 33:119-123.

Roberts CW, Biegel JA. 2009. The role of SMARCB1/INI1 in development of rhabdoid tumor. Cancer Biol Ther 8:412-416.

Roberts CW, Galusha SA, McMenamin ME, Fletcher CD, Orkin SH. 2000. Haploinsufficiency of Snf5 (integrase interactor 1) predisposes to malignant rhabdoid tumors in mice. Proc Natl Acad Sci USA 97:13796–13800.

Roberts CW, Leroux MM, Fleming MD, Orkin SH. 2002. Highly penetrant, rapid tumorigenesis through conditional inversion of the tumor suppressor gene Snf5. Cancer Cell 2:415-425.

Singh AP, Foley JF, Rubino M, Boyle MC, Tandon A, Shah R. 2016. Brg1 enables rapid growth of the early embryo by suppressing genes that regulate apoptosis and cell growth arrest. Mol Cell Biol 36:1990-2010.
Sohn DH, Lee KY, Lee C, Oh J, Chung H, Jeon SH. 2007. SRG3 interacts directly with the major components of the SWI/SNF chromatin remodeling complex and protects them from proteasomal degradation. J Biol Chem 282:10614-10624.

Teif VB, Rippe K. 2009. Predicting nucleosome positions on the DNA: combining intrinsic sequence preferences and remodeler activities. Nucleic Acids 37:5641–5655.

Telford NA, Watson AJ, Schultz GA. 1990. Transition from maternal to embryonic control in early mammalian development: a comparison of several species. Mol Reprod Dev 26:90-100.

Tseng YC, Cabot B, Cabot RA. 2017. ARID1A, a component of SWI/SNF chromatin remodeling complexes, is required for porcine embryo development. Mol Reprod 84:1250-1256.

Whitworth KM, Agca C, Kim JG, Patel RV, Springer GK, Bivens N. 2005. Transcriptional profiling of pig embryogenesis by using a 15K member unigene set specific for pig reproductive tissues and embryos. Biol Reprod 72:1437-1451.

Yoshioka K, Suzuki C, Tanaka A, Anas IM, Iwamura S. 2002. Birth of piglets derived from porcine zygotes cultured in a chemically defined medium. Biol Reprod 66:112-119.

You JS, De Carvalho DD, Dai C, Liu M, Pandiyan K, Zhou, XJ. 2013. SNF5 is an essential executor of epigenetic regulation during differentiation. PLoS Genetics 9:1003459.

Yuan Y, Spate LD, Redel BK, Tian Y, Zhou J, Prather RS. 2017. Quadrupling efficiency in production of genetically modified pigs through improved oocyte maturation. Proc Natl Acad Sci USA 114: 5796-5804.

Zhang X, Li B, Li W, Ma L, Zheng D, Li L. 2014. Transcriptional repression by the BRG1-SWI/SNF complex affects the pluripotency of human embryonic stem cells. Stem Cell Reports 3:460-474.

CHAPTER 4. DISRUPTION OF BRD7, A SWI/SNF CHROMATIN REMODELING COMPLEX SUBUNIT ALTERS THE DEVELOPMENT OF CLEAVAGE STAGE PORCINE EMBRYOS

4.1 Abstract

The objective was to determine the developmental requirements of a PBAF SWI/SNF chromatin remodeling complexes-specific subunit of BRD7. SWI/SNF chromatin remodeling complexes are large multi-subunits complexes; the unique collection of subunits characterize the activities of a given SWI/SNF complex. BRD7 is required for cleavage development and disruption of BRD7 will lead to abnormality during cleavage development in the porcine embryo. An RNA interference was employed to determine the developmental requirements of BRD7 in porcine embryos. Our findings indicate that BRD7 depletion reduces preimplantation porcine embryo developmental competency.

4.2 Introduction

In sexual reproductions, two gametes forming the zygote upon fertilization and the zygote develops into a new individual. The dynamic regulation of gene expression during preimplantation allows fertilized oocyte undergoes cleavage divisions, develops into a morula, and then completes the first cell differentiation to form the blastocyst with two distinct cell linages, the trophectoderm (TE) and the inner cell mass (ICM). Several events have been characterized as milestones during this cleavage developmental period, including zygotic genome activation and formation of blastocyst (Marcho *et al*., 2015). It is critical to establish the proper epigenetic statues to accomplish these tasks.

Epigenetics is considered as the study of heritable changes in gene expression without alteration in the DNA sequence. To regulate transcription, different modifications are employed to restructure the chromatin and nucleosome so that the transcriptional machinery can access to the DNA (Waddington, 1942). Epigenetic modifications can be classified into covalent and non-covalent. DNA methylation, histone methylation and histone acetylation are well-known covalent modifications. The non-covalent modification is carried out by a group of enzymes named

chromatin remodeling complexes (Bird, 1986). It has been evidenced that both covalent and non-covalent modification are required for preimplantation embryo development. The parental genomes are globally demethylated right after fertilization and followed by lineage-specific reacquisition of methylation; ablation of methyltransferases leads to embryo lethality (Li *et al*., 1992; Mayer *et al*., 2000; Sanz *et al*., 2010; Cantone and Fisher, 2013). Transcriptional activation directed by acetylation on core histones have been observed in two-cell stage mouse embryo which reflects the zygotic genome activation (Wiekowski *et al*., 1997).

The SWI/SNF (SWItch/Sucrose Non-Fermentable) family of chromatin remodeling complexes are evolutionarily conserved in eukaryotes. These complexes are composed of multi-protein subunits and carry out the no-covalent epigenetic modifications. BRM (Brahma) and BRG-1 (Brahma-related gene-1) are ATPases catalytic subunits which hydrolyze ATP to restructure nucleosomes thereby increase DNA accessible during transcription (Stern *et al*., 1984; Cairns *et al*., 1994). A series of BAFs (BRG1 associated factors) associate with either BRM or BRG1 to create a functional SWI/SNF chromatin-remodeling complex. Which BAFs and catalytic subunit decide the identity of a given SWI/SNF complex and dictate where that complex will act (Cairns *et al*., 1994). In human, the complexes can be characterized into BAF and PBAF (Polybromo-associated BAF) biochemically and genetically. The BAF complex have either hBRM (human Brahma) or BRG1 as its catalytic subunit meanwhile PBAF only contains BRG1 as the ATPase. BAF and PBAF share the same core components, including BAF47, BAF53, BAF57, BAF155, BAF170 and actin. ARID2, BAF45D, and BRD7 are only identified in PBAF while ARID1, BCL7, and BCL11 belong to BAF (Phelan *et al.*, 1999). Some SWI/SNF complexes are unique to specific cell types, including pnBAF, esBAF, and nBAF (found in neural progenitor cells, embryonic stem cells, and neurons, respectfully) (Lessard *et al*., 2007; Ho *et al*., 2009; Sokpor *et al*., 2017).

SWI/SNF chromatin remodeling complexes are critical during embryo development. Mice knockout studies evidence the necessary of these complexes in embryos. Although depletion of Brg1, Baf47, Baf57 and Baf155 in mice embryo lead to embryo lethality, the phenotypes are different (Bultman *et al*., 2000; Klochendler-Yeivin *et al*., 2000; Wang *et al*., 2005; Ho *et al*., 2019). For example, BRG1 null mice embryos die before implantation with morphologically normal blastocyst phenotype but they failed to hatch from zona pellucidae and cannot finish

implantation meanwhile the BAF47 null embryos fail to differentiate into trophoblast therefore cannot develop into blastocyst (Bultman *et al*., 2000; Klochendler-Yeivin *et al*., 2000).

BRD7 (Bromodomain-containing protein 7) is in bromodomain-containing protein family and is first identified as a tumor suppressor that inhibits the growth of nasopharyngeal carcinoma cell growth by down regulating the ERK pathways (Peng *et al*., 2007; *Yu et al*., 2016). This BAF subunit can be found in all PBAF and has a hydrophobic domain that binds to methylated and acetylated lysine residues. The modified lysine residues can be found on histone tails. Tae and his colleagues have found that BRD7 is localized with PRMT5 and PRC2 on suppressor of tumorigenecity 7 (ST7) and retinoblastoma-like protein 2 (RBL2) promoters in β cell lines and assists the methylation of H3R8, H4R3 and H3K27 on the target genes. (Nagy and Tora, 2007; Tae *et al*., 2011). In addition, BRD7 is also important to maintain normal biological function for individuals. For example, BRD7 have been found to involved in glucose metabolism and insulin signaling pathway; BRD7 deficiency can causes type 2 diabetes (Park *et al*., 2014).

The most well-studied BRD7 function is related to its inhibitory function in terms of cell cycle and cell growth. BRD7 downregulates the promoter activity of E2F3, a gene required for cell cycle proceeds (Zhou *et al*., 2006). BRD7 is expressed in many tissues, including organs, brain, skin, reproductive tracts, and immune system (Zhou *et al*., 2004; Drost *et al*., 2010). Evidences indicate that BRD7 mutation leads to cancers and leukemia (Yu *et al*., 2016). BRD7 is required for proper embryo development. In mice study, Brd7 heterozygous embryos are vital with no major defects while Brd7 null embryos are dead without proper limbs, blood vessels and organs at E16.5 (Kim *et al*., 2016). In another conditional Brd7 knockout study in mice, Brd7 is required for spermatogenesis. Brd7 knockout mice are infertile with deformed acrosome, and the spermatogenesis is complete hauled. This study also indicates several DNA repair genes are down regulated upon Brd7 knockout (Wang *et al*., 2016).

Previous works suggest that BRD7 is transported between nuclear and cytoplasm during cleavage development. The shuttling of BRD7 indicates that it may serve a critical role in chromatin remodeling during cleavage (Crodian *et al*., 2019). According to this work, we hypothesize that BRD7 is required for cleavage development and disruption of BRD7 will lead to abnormality

during cleavage development in the porcine embryo. To test our hypothesis, an RNA interference-mediated knockdown assay is performed to determine the developmental requirements of BRD7 in porcine embryos. Our results indicate that the loss of BRD7 deceases development competence of preimplantation porcine embryos significantly. This preliminary data can contribute to our future investigations to BRD7 mediated PBAF function.

4.3 Materials and Methods

Oocyte collection

All Chemicals used in this study were all purchased from Sigma Chemical Company (St. Louis, MO) unless stated otherwise. Prepubertal gilt (*Sus scrofa*) ovaries were provided by a local slaughterhouse and transported to the laboratory in a container filled with 35°C saline. Ovaries were washed with warm saline three times before aspiration. Follicular fluid containing cumulus-oocyte-complexes (COCs) was manually collected by 10-gauge needle and 10 cc sterile syringe from antral follicles (3–5 mm in diameter). COCs with multiple layers of cumulus cells were then selected from the follicular fluid and resuspended in 4-(2-hydroxyethyl)-1-piperazineethanesulphonic acid (HEPES)-buffered medium with 0.01% polyvinyl alcohol (PVA) (Abeydeera et al., 1998). COCs with multiple layers of intact cumulus cells were collected for further experiments in this study. Germinal vesicle (GV)-stage oocytes used in this study were placed in 0.1% hyaluronidase in HEPES-buffered medium and vortexed in medium speed for 8 minutes to denude the oocytes.

In vitro maturation

COCs (70-100) were matured in 500 µl of tissue culture medium 199 (TCM199) supplemented with 0.14% PVA, 10 ng/mL epidermal growth factor, 20 ng/mL insulin-like growth factor 1 (IGF1; Prospec Protein Specialists), 40 ng/mL fibroblast growth factor 2 (FGF2; PeproTech), 20 ng/mL leukaemia inhibitory factor (LIF; MilliporeSigma), 0.57 mM cysteine, 0.5 IU/ml FSH, and 0.5 IU/ml LH (Yuan *et al.,* 2017). COCs were matured at 39°C and 5% CO_2 in air, 100% humidity for 42-44 hours (Abeydeera *et al.,* 1998). Cumulus cells on matured COCs were denuded by vortex for 4 minutes in 0.1% hyaluronidase in HEPES-buffered medium.

In vitro fertilization and embryo culture

Denuded matured oocytes were fertilized with diluted semen in a modified Tris-buffered medium (mTBM) (30 oocytes in 50 µl mTBM droplet) according to a practiced protocol (Abeydeera and Day 1997). Semen used in this study was provided from Purdue's Animal Science Research and Educational Center. The boar was selected and proven fertility. The fresh collected semen was extended in a commercial semen extender (EnduraGuard Plus; Mofa Global, Verona, WI) and stored at 18°C for up to three days. The procedure of sperm preparation for *in vitro* fertilization has been established in our lab. Briefly, 1 mL of extended semen was gently mixed with 9 ml of prewarmed Dulbecco's phosphate buffered Saline (DPBS) containing 1 mg/ml BSA and centrifuged at 900xg in room temperature for 4 minutes, three times. The sperm pellet was resuspended with mTBM. 50 µl of sperm suspension were added into mTBM droplets to a final concentration of 5×10^5 spermatozoa /mL; after 5 hours of incubation at 39°C and 5% CO_2, mixed gametes were washed and transferred to the embryo culture medium, Porcine Zygote Medium 3 (PZM3) (Yoshioka *et al.,* 2002), supplemented with 3 mg/ml fatty acid-free bovine serum albumin (BSA) at 39°C, 5% CO_2 and 100% humidity for 48 hours and 7 days in order to collect 4-cell stage and blastocyst stage embryos.

RNA interference

The BLOCK-iT™ RNAi Designer software (Invitrogen) was employed to design *BRD7* siRNA based on the full-length porcine *BRD7* open reading frame (XM_013992001). Custom made Stealth™ double stranded RNAi nucleotides targeting porcine *BRD7* were 5'-CAAAUGAUUUCAGCAUCCAUGAGUU and 5'- AACUCAUGGAUGCUGAAAUCAUUUG. The scrambled version of nonsense Stealth™ siRNA nucleotides, 5'-CAAUUAGGACUCUACGUACAUAGUU and 5'- AACUAUGUACGUAGAGUCCUAAUUG was used as control. All siRNA nucleotides acquired were aliquoted and diluted in DEPC treated water and stored at –20°C. The final concentration of siRNA used in this study was 1 µM.

Microinjection

Five hours after *in vitro* fertilization, Sperm were removed from presumptive zygotes by vortexing embryos in 0.1% hyaluronidase in HEPES-buffered medium for 4 minutes. Presumptive zygotes were then assigned to three treatments: *BRD7* siRNA injected, nonsense siRNA injected, and non-

injected controls. All embryos were placed in HEPES-buffered medium containing 3mg/ml BSA before the microinjection was performed. 5μl of 1μM siRNA were loaded into the Injection pipette and a Femtojet microinjector (Eppendorf, Hauppauge, NY, USA) was employed to perform microinjection. Embryos that lysed immediately after microinjection were excluded from analysis and removed. Surviving embryos after microinjection were cultured in PZM3 medium at 39°C and 5% CO_2. A small portion of embryo was removed after 48 hours of culture to determine the effectiveness of knockdown by immunocytochemical staining; the rest embryos were cultured for seven days to determine the developmental competence upon each treatment. Embryos were stained with Hoechst 33342 (5 μg/ml) to visualize nuclei by an epifluorescent microscope and the nuclei counting numbers were collected. An immunocytochemical staining approach was employed to determine changes in BRD7 levels in each treatment group.

Effectiveness of interfering RNAs targeting BRD7

The effectiveness of knockdown *BRD7* transcripts by the designed interfering RNAs was determine by both RT-PCR. Briefly, GV-stage oocytes were used and assigned to one of the treatments: *BRD7* siRNA injected (*BDR7* siRNA), nonsense siRNA injected (control siRNA), and non-injected controls (non-injected). Microinjections were performed and all oocytes were incubated in TCM-199 maturation medium for 30 hours according to the in vitro maturation protocol mentioned above. Messenger RNA was then isolated from intact oocytes from each treatment and RT-PCR was performed to determine *BRD7* transcript abundance. RNA from each treatment was isolated by commercial RNA isolation kit, DYNABEADS RNA Isolation Kit (Invitrogen Corporation, Carlsbad, CA, USA) according to the manufacturer's protocol. All oocytes were washed in HEPES-buffered medium three times, placed in 100 μl DYNABEADS lysis buffer, and gently mixed for 10 minutes at room temperature. The Lysates were stored at -80°C overnight (12-16 hours). Upon thawing, mRNA was isolated, and reverse transcribed in a 20 μl reaction using the iScript kit (Bio-rad, Hercules, CA, USA) according to the manufacturer's protocol (Lonergan *et al.*, 2003).

Quantitative PCR

Primers used to amplify *BRD7* in this experiment were designed from publicly available sequence data in GenBank XM_013992001 and the sequence for *BRD7* primer sets are forward: 5'-

GAAGTCACCGAGCTCTCCAC; and reverse: 5'- GGTCCCGATCTCGCTCTTT, product size is 190 nucleotides. The *BRD7* PCR products were cloned into pENTR^{TM}/SD/D-TOPO vector (Invitrogen, Carlsbad, CA, USA). The amplification efficiency of the primer sets was determined by constructing the standard curve. Briefly, the standard curve for *BRD7* was created by performing RT-PCR with known *BRD7* templates. The curve was used to determine the range of Ct values (threshold cycles) from different primer sets that produced a linear amplification of *BRD7*. Housekeeping gene, *YWHAG* (Genbank accession number CO94522), was used to normalize template input; *YWHAG* has been referenced to transcript stably through cleavage development (Whitworth *et al.*, 2005). The *BRD7* transcription abundance was determined relative to a housekeeping gene, *YWHAG*. *YWHAG* primers were forward: 5'-TCCATCACTGAGGAAAACTGCTAA; and reverse 5'-TTTTTCCAACTCCGTGTTTCTCTA, product size 130 nucleotides (Whitworth *et al.*, 2005).

A PCR master mix was prepared for each gene as follows: 1µl of 5µM forward primer, 1µl of 5µM reverse primer and 3µl of cDNA from each treatment were mix with 10 µl of SybrGreen Master mix (Bio-Rad). For each replicate, cDNA from each treatment oocyte was used to amplify *BRD7* and *YWHAG*; reactions for each biological replicate were performed within the same PCR run and all genes were run in duplicates, and three biological replicates were performed. The MyiQ single color real-time thermal cycler (Bio-Rad) was employed and programed as follow: 5 minutes initial denaturation at 94°C, followed by 45 cycles of 5 seconds at 94°C, 30 seconds at 60°C, and 30 seconds at 72°C. Fluorescence data were collected during the extension step of each cycle; a melting curve was generated to determine each PCR amplicons.

Immunocytochemical staining

48 hours after microinjection, embryos assigned for all treatments in the interfering RNA assay were fixed in 3.7% paraformaldehyde at 4°C for 1 hour following by three washes in phosphate-buffered saline (PBS) containing 0.1% Tween-20 (PBST) (the length of washing step in this immunocytochemical staining procedure was 10 min. for each washing). Fixed embryo were then placed in 1% Triton X-100 in PBS an hour for permeabilization and incubated in blocking solution (0.1 M glycine, 1% goat serum, 0.01% Triton X-100, 1% powdered nonfat dry milk, 0.5% BSA and 0.02% sodium azide in PBS) overnight (12-16 hours) (Prather and Rickords 1992). Embryos

were incubated with primary antibody against BRD7 (Abcam, Cambridge, MA, USA, catalog number cat# ab56036) (1:500 in PBST) at 4°C overnight (12-16 hours). After first antibody incubation, three washes with PBST were performed and embryos were incubated with secondary antibody (goat-anti-rabbit-IgG, fluorescein isothiocyanate (FITC)-conjugated, 1:500; Sigma–Aldrich. St. Louis, MO) in PBST at 4°C overnight (12-16 hours). Embryos were washed with PBST three times again and stained with Hoechst 33342 (5 µg/ml) for 20 minutes. Processed embryos were mounted on slides in Vectashield mounting medium (Vector Laboratories, Inc., Burlingame, CA, USA) and slides were sealed with nail polish. Nikon A1R_MP confocal microscope was employed to examine slides. The florescent signals were checked by laser lines at 408 nm (Hoechst 33342) and 488 nm (FITC). The control groups were included by a subset of embryos from each treatment stained with secondary antibody alone (to control for non-specific binding of secondary antibody) and embryos incubated with no antibodies (to control for background fluorescence).

Statistical analysis

Average nuclei numbers from the *BRD7* knockdown experiment were compared using a two-way ANOVA using GLM procedures to perform multiple comparison of main effect means; treatments and replicates were considered as the main factors. Data pertaining to the percentage of morphological blastocyst stage embryos in the *BRD7* knockdown experiment were subjected to arcsine transformation; transformed values were analyzed with one-way ANOVA and compared by using Tukey's multiple comparison test. A p-value less than 0.05 was considered significant. The relative expression of each gene were calculated from the average Ct values of each duplicate using the $2^{-\triangle\triangle Ct}$ method. The $2^{-\triangle\triangle Ct}$ values were imported and analyzed by one-way ANOVA. Differences were compared using Tukey's multiple comparison test. Treatments were considered as the main factors; a p-value < 0.05 was considered significant.

4.4 Results

Efficiency of BRD7 knockdown by interfering RNAs

Messenger RNA was isolated from oocytes collected from each treatment 30 hours after microinjection. cDNA was synthesized and PCR was performed to determine the relative transcript abundance of *BRD7* in each treatment group. The results indicate that the interfering RNA we

designed was able to target *BRD7* transcript and knock it down significantly. (*BRD7* siRNA vs control siRNA and non-injected, $p<0.05$; Figure 6).

Immunocytochemical staining was employed to identify the level of reduction of BRD7 protein at 4-cell stage porcine embryos. *In vitro* produced porcine embryos were assigned to each treatment, cultured for 48 hours. Antibody against BRD7 was used to visualize BRD7 in cellular components. Our results indicate that BRD7 protein is dramatically reduced in the *BRD7* siRNA group while the other two control groups have normal BRD7 abundance (*BRD7* siRNA n=11 vs control siRNA and non-injected, n=14 and n=8, respectively; Figure 7).

BRD7 knockdown reduces preimplantation porcine embryo development competence significantly

I*n vitro* produced porcine zygotes were assigned for interfering RNA assay targeting BRD7, including three treatments mentioned above. After seven days of embryo culture, all embryos in the same treatment were collected and processed for nuclei counting (n=309, 383 and 309 for *BRD7* siRNA, control siRNA and non-injected, respectively; Table 2). The results indicate that embryos from the *BRD7* siRNA treatment only have average 3.15 nuclei per embryo while other controls reach 5.43 and 5.14 nuclei per embryo (control siRNA and non-injected, respectively; $p<0.05$; Table 2). This reduction is significant. In addition, fewer embryos in the *BRD7* siRNA treatment reach blastocyst stage as compared to controls (3.8% blastocysts for *BRD7* siRNA vs 8.47% and 9.89% blastocysts for control siRNA and non-injected, respectively, $p<0.05$; Table 2). The blastocysts in the *BRD7* siRNA treatment also have significant fewer number of nuclei as compared to the other controls (18.33 nuclei/blastocyst [*BRD7* siRNA] vs 25.78 nuclei/blastocyst [control siRNA] and 22.58 nuclei/blastocyst [non-injected], $p<0.05$; Table 2).

Table 2. Knockdown of BRD7 reduces porcine embryo developmental potential *in vitro*

Treatment	Number (%) of embryos at the blastocyst stage	Average nuclei number per embryo*	Average nuclei number per blastocyst	N
BRD7 siRNA	12 (3.8%)[a]	3.15[a]	18.33[a]	309
control siRNA	30 (8.47%)[b]	5.43[b]	25.78[b]	383
Non-injected	39 (9.89%)[b]	5.14[b]	22.58[b]	309

*All embryos were included in the analysis; degenerated embryos were considered as having zero nuclei for the purpose of determining nuclei number. Superscripts indicate differences at $p<0.05$.

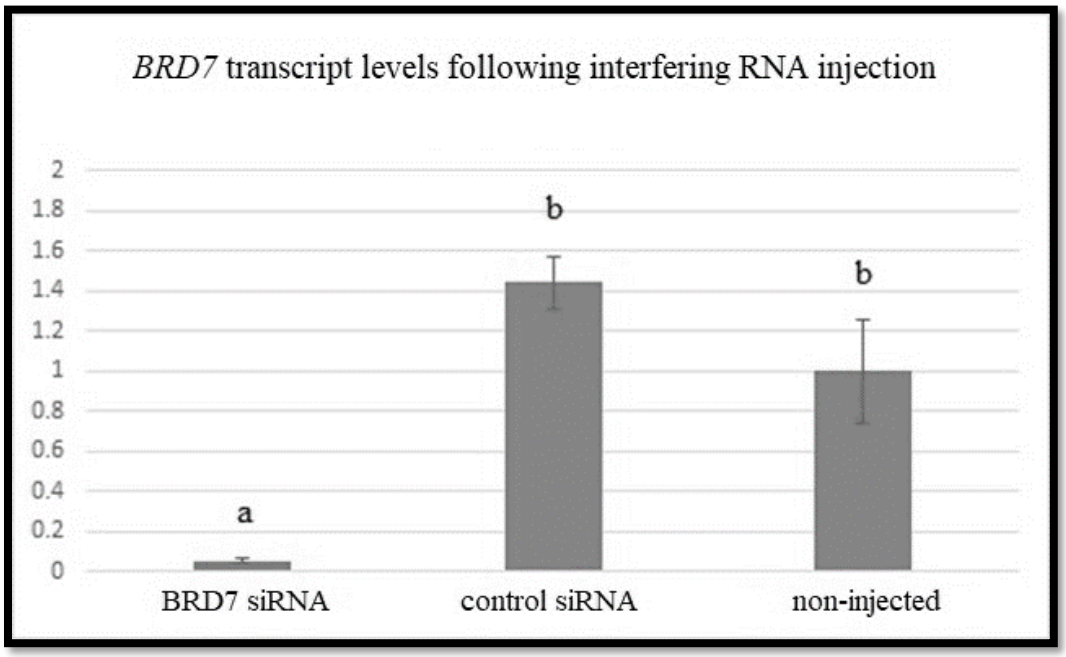

Figure 6. Quantitative PCR results of GV-stage oocytes 30 hours after injection of interfering RNAs targeting *BRD7*. ΔCt values were calculated by subtracting the Ct value for *BRD7* from the Ct value for *YWHAG* in each treatment. The ΔCt value for the non-injected treatment group was used as the calibrator to calculate the ΔΔCt values. Y-axis in this graph represents $2^{-\Delta\Delta Ct}$ values. The average of three independent experimental replicates is shown; error bars represent standard deviation. a, b superscripts denote statistically significant differences ($p<0.05$).

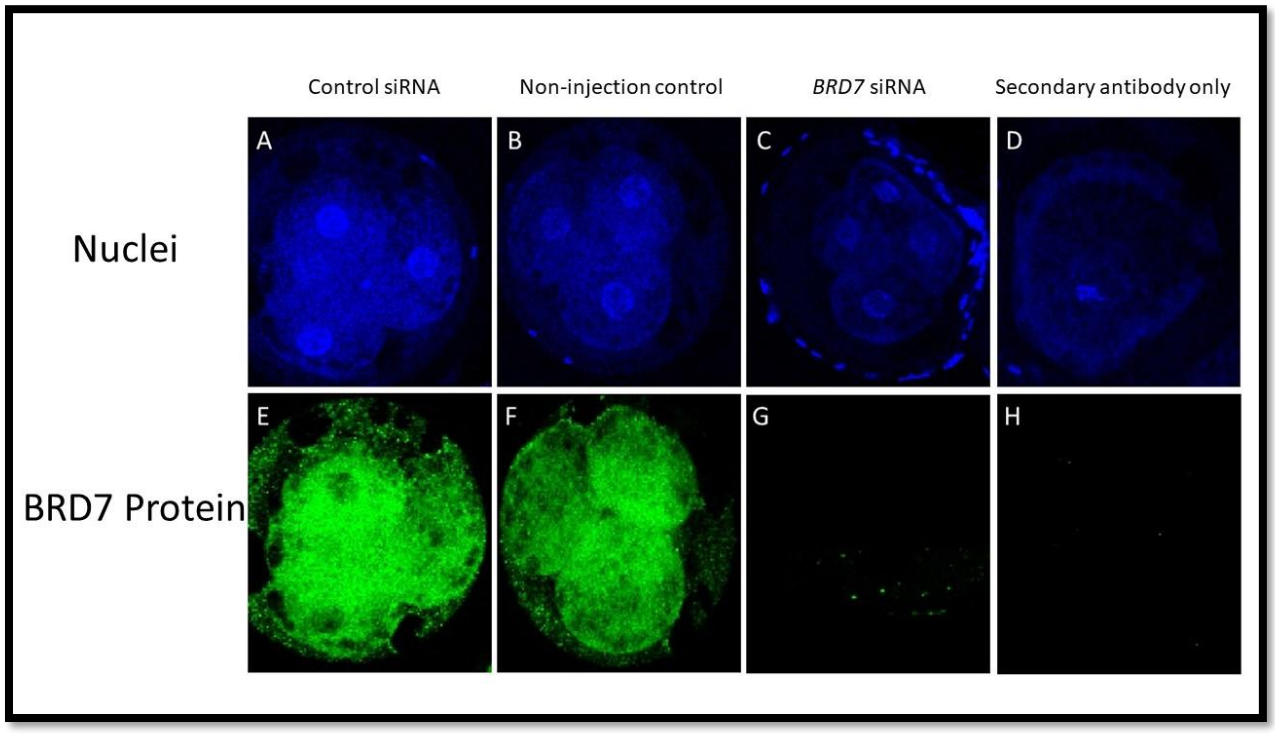

Figure 7. Representative images of 4-cell stage embryos 48 hours after *BRD7* interfering RNA injected. Panels C and G represent the images of a 4-cell stage embryo injected with *BRD7* interfering RNAs (*BRD7* siRNA); panels A and E contain representative images of a 4-cell stage embryo injected with control RNAs (control siRNA); panels B and F are images of a 4-cell stage embryo from the non-injected control group (non-injected); panels D and H are secondary antibody only images. DNA staining are shown in panels A, B, C, and D with blue fluorescence; panels E, F, G and H show the staining of BRD7 in green fluorescence.

4.5 Discussion

A series of dynamic changes happened to the mammalian embryo during the first week of embryo development. After fertilization, protamine bound to the DNA derived from sperm are replaced by histone proteins found in the oocyte cytoplasm (Oliva and Dixon, 1991). The presumptive zygote undergoes cleavage divisions, which involves a series of rapid cell division while the embryo increases the total cell number but not the total cytoplasmic volume. In addition, the embryo relies on stores of mRNAs that found in the oocyte cytoplasm that were produced by the oocyte prior to ovulation to direct embryo development until a species-specific timepoint when the embryo starts to synthesize its own mRNA (Roberts and Graziosi, 1977). This timepoint in development is known as the maternal-to-zygotic transcription transition (MZTT), followed by zygotic genome activation (ZGA) (Newport and Kirschner, 1982; Davidson, 1986). As cleavage divisions continue, the embryo reaches a stage referred to as the morula stage. Compaction takes place during morula stage where blastomeres start to differentiate. Ultimately the embryo reaches what is referred to as the blastocyst stage, a stage at which the embryo develops a fluid filled cavity, known as the blastocoele, in the extracellular space at the center of the embryo (Lo and Gilula, 1979). At this point of development, the first differentiation event has taken place with the formation of the trophectoderm (TE, the outer cells of the blastocyst) which are limited to contributing only to extraembryonic tissues, and the inner cell mass, a cluster of cells at the center of the blastocyst that will ultimately give rise to the fetus (Marcho *et al*., 2015). These processes require precise regulation of gene transcription; chromatin remodeling is an epigenetic modification that is closely linked with transcription regulation.

The ATP-dependent chromatin remodeling complexes can be classified into different families, including INO80, ISWI, CHD and SWI/SNF. The SWI/SNF chromatin remodeling complexes were first identified in yeast and later found to be conserved in all eukaryotes (Stern *et al*., 1984, Sudarsanam and Winston, 2000). The variety functions of SWI/SNF complexes have been reported, including DNA repair, DNA replication, gene splicing, and epigenetic remodeling during cell proliferation and cell differentiation (Hargreaves and Crabtree, 2011). Each SWI/SNF chromatin remodeling complex contains an ATPase, either BRM or BRG1; the ATPase serves at

the catalytic subunit and utilizes the energy from ATP hydrolysis to restructure nucleosomes alter the accessibility of transcriptional machinery to the underlying chromatin (Wang *et al*., 1996).

In addition to the ATPase, nine to fifteen additional subunits known as BAFs interact with the ATPase to create functionally distinct SWI/SNF complexes. SNF5, BAF155, and BAF170 are considered core subunits and conserved in canonical SWI/SNF complexes (including BAF and PBAF). SWI/SNF complexes can be categorized as BAF complexes; BAF complexes contain the subunits ARID1, BCL7, and BCL11. Alternatively PBAF complexes contain ARID2, BAF45D, and BRD7 (Clapier and Cairns, 2009). The GBAF (glioma tumor suppressor candidate region gene 1 [GLTSCR1]) complexes lack the SNF5 subunit (Alpsoy and Dykhuizen, 2018).

BRD7 is expressed in many tissues, including organs, reproductive tracts, and preimplantation embryo (Zhou *et al*., 2004; Drost *et al*., 2010; Cabot *et al*., 2017). The hydrophobic domain on the BRD7 has been suggested binding to the lysine residues. *In vitro* study indicates that BRD7 binds the H3K14ac peptide in vitro and can interact with acetylated proteins (Cong *et al*., 2006). It is also reported that BRD7 co-localizes with PRMT5 and PRC2 on suppressor of several genes in B cell lines and assists the methylation of H3R8, H4R3 and H3K27 on the target genes. (Nagy and Tora, 2007; Tae *et al*., 2011).

BRD7 has been shown to be required for proper embryo development. BRD7 null mouse embryos die at E16.5; these embryos lack proper limb development and have malformations in blood vessels and major organs (Kim *et al*., 2016). Our RNAi-mediated knockdown of BRD7 indicates that BRD7 is required for proper cleavage development in porcine embryos. We find the average cell number in BRD7-depleted embryos is significantly decreased. The proportion of BRD7-depleted embryos that develop into blastocyst is significantly less than control treatments (Table 2). BRD7 is PBAF-specific and it is possible that losing bromodomain can disrupt the function of PBAF (Ho *et al.*, 2019). The reduction of development potential caused by BRD7 depletion in preimplantation embryo may relate to the role of PBAF during early embryo development.

Comparing the results from RNAi-mediated knockdown assays targeting different subunits we had already performed, including SNF5, ARID1A and BRD7. BRD7 knockdown embryos have

reduced development competence phenotype but embryos from ARID1A and SNF5 knockdown have arrested at specific embryonic stage (4-cell stage for ARID1A knockdown and before cleavage for SNF5 knockdown). The similar results can be observed in mouse embryo. Both Arid1a and Snf5 null mouse embryo died around E7 while Brd7 null embryos died at E16.5.
SNF5 is conserved in both PBAF and BAF complexes. Besides the DNA binding ability, SNF5 is critical to interact with other cores in the complex to maintain the correct configuration of the complex. The interaction between SNF5 and the SWIRM domain on BAF155 is required for constructing the structure of a SWI/SNF chromatin remodeling complex (Sen *et al*., 2017; Yan *et al*., 2017). It is understandable that SNF5 depletion results in disruption of genes that regulated by the SNF5 plus the deformed SWI/SNF complexes. The combination of these factors leads to the early embryo lethality while the BRD7 is specific to the less abundant PBAF complexes.

These results indicate that either BRD7 mediated SWI/SNF chromatin remodeling complex action participates in embryo development at much less degree or there are some unknown mechanisms that compensates the losing of BRD7 during preimplantation embryo development.
The functional redundancy of BAFs has been reported in several studies. BRG-1 can compensate the loss of BRM suggesting that BAFs can be functionally redundant (de la Serna *et al*., 2001; Strobeck *et al*., 2002). BRD9, another bromodomain containing protein family has been reported to have similar bromodomain to BRD7(Wang *et al*., 2019; Karim *et al*., 2020). Evidences suggest that both BRD7 and BRD9 recognize and bind to acetylated vitamin D receptor (VDR) in β cells. The binding of BRD9 turns the receptor into an inactive state. The ligand, vitamin D, then binds to BRD7 instead of VDR, which recruits PBAF to restructure chromatin and promote enhancer to response to inflammatory stress (Wei *et al*., 2018). Base on the similarity of bromodomain, BRD7 and BRD9 may share the same function during early embryo development or have uncovered mechanisms to compensate the function for each other. A BRD9 knockdown and BRD7/BRD9 double knockdown assay can be done but the newly discovered GBAF which contains BRD9 as a core subunit can be affected by BRD9 depletion.

Although BRD7 has been generally considered as a tumor suppressor, BRD7 could be a key subunit to reveal the role that BAF complexes, PBAF complexes and GBAF complexes play during preimplantation embryo development. In summary, the collective data presented here

demonstrate that disruption of BRD7 reduces porcine embryo development potential. In addition, the early embryo lethality resulted from ARID1A and SNF5 knockdown indicates the subfamily of SWI/SNF chromatin remodeling complexes, BAF, PBAF may participate in embryo development in different degree. Further investigations need to be done to identify the network of SWI/SNF chromatin remodeling complexes and unique function of each subunit during preimplantation embryo development.

4.6 References

Abeydeera LR, Day BN. 1997. Fertilization and subsequent development in vitro of pig oocytes inseminated in a modified Tris-buffered medium with frozen–thawed ejaculated spermatozoa. Biol Reprod 57:729-734.

Abeydeera LR, Wang WH, Prather RS, Day BN. 1998. Maturation in vitro of pig oocytes in protein-free media: fertilization and subsequent embryo development in vitro. Biol Reprod 58: 1316-1320.

Bird AP. 1986. CpG-rich islands and the function of DNA methylation. Nature 321:209–213.

Bultman S, Gebuhr T, Yee D, La Mantia C, Nicholson J, Gilliam A, Randazzo F, Metzger D, Chambon P, Crabtree G, Magnuson T. 2000. A Brg1 null mutation in the mouse reveals functional differences among mammalian SWI/SNF complexes. Mol Cell 6:1287–1295

Cabot B, Tseng YC, Crodian JS, Cabot R. 2017. Differential expression of key subunits of SWI/SNF chromatin remodeling complexes in porcine embryos derived in vitro or in vivo. Mol Reprod Dev 84(12):1238-1249.

Cairns BR, Kim YJ, Sayre MH, Laurent BC, Kornberg RD. 1994. A multisubunit complex containing the SWI1/ADR6, SWI2/SNF2, SWI3, SNF5, and SNF6 gene products isolated from yeast. Proc Natl Acad Sci USA 91:1950-1954.

Cantone I, Fisher AG. 2013. Epigenetic programming and reprogramming during development. Nat Struct Mol Biol 20:282–289.

Cong P, Jie Z, Ying LH, Ming Z, Li WL, Hong ZQ, Xin YY, Wei X, Rong SS, Ling LX. 2006. The transcriptional regulation role of BRD7 by binding to acetylated histone through bromodomain. J. Cell. Biochem 97:882-892.

Crodian JS, Weldon BM, Tseng YC, Cabot B, Cabot R. 2019. Nuclear trafficking dynamics of Bromodomain-containing protein 7 (BRD7), a switch/sucrose non-fermentable (SWI/SNF) chromatin remodelling complex subunit, in porcine oocytes and cleavage-stage embryos. Reprod Fertil Dev 31(9):1497-1506.

Davidson EH. 1986. Gene Activity in Early Development. Academic Press.

De la Serna IL, Carlson KA, Imbalzano AN. 2001. Mammalian SWI/SNF complexes promote MyoD-mediated muscle differentiation. Nat. Genet 27:187-190.

Drost J, Mantovani F, Tocco F. 2010. BRD7 is a candidate tumour suppressor gene required for p53 function. Nat Cell Biol 12:380-389.

Henery CC, Miranda M, Wiekowski M, Wilmut I, DePamphilis ML. 1995. Repression of gene expression at the beginning of mouse development. Dev Biol 169:448-460.

Hargreaves DC, Crabtree GR. 2011. ATP-dependent chromatin remodeling: genetics, genomics and mechanisms. Cell Res 21:396–420.

Ho L, Ronan JL, Wu J, Staahl BT, Chen L, Kuo A, Lessard J, Nesvizhskii AI, Ranish J, Crabtree GR. 2009. An embryonic stem cell chromatin remodeling complex, esBAF, is essential for embryonic stem cell self-renewal and pluripotency. Proc Natl Acad Sci USA 2009 106(13):5181-5186.

Ho PJ, Lloyd SM, Bao X. 2019. Unwinding chromatin at the right places: how BAF is targeted to specific genomic locations during development. Development 146(19):dev178780.

Karim RM, Chan A, Zhu JY, Schönbrunn E. 2020. Structural Basis of Inhibitor Selectivity in the BRD7/9 Subfamily of Bromodomains. J Med Chem 63(6):3227-3237.

Kim Y, Andrés Salazar Hernández M, Herrema H, Delibasi T, Park SW. 2016. The role of BRD7 in embryo development and glucose metabolism. Journal of cellular and molecular medicine 20(8):1561–1570.

Klochendler-Yeivin A, Fiette L, Barra J, Muchardt C, Babinet C, Yaniv M. 2000. The murine SNF5/INI1 chromatin remodeling factor is essential for embryonic development and tumor suppression. EMBO Rep 1(6):500–506.

Kornberg RD. 1974. Chromatin structure: a repeating unit of histones and DNA. Science 184(4139):868-871.

Lessard J, Wu JI, Ranish JA, Wan M, Winslow MM, Staahl BT, Wu H, Aebersold R, Graef IA, Crabtree GR. 2007. An essential switch in subunit composition of a chromatin remodeling complex during neural development. Neuron 55(2):201-215.

Li E, Bestor TH, Jaenisch R. 1992. Targeted mutation of the DNA methyltransferase gene results in embryonic lethality. Cell 69:915–926.

Lo CW, Gilula NB. 1979. Gap junctional communication in the preimplantation mouse embryo. Cell 18:399–409.

Lonergan P, Rizos D, Gutierrez-Adan A, Fair T, Boland MP. 2003. Effect of culture environment on embryo quality and gene expression-experience from animal studies. Reprod Biomed Online 7:657-663.

Marcho C, Cui W, Mager J. 2015. Epigenetic dynamics during preimplantation development. Reproduction (Cambridge, England), 150(3), R109–R120.

Mayer W, Niveleau A, Walter J, Fundele R, Haaf T. 2000. Demethylation of the zygotic paternal genome. Nature 403:501-502.

Nagy Z, Tora L. 2007. Distinct GCN5/PCAF-containing complexes function as co-activators and are involved in transcription factor and global histone acetylation. Oncogene 26:5341-5357.

Neigeborn L, Carlson M. 1984. Genes affecting the regulation of SUC2 gene expression by glucose repression in Saccharomyces cerevisiae. Genetics 108(4):845–858.

Newport J, Kirschner M. 1982. A major developmental transition in early Xenopus embryos: II. Control of the onset of transcription. Cell 30(3):687-696.

Oliva R, Dixon GH. 1991. Vertebrate protamine genes and the histone-to-protamine replacement reaction. Prog Nucleic Acid Res Mol Biol 40:25-94.

Park SW, Herrema H, Salazar M. 2014. BRD7 regulates XBP1s' activity and glucose homeostasis through its interaction with the regulatory subunits of PI3K. Cell Metab 20:73-84.

Peng C, Liu HY, Zhou M, Zhang LM, Li XL, Shen SR, Li GY. 2007. BRD7 suppresses the growth of Nasopharyngeal Carcinoma cells (HNE1) through negatively regulating beta-catenin and ERK pathways. Mol Cell Biochem 303(1-2):141-149.

Phelan ML, Sif S, Narlikar GJ, Kingston RE. 1999. Reconstitution of a core chromatin remodeling complex from SWI/SNF subunits. Mol Cell 3:247–253.

Prather RS, Rickords LF. 1992. Developmental regulation of a snRNP core protein epitope during pig embryogenesis and after nuclear transfer for cloning. Mol Reprod Dev 33:119-123.

Roberts DB, Graziosi G. 1977. Protein synthesis in the early Drosophila embryo; analysis of the protein species synthesized. J Embryol Exp Morphol 41:101-110.

Sanz LA, Kota SK, Feil R. 2010. Genome-wide DNA demethylation in mammals. Genome biology. 11(3):110.

Sen P, Luo J, Hada A. 2017. Loss of Snf5 Induces Formation of an Aberrant SWI/SNF Complex. Cell Rep 18(9):2135-2147.

Stern M, Jensen R, Herskowitz I. 1984. Five SWI genes are required for expression of the HO gene in yeast. J Mol Biol 178(4):853-868.

Sokpor G, Xie Y, Rosenbusch J, Tuoc T. 2017. Chromatin Remodeling BAF (SWI/SNF) Complexes in Neural Development and Disorders. Front Mol Neurosci 10:243.

Strobeck MW, Reisman DN, Gunawardena RW, Betz BL, Angus SP, Knudsen KE, Kowalik TF, Weissman BE, Knudsen ES. 2002. Compensation of BRG-1 function by Brm: insight into the role of the core SWI-SNF subunits in retinoblastoma tumor suppressor signaling. J. Biol. Chem 277:4782-4789.

Sudarsanam P, Winston F. 2000. The Swi/Snf family nucleosome-remodeling complexes and transcriptional control. Trends Genet 16:345-351.

Tae S, Karkhanis V, Velasco K. 2011. Bromodomain protein 7 interacts with PRMT5 and PRC2 and is involved in transcriptional repression of their target genes. Nucleic Acids Res 39(13):5424-5438.

Waddington CH. 1942. The epigenotype. Int J Epidemiol 41(1):10-13.

Wang W, Côté J, Xue Y, Zhou S, Khavari PA, Biggar SR, Muchardt C, Kalpana GV, Goff SP, Yaniv M, Workman JL, Crabtree GR. 1996. Purification and biochemical heterogeneity of the mammalian SWI-SNF complex. EMBO J 15(19):5370-5382.

Wang L, Baiocchi RA, Pal S, Mosialos G, Caligiuri M, Sif S. 2005. The BRG1- and hBRM-associated factor BAF57 induces apoptosis by stimulating expression of the cylindromatosis tumor suppressor gene. Mol Cell Biol 25:7953-7965.

Wang H, Zhao R, Guo C, Jiang S, Yang J, Xu Y, Liu Y, Fan L, Xiong W, Ma J, Peng S, Zeng Z, Zhou Y, Li X, Li Z, Li X, Schmitt DC, Tan M, Li G, Zhou M. 2016. Knockout of BRD7 results in impaired spermatogenesis and male infertility. Scientific reports 6:21776.

Wang X, Wang S, Troisi EC. 2019. BRD9 defines a SWI/SNF sub-complex and constitutes a specific vulnerability in malignant rhabdoid tumors. Nat Commun 10:1881.

Wei Z, Yoshihara E, He N, Hah N, Fan W, Pinto AFM, Huddy T, Wang Y, Ross B, Estepa G, Dai Y, Ding N, Sherman MH, Fang S, Zhao X, Liddle C, Atkins AR, Yu RT, Downes M, Evans RM. 2018. Vitamin D Switches BAF Complexes to Protect β Cells. Cell 173(5):1135-1149.

Whitworth KM, Agca C, Kim JG, Patel RV, Springer GK, Bivens N. 2005. Transcriptional profiling of pig embryogenesis by using a 15K member unigene set specific for pig reproductive tissues and embryos. Biol Reprod 72:1437-1451.

Wiekowski M, Miranda M, Nothias JY, DePamphilis ML. 1997. Changes in histone synthesis and modification at the beginning of mouse development correlate with the establishment of chromatin mediated repression of transcription. J Cell Sci 110:1147-1158.

Yan L, Xie S, Du Y, Qian C. 2017. Structural Insights into BAF47 and BAF155 Complex Formation. J Mol Biol 429(11):1650-1660.

Yoshioka K, Suzuki C, Tanaka A, Anas IM, Iwamura S. 2002. Birth of piglets derived from porcine zygotes cultured in a chemically defined medium. Biol Reprod 66:112-119.

Yu X, Li Z, Shen J. 2016. BRD7: a novel tumor suppressor gene in different cancers. Am J Transl Res 8(2):742-748.

Yuan Y, Spate LD, Redel BK, Tian Y, Zhou J, Prather RS. 2017. Quadrupling efficiency in production of genetically modified pigs through improved oocyte maturation. Proc Natl Acad Sci USA 114: 5796-5804.

Zhou J, Ma J, Zhang BC. 2004. BRD7, a novel bromodomain gene, inhibits G1-S progression by transcriptionally regulating some important molecules involved in ras/MEK/ERK and Rb/E2F pathways. J Cell Physiol 200:89-98.

Zhou M, Liu H, Xu X, Zhou H, Li X, Peng C, Shen S, Xiong W, Ma J, Zeng Z, Fang S, Nie X, Yang Y, Zhou J, Xiang J, Cao L, Peng S, Li S, Li G. 2006. Identification of nuclear localization signal that governs nuclear import of BRD7 and its essential roles in inhibiting cell cycle progression. J Cell Biochem 98(4):920-30.

CHAPTER 5. DEPLETION OF THE SWI/SNF CHROMATIN REMODELING COMPLEX SUBUNIT, ARID1A, DOWNREGULATES CDH1 GENE EXPRESSION AND E-CADHERIN PROTEIN ABUNDANCE IN PORCINE 4-CELL STAGE EMBRYOS.

5.1 Abstract

The objective was to investigate the mechanism involving in early embryo lethality caused by ARID1A depletion. ARID1A is a SWI/SNF chromatin remodeling complexes subunit found exclusively in BAF sub complexes. Our previous study revealed the critical requirement of ARID1A during preimplantation porcine embryo development. ARID1A-depleted porcine embryos arrest at 4-cell stage. We hypothesized that the lethality we observed upon *ARID1A* knockdown in porcine embryos was due in part to down regulation of *CDH1* mediated by direct interaction between ARID1A and the CDH1 promoter. To test our hypothesis, we first determined *CDH1* transcript abundance in ARID1A-depleted porcine 4-cell stage embryos. We next performed an immunocytochemical staining to determine the intracellular localization patterns of E-cadherin in GV stage porcine, 2-cell stage, 4-cell stage and blastocyst. We found both *CDH1* transcript and E-cadherin were down regulated in ARID1A depleted 4-cell stage embryos. We also found that E-cadherin was nuclear localized in GV stage oocytes and 2-cell stage embryo, then adopted nuclear and cell membrane localization in 4-cell stage and blastocyst stage embryos.

5.2 Introduction

The evolutionally conserved SWI/SNF (SWItch/Sucrose Non-Fermentable) family of chromatin remodeling complexes can be found in all eukaryotes, from yeast to human (Neigeborn and Carlson, 1984). All SWI/SNF chromatin remodeling complexes contain one of two catalytic subunits, either BRM (Brahma) or BRG1 (Brahma-related gene-1); BRM and BRG1 are ATPases. SWI/SNF chromatin remodeling complexes possess a series of protein subunits referred to as BRM/BRG1-associated factors (BAFs) to form complexes that remodel chromatin by altering nucleosome spacing. The collection of BAFs determine the identity of a given SWI/SNF chromatin-remodeling complex and dictate where that complex will act (Smith *et al*., 2003).

Examples of SWI/SNF chromatin remodeling complexes include the BAF complex, the PBAF complex and the GBAF complex (Ho *et al*., 2019). BAF and PBAF complexes share many of the same core components, including BAF47, BAF53, BAF57, BAF155, BAF170 and actin. ARID2, BAF45D, and BRD7 have been found to be unique subunits present in PBAF complexes, while ARID1, BCL7, and BCL11 have been found to be unique to BAF complexes (Phelan *et al.*, 1999). The composition of the most recently discovered SWI/SNF complex, the GBAF complex, differs from the BAF and PBAF complexes. GBAF complexes do not appear to contain SMARCB1, a core subunit found in both BAF and PBAF complexes. GBAF complexes have been shown to contain a BAF155 dimer, as well as the unique subunits GLTSCR1, GLTSCR1L and BRD9 (Alpsoy and Dykhuizen, 2018).

About 30 genes encoding BAF subunits have been identified in the human genome and the expression level of these subunits differs across various cell types (Mashtalir *et al*., 2018). This suggests that the composition of SW/SNF complexes is tissue-specific (Toto *et al*., 2016; Hota *et al*., 2019). Previous work from our laboratory revealed that while many BAFs have similar intracellular localization patterns in porcine embryos at the pronuclear, 4-cell and blastocyst stages of development, some subunits adopt a change in intracellular localization at discrete developmental stages. For example, ARID2 was tightly associated with chromatin in GV stage oocytes and had weak nuclear localization in pronuclear stage embryos. ARID2 then localized predominately in the nuclei at both 4-cell and blastocyst-stage embryos. BRD7, on the other hand, adopted cytoplasmic localization in both 4-cell and blastocyst stage embryos. In addition, we also found that BAF170 and ARID1B differ in their intracellular localization between embryos produced in vitro, and embryos recovered from bred gilts (in vivo-derived embryos). The expression of BAF170 is stronger in *in vitro* produced blastocysts compared to *in vivo*-derived blastocysts. ARID1B is not detectable in most *in vitro* produced blastocysts but only one of seven *in vivo*-derived blastocysts possessed detectable ARID1B. This data indicates that *in vitro* manipulation may disrupt the timing of chromatin remodeling and perturb the epigenetic state during early preimplantation embryo development. In a separate study, we found that transcript levels of *ARID1A* and *SNF5* change over the course of cleavage development (Tseng, *et al*., 2017), suggesting the action of a given SWI/SNF chromatin remodeling complex and its components is stage-dependent during preimplantation embryo development.

Studies involving knockout mouse models indicate differing developmental requirements for discrete BAF subunits. For example, *Snf5*-null mice fail to reach the blastocyst stage of development, but *Brd7*-null mice survive until E16.5 but display abnormal limb development, abnormal blood vessels and organs at E16.5. A*rid1a*-null mice are reported to arrest at E6.5 and fail to complete gastrulation where mesoderm is missing (Klochendler-Yeivin *et al*., 2000; Gao *et al*., 2008; Kim *et al*., 2016). A single point mutation in the ARID domain (V1068G) in mice disrupts SWI/SNF complex binding ability to chromatin and leading to embryo death at E13.5 (Chandler *et al*., 2013). Loss of ARID1A in both mouse and pig models lead to early embryonic lethality. ARID1A depleted pig embryos arrest at 4-cell stage which occur earlier than what has been observed in *Arid1a*-null mice. It is understandable that the ablation approaches used in these studies are different. The knockout mice lack any zygotic *Arid1a* but the maternal derived *Arid1a* may enable embryos to develop into a later stage compared to the RNAi approach we employed. In the *SNF5* knockout study published by Klochendler-Yeivin, the author has reported that the maternal stored *Snf5* transcript affects the phenotype of *Snf5*-null embryo (Klochendler-Yeivin *et al*., 2000; Gao *et al*., 2008; Li *et al*., 2010; Tseng *et al.*, 2017).

ARID1A/B (AT-rich interactive domain-containing protein 1A/B), BCL7, and BCL11 are exclusively found in the BAF complex; the BAF complex is thought to be the most abundant SWI/SNF chromatin remodeling complex (Yan *et al*., 2005). The AT-rich interacting domains (ARIDs) within ARID1A and ARID1B shares 90% similarity. A mass spectrometry study from human cells revealed that the primary role of ARID1A/B in SWI/SNF complexes is DNA binding, rather than complex structure (Mashtalir *et al*., 2018).

These evidences presented above indicate that ARID1A and ARID1B are crucial for guiding the SWI/SNF complexes to specific loci. *ARID1A* is considered as tumor suppressor gene and found commonly mutated in several cancers (Kelso *et al*., 2017; Mathur *et al.*, 2017). It is not surprising since ARID1A have been reported to directly interact with p53, which is considered as tumor antigen and responsible for regulating the cell cycle and DNA repair (Guan *et al*., 2011). Despite the role of tumor suppressor, ARID1A is essential for embryo development. It appears that ARID1A/B are required to maintain the pluripotency in embryonic stem cells (Gao *et al*., 2008;

Lei *et al*., 2015) but how loss of ARID1A contributes to early embryo developmental arrest remains unresolved.

Chromatin immunoprecipitation studies suggest that ARID1A directly interacts with the promoter region of several genes that could affect early embryo development potential. The gene *CDH1* encoding the cell-cell adhesion molecule cadherin-1 is one of them (Wu and Roberts, 2013; Yan *et al*., 2014; Sun *et al*., 2018). Cadherin-1 (also referred to as E-cadherin) is a calcium-dependent transmembrane glycoprotein (Yoshida-Noro *et al*., 1984). This protein is one of the most important cell-cell adhesion protein localized on the surfaces of epithelial cells (Gumbiner, 1996). It is also critical to maintain the correct organization of cytoskeleton (Chen *et al*., 2014). In mice, E-cadherin can be detected six hours after activation (Clayton *et al*., 1993). E-cadherin has been reported to be necessary for proper inner cell mass and trophectoderm formation during embryo development (Marikawa and Alarcón, 2009). *Cdh1*-null mouse embryos fail to accumulate E-cadherin during early cleavage stages, resulting in a loss of cell polarity and cell integrity and ultimately results in developmental arrest before embryo compaction at the morula stage prior to blastocyst formation (Larue *et al*., 1994).

In our previous study, we have found that ARID1A depleted porcine embryos arrest at 4-cell stage (Tseng *et al*., 2017). Since ARID1A has been reported to directly interact with the *CDH1* promoter region in human (Yan *et al*., 2014), we hypothesized that the lethality we observed upon *ARID1A* knockdown in porcine embryos was due in part to down regulation of *CDH1* mediated by direct interaction between ARID1A and the CDH1 promoter. To test our hypothesis, we first determined *CDH1* transcript abundance in ARID1A-depleted porcine 4-cell stage embryos. We next performed an immunocytochemical staining to determine the intracellular localization patterns of E-cadherin in GV stage porcine, 2-cell stage, 4-cell stage and blastocyst stage porcine embryo. Lastly, we attempted to develop a chromatin immunoprecipitation assay to identify the direct interaction between ARID1A-containing SWI/SNF chromatin remodeling complexes and the *CDH1* promoter region. Our results indicate that transcript levels of *CDH1* are significantly reduced in ARID1A-depleted porcine embryos, as compared to wild-type porcine embryos. Taken together, our work demonstrates that *CDH1* transcript is disrupted by ARID1A-depletion and potentially distort preimplantation porcine embryo development.

5.3 Materials and Methods

Oocyte collection

All chemicals used in these experiments were purchased from Sigma Chemical Company (St. Louis, MO) unless specifically stated. Ovaries from prepubertal gilt (*Sus scrofa*) were obtained from a local slaughterhouse and transported to the laboratory in an insulated container containing 35°C saline. Follicular fluid containing cumulus-oocyte-complexes (COCs) was aspirated manually form antral ovarian follicles (3–5 mm in diameter) using a 10-gauge needle and 10 cc sterile syringe. COCs suspended in aspirated follicular fluid were allowed to settle by gravity; follicular fluide was then removed and COCs resuspended in HEPES-buffered medium containing 0.01% polyvinyl alcohol (HEPES-PVA; Abeydeera et al., 1998). COCs with multiple layers of intact cumulus cells were collected for further processing. For studies involving germinal vesicle (GV)-stage oocytes, COCs were placed in 0.1% hyaluronidase in HEPES-PVA, vortexed for 8 minutes to remove cumulus cells, rinsed in HEPES-PVA, and allocated to experiments. For experiments involving matured porcine oocytes, COCs were placed in in vitro maturation medium (see below).

In vitro maturation

Between 70-100 COCs were placed in 500 µl of Tissue Culture Medium 199 (TCM199) supplemented with 0.14% PVA, 40 ng/ml fibroblast growth factor 2 (FGF2; PeproTech), 10 ng/ml epidermal growth factor, 20 ng/ml leukemia inhibitory factor (LIF; MilliporeSigma), 0.57 mM cysteine, 20 ng/ml insulin-like growth factor 1 (IGF1; Prospec Protein Specialists), 0.5 IU FSH, and 0.5 IU LH, (Yuan *et al.*, 2017) under mineral oil at 39°C and 5% CO_2 in air, 100% humidity for 42-44 hours for maturation (Abeydeera *et al.*, 1998). Cumulus cells were removed from matured COCs by vortexing for 4 minutes in 0.1% hyaluronidase in HEPES-PVA.

In vitro fertilization and embryo culture

Groups of 30 matured oocytes placed in 100 µl of modified Tris-buffered medium (mTBM) with 5×10^5 spermatozoa/ml (Abeydeera and Day, 1997). Semen used in *in vitro* fertilization was collected from a boar of proven fertility housed at the Purdue Animal Science Research and Educational Center. Freshly collected semen was mixed with a commercial semen extender (EnduraGuard Plus; Mofa Global, Verona, WI); extended semen was stored at 18°C for up to three

days. The sperm was prepared for *in vitro* fertilization by mixing 1 ml of extended semen mixed with 9 ml of 39ºC Dulbecco's phosphate buffered Saline (DPBS) containing 1 mg/ml BSA and centrifuged at 900xg for 4 minutes. The resultant sperm pellet was resuspended in DPBS; this process was repeated three times. Following the final wash in DPBS, the sperm pellet was resuspended in 100 µl of mTBM. This sperm suspension was diluted in mTBM such that oocytes were fertilized in the presence of 5×10^5 sperm/ml. After 5 hours of gamete co-incubation at 39°C and 5% CO_2, presumptive zygotes were washed three times in Porcine Zygote Medium 3 supplemented with 3 mg/ml fatty acid-free BSA (PZM3; Yoshioka *et al*., 2002). Group of 15 presumptive zygotes were then placed in 30 µl droplets of PZM3 under mineral oil and cultured at 39°C, 5% CO_2 and 100% humidity for 48 hours or 7 days in order to collect 4-cell stage or blastocyst stage embryos, respectively.

RNA interference

The interfering RNAs used to knock down *ARID1A* transcript abundance were previously reported by our group (Tseng *et al*., 2017). Briefly, Custom made Stealth™ RNAi nucleotides targeting porcine *ARID1A*, 5'- CGGACAGCAUCAUGCAUCCUUCUAU and nonsense Stealth™ RNAi nucleotides were 5'- CGGCGACUAGUAUACUCCCUACUAU were designed by the BLOCK-iT™ RNAi Designer (Invitrogen) based on the full-length porcine *ARID1A* open reading frame. The nonsense siRNA was designed so that it was not complimentary to *ARID1A* and maintained the same molecular weight as *ARID1A* siRNA. The final concentration of interfering RNAs used in this study was 1 µM.

Microinjection

Presumptive porcine zygotes were vortexed in 0.1% hyaluronidase in HEPES-buffered medium for 4 minutes to remove sperm immediately after gamete co-incubation. Embryos were allocated to one of three treatment groups as follows: injection with *ARID1A* interfering RNAs (*ARID1A*-siRNA), injection with nonsense RNAs (control-siRNA), and non-injection controls (non-injected). All presumptive zygotes were placed in HEPES-buffered medium containing 3mg/ml BSA (HEPES-BSA). Microinjection needles were loaded with 5 µl of 1 µM siRNA and fixed to a Femtojet microinjector (Eppendorf, Hauppauge, NY, USA). Cells that lysed upon microinjection were discarded and excluded from analysis. Presumptive zygotes that remained intact following

microinjection were cultured in PZM3 for 48 hours, at which point 4-cell stage embryos were collected for mRNA isolation used in *CDH1* transcript analysis. This procedure was repeated to generate ARID1A knockout embryos used in immunocytochemical staining.

CDH1 transcript abundance in 4-cell stage porcine embryos following ARID1A knockdown

The transcript abundance of *CDH1* was measured in 4-cell stage embryos from the *ARID1A*-siRNA, control siRNA, and non-injected treatment groups described in the section entitled, '*Microinjetion*' above. Morphological 4-cell stage embryos from the three treatment groups were collected 48 hours after microinjection; messenger RNA was isolated from embryos using a commercial RNA isolation kit, DYNABEADS RNA Isolation Kit (Invitrogen Corporation, Carlsbad, CA, USA) according to the manufacturer's protocol. Briefly, embryos were washed in HEPES-PVA three times then placed in 100 μl DYNABEADS lysis buffer. Embryos were gently mixed in lysis buffer for 10 minutes at room temperature. The lysates were stored at -80°C until further processing. Upon thawing, mRNA was isolated, and reverse transcribed in a 20 μl reaction using the iScript kit (Bio-rad, Hercules, CA, USA) according to the manufacturer's protocol (Lonergan *et al.*, 2003). Resultant cDNA was used to perform quantitative PCR to determine relative levels of *CDH1* transcript in each treatment.

Quantitative PCR

Primers used to amplify *CDH1* in this experiment were designed from publicly available sequence data in GenBank (NM_001163060); the sequence for *CDH1* primers are forward: 5'-CACCAGATGTGCACGTATGCGACT; and reverse: 5'- GTTGTCCCGGGTGTCATCTT; product size is 194 base pairs. The *CDH1* PCR products were cloned into pENTR^{TM}/SD/D-TOPO vector (Invitrogen, Carlsbad, CA, USA) and sequenced to confirm their identity. The amplification efficiency of *CDH1* primer set was determined by constructing a standard curve. Briefly, the standard curve for *CDH1* was generated by performing PCR with known concentration of serially diluted *CDH1* template in the pENTR vector. The standard curve was used to determine the range of Ct values (threshold cycles) for which the *CDH1* primer set produced linear amplification of *CDH1*. The housekeeping gene, *YWHAG* (Genbank accession number CO94522), was used to normalize template input; *YWHAG* has been reported to maintain a constant level of transcript abundance from the GV stage oocyte to the blastocyst stage of embryo development (Whitworth

et al., 2005). *YWHAG* primers were forward: 5'-TCCATCACTGAGGAAAACTGCTAA; and reverse 5'-TTTTTCCAACTCCGTGTTTCTCTA, product size 130 base pairs (Whitworth *et al.*, 2005).

A PCR master mix was prepared for each gene as follows: 1 µl of 5 µM forward primer, 1 µl of 5 µM reverse primer and 3 µl of cDNA from each treatment were mix with 10 µl of SybrGreen Master mix (Bio-Rad). For each replicate, cDNA from each treatment was used to amplify *CDH1* and *YWHAG*; reactions for each biological replicate were performed within the same PCR run and all genes were run in duplicate, and three biological replicates were performed. The MyiQ single color real-time thermal cycler (Bio-Rad) was employed and programed as follow: 5 minutes initial denaturation at 94°C, followed by 45 cycles of 5 seconds at 94°C, 30 seconds at 60°C, and 30 seconds at 72°C. Fluorescence data were collected during the extension step of each cycle; a melting curve was generated to determine the identity of each PCR amplicon.

Immunocytochemical staining

Embryos were subjected to an immunocytochemical staining assay to determine the intracellular localization of CHD1 in porcine embryos using an established immunocytochemical staining protocol (Cabot *et al*., 2017; Tseng *et al*., 2017). Briefly, 48 hours after microinjection, 4-cell stage embryos from each of the three treatment groups (*CDH1*-siRNA, control-siRNA, and non-injected) were fixed in 3.7% paraformaldehyde at 4°C for one hour. Fixed cells were moved through three, 15-minute washes in phosphate buffered saline (PBS) containing 0.1% Tween-20 (PBST); embryos were stored in PBST for up to 18 hours. Following the three washes, embryos were permeabilized by incubation for one hour in PBS containing 1% TritonX-100; cells were then incubated in blocking solution at 4°C (0.1 M glycine, 1% goat serum, 0.01% Triton X-100, 1% powdered nonfat dry milk, 0.5% BSA and 0.02% sodium azide in PBS for 12-16 hours (Prather and Rickords, 1992). Embryos were then washed three times in PBST (15 minutes each wash). Embryos were co-incubated at 4°C for 12-16 hours with primary antibody against E-cadherin (BD Biosciences, San Jose, CA, USA, cat# 610181) and ARID1A (Abcam, Cambridge, MA, USA, cat# ab182560); each antibody was diluted to 1:500 in PBST. Following incubation with primary antibodies, cells were processed through a series of three washes in PBST (15 minutes each wash). Embryos were co-incubated at 4°C for 12-16 hours with two secondary antibodies: goat-anti-

mouse IgG, fluorescein isothiocyanate (FITC)-conjugated (Sigma catalog number F0257) diluted 1:500 in PBST to detect E-cadherin and goat-anti-rabbit-IgG, tetramethyl rhodamine isothiocyanate (TRITC)-conjugated (Sigma catalog number 6778) diluted 1:500 in PBST to detect ARID1A protein. Embryos were washed with PBST three times (each wash lasting 15 minutes); cells were then stained with Hoechst 33342 (5 μg/ml) for one hour, washed in PBST, and mounted on slides in Vectashield mounting medium (Vector Laboratories, Inc., Burlingame, CA, USA). Samples were examined using an inverted Nikon A1R_MP multi-photon confocal microscope, (Nikon Instruments Inc., Melville, NY) using de-scanned detectors and laser lines at 408 nm (Hoechst), 488 nm (FITC), and 561 nm (TRITC). Control groups for immunocytochemical staining included by a subset of embryos from each treatment stained with secondary antibody alone (to control for non-specific binding of secondary antibody). The intracellular localization of CDH1 was also determined in GV-stage oocytes and in vitro produced embryos at the 2-cell, 4-cell, and blastocyst stages of development using the above described protocol, omitting the ARID1A antibody and respective secondary antibody.

ARID1A ChIP assay

Acquisition of Porcine fibroblast

Porcine fetal fibroblast cells (PFFs) were generously provided by by our lab members, Jennifer Crodian and Birgit Cabot. Briefly, Briefly, PFFs were derived from fetuses on Day 28 of gestation. After removal of extraembryonic tissue, fetal tissue was cut into 1 mm^2 pieces with sterile scauple blades in the presence of 1% trypin. Tissues pieces were suspended in Dulbecco's modified Eagle's medium containing 1% L-glutamine (Gibco), 1% sodium pyruvate (Gibco), 1% MEM-nonessential amino acids (Sigma), and 1% penicillin-streptomycin (Gibco; DMEM), supplemented with 15% fetal bovine serum (DMEM-FBS). Tissue pieces were centrifuged at 250g for 9 minutes, resuspended in DMEM-FBS, and plated on culture dishes (Kühholzer *et al*., 2001).

Crosslinking of ARID1A and DNA

PFFs were harvested from the culture dish by incubation in 1% trypsin. The trypsin coated culture plate was washed with DMEM-FBS and the cell suspension centrifuged at 400xg for 7 minutes. The cell pellet was resuspended in DMEM-FBS; 6 $x10^6$ PFFs were use then pelleted by

centrifugation. This cell pellet was resuspended in ice cold phosphate buffered saline (Gibco, pH 7.2), centrifuged at 400xg for 7 minutes. The cell pellet was resuspended in buffer A (20 mM HEPES, pH 7.9, 25 mM KCl, 10% glycerol, 0.1% NP-40, supplemented with protease inhibitors (Thermo Scientific) and incubated on ice for 7 minutes. Nuclei were isolated by centrifugation at 645g for 10 min at 4°C. Pellets were resuspended in 1ml lysis buffer (50 mM HEPES, pH 7.5, 150 mM NaCl, 0.5% NP-40, supplemented with protease inhibitors). Bicinchoninic acid assay (BCA) was employed to assess protein concentration in the lysate. Ten ml of fixation buffer (50 mM Hepes, 1 mM EDTA, 0.5 mM EGTA, 100 mM NaCl) containing 1% formaldehyde (Thermo Scientific) was added to the lysate to crosslink protein and DNA. Following an 8 minutes incubation at room temperature, crosslinking was terminated by the addition of glycine (final concentration of 125 mM) and incubated for 5 minutes on ice. The solution was centrifuged at 1200xg at 4°C for 5mininutes, pellets were washed three times with PBS and resuspended in 10 ml of Rinse Buffer 1 (50 mM HEPES, 140 mM NaCl, 1 mM EDTA, 10% glycerol, 0.5% NP40, 0.25% Triton X100) and then incubated on ice for 10 minutes and pelleted by centrifugation at 1200g at 4°C for 5 minutes. The pellet was resuspended in 5 ml of Rinse Buffer 2 (10 mM Tris base, 1 mM EDTA, 0.5 mM, EGTA, 200 mM NaCl) and incubated on ice for 5 minutes. The suspension was then centrifuged at 1200xg at 4°C for 5 minutes (Porter and Dykhuizen, 2017).

Shearing

The pellet were then resuspended in 1 ml of ChIP IP Buffer (50 mM Hepes, pH 7.5, 300 mM NaCl, 1 mM EDTA, 1% Triton X-100, 0.1% deoxycholate, 0.1% SDS, plus protease inhibitors) and sonicated with a Branson Sonifier 250 probe sonicator for 6 minutes (30 seconds bursts followed by 30 seconds on ice repeatedly for total 6 minutes). Debris was removed by centrifugation at 20,000xg for 10 minutes at 4 °C and the supernatant was collected. The supernatant contained sheared chromatin; 25 µl of sheared chromatin was added into 75 µl of TE buffer containing 1% SDS and 50µg/ml of RNAase (AMRESCO) and incubated at 37°C for 30 minutes. Proteinase K (New England Biolabs) was added to a final concentration of 200 µg/ml; the solution was incubated at 55°C for 3 hours, then incubated at 65°C for 16-18 hours. Following incubation, 230 µl of TE buffer,165 µl of phenol, and 165 µl of chloroform was added. The solution was vortexed at maximum speed for 1 minute and centrifuged at 10,000xg for 1 minute. DNA was precipitated from the supernatant with 1 µl glycogen, 30 µl 3M NaOAc, and 330 µl isopropanol. The solution

was centrifuged at 10,000xg for 30 minutes at 4°C, the pellet was washed with 70% ethanol and dried. The pellet was resuspended in 25 µl TE buffer. The shearing was assayed by running 10 µl of the sample on a 1% agarose gel (Porter and Dykhuizen, 2017).

Immunoprecipitation

450 µl of ChIP IP Buffer with sheared product was precleared with 15 µl of Dynabeads Protein A (Thermo Scientific) to minimize non-specific binding and then incubated with 5 µl of antibody against ARID1A (Abcam, Cambridge, MA, USA, cat# ab182560) for 3 hours. 15 µl of washed Dynabeads was added and incubated for another hour. Dynabeads were collected and washed two times for 5 minutes with ChIP IP Buffer and washed with Deoxycholate Buffer (10 mm Tris, pH 8, 250 mm LiCl, 0.5% NP40, 0.5% deoxycholate) and 1× Tris-EDTA Buffer (10 mm Tris-HCl, 1 mm EDTA pH 8.0). Beads were rotated at room temperature for 30 minutes in 150 µl of Elution Buffer 2 (1% SDS, 100 mM $NaHCO_3$) for 30 minutes. The elution step was repeated a second time and the resulting sample was suspended in SDS gel loading buffer and subjected for western blot analysis (Porter and Dykhuizen, 2017). Briefly, 20 µl eluted proteins was mixed with 4 µl of 6x Laemmli SDS Sample buffer and boiled for 10 minutes at 95°C. Samples were loaded and separated on a 10% SDS-polyacrylamide gel (Bio-Rad) at 90V for 90 minutes then transferred to a nitrocellulose membrane (Thermo Scientific) by semidry electroblotting system. The membrane was blocked with 5% skim milk in PBS containing 0.1% Tween-20 (PBST) (Sigma) at room temperature for 2 hours and then incubated with 5 ml of blocking buff and primary antibody against ARID1A (1:1000) (Abcam, Cambridge, MA, USA, cat# ab182560) 12-16 hours at 4°C. The membrane was washed in TBST three times, 10 minutes each. The membrane was incubated with blocking buffer and HRP-conjugated goat anti-rabbit secondary antibodies (1:500) at room temperature for 2 hours. The membrane was washed in TBST three times, 10 minutes each. The membrane signal was developed using Clean-Blot IP Detection Kit (Thermo Scientific) and visualized using a FluorChem R camera system (ProteinSimple).

Statistical analysis

Statistical Analysis Software (SAS, SAS Institute, Cary, NC, USA) was used to analyze the relative expression of *CDH1*. The average Ct values of each duplicate using the $2^{-\triangle\triangle Ct}$ method were calculated and the $2^{-\triangle\triangle Ct}$ values were imported into Statistical Analysis Software (SAS, SAS

Institute, Cary, NC, USA). The linear model was processed by SAS LR program and analyzed by one-way ANOVA; treatment was considered as the main factor. The differences were compared using Tukey's multiple comparison test ; a p-value < 0.05 was considered significant.

5.4 Results

The intracellular localization of E-cadherin in GV stage oocyte, 2-cell, 4-cell, and blastocyst stage embryos.

Immunocytochemical staining was employed to identify the intracellular localization patterns of E-cadherin in GV stage oocytes, 2-cell, 4-cell and blastocyst stage porcine embryos. Our results indicate that E-cadherin is present in the nucleus in both GV stage oocytes (n=13/17) and 2-cell stage embryos (n=9/12). E-cadherin was detected in the nuclei and on the cell membrane at 4-cell (n=11/13) and blastocyst (n=9/9) stages of development. (Figure 8).

ARID1A depletion disrupts E-cadherin and CDH1 transcript in 4-cell stage embryos

Embryos injected with ARID1A interfering RNAs (ARID1A-siRNA) showed minimal staining for E-cadherin, and lacked detectable nuclear E-cadherin staining, as compared to controls. From a total of 31 4-cell stage embryos in the *ARID1A*-siRNA treatment group, 24 embryos show a reduction in E-cadherin staining. In contract, the majority of control embryos displayed nuclear E-cadherin staining (control-siRNA n=30/34 and non-injected n=21/24, respectively). Representative images of these embryos are shown in Figure 9. Transcript levels of *CDH1* were significantly reduced in 4-cell stage embryos upon *ARID1A* knockdown (*ARID1A* siRNA vs control siRNA and non-injected, $p<0.05$; Figure 10).

Optimization of ARID1A chromatin immunoprecipitation assay conditions

The PFF nuclear extract was fixed in 1% formaldehyde for 4, 6, 8, 10 minutes and sheared for 2.5, 5, 7.5 minutes. The size of sheared products was measured by gel electrophoresis on a 1% agarose gel (Figure 11). Our results indicate that 8 minutes of crosslinking, followed by 6 minutes of shearing provides 200-300bp DNA fragments. The immunoprecipitated output was analyzed by Western blot and the result indicates the presence of a protein band of 230-250 kDa when probed with an antibody against ARID1A (Figure 12).

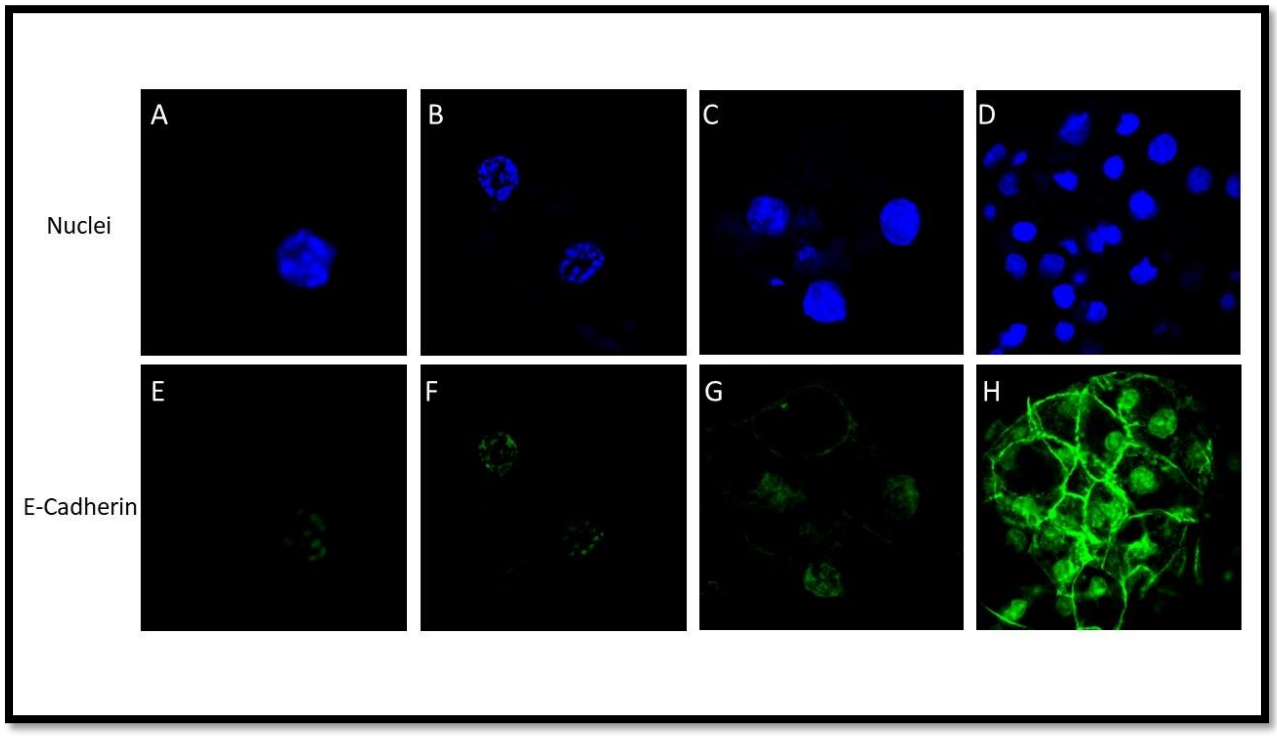

Figure 8. Representative images of E-cadherin at GV-stage oocyte and different stages of porcine embryo. Panels A and E represent the images of a GV stage oocyte; panels B and F contain representative images of a 2-cell stage embryo; panels C and G are images of a 4-cell stage embryo; panels D and H are a blastocyst stage embryo. DNA staining are shown in panels A, B, C, and D with blue fluorescence; panels E, F, G and H show the staining of E-cadherin in green fluorescence.

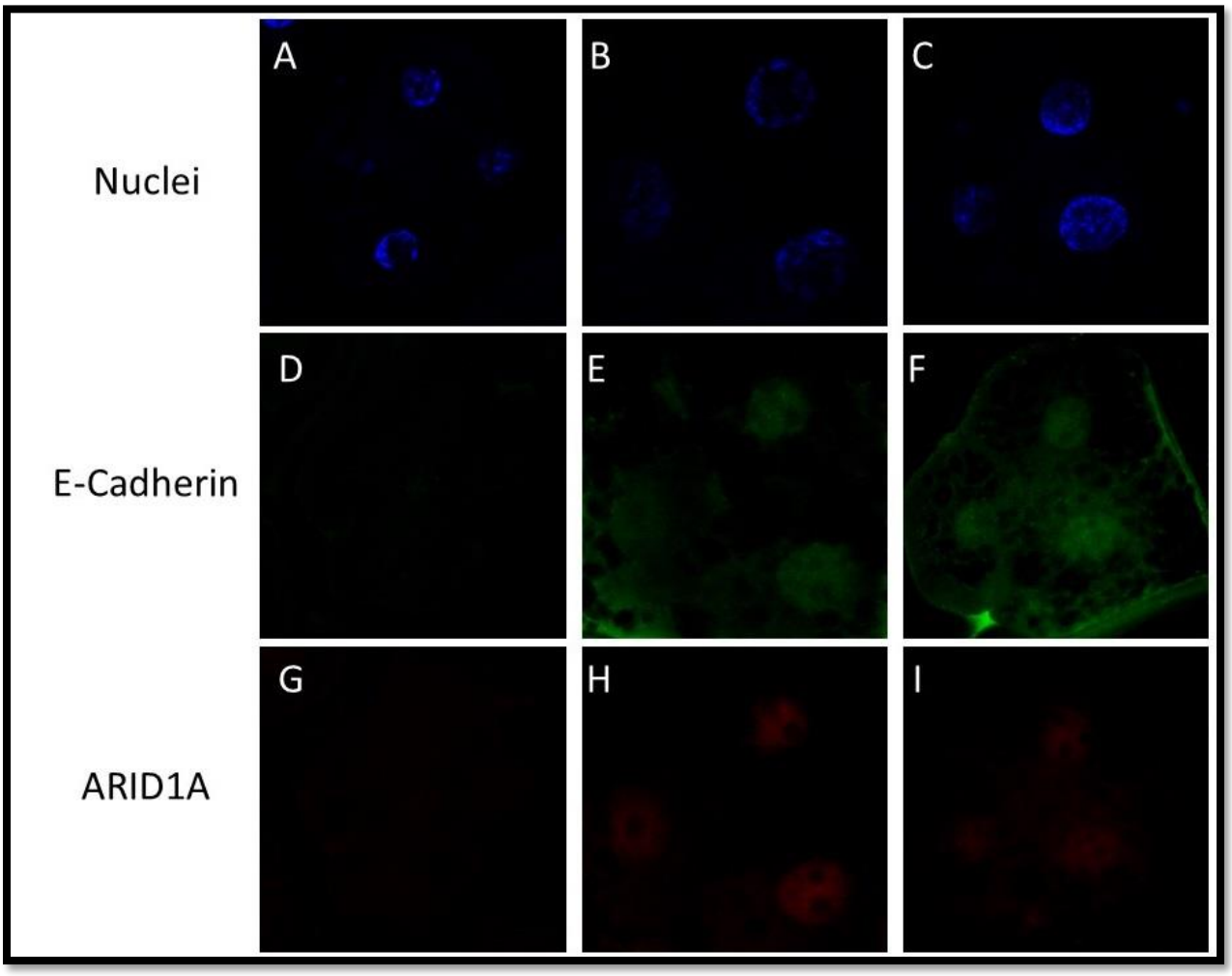

Figure 9. Representative images of 4-cell stage embryos 48 hours after *ARID1A* interfering RNA injected. Panels A, D, and G represent the images of a 4-cell stage embryo injected with *ARID1A* interfering RNAs (*ARID1A* siRNA); panels B, E, and H contain representative images of a 4-cell stage embryo injected with control RNAs (control siRNA); panels C, F, and I are images of a 4-cell stage embryo from the non-injected control group (non-injected). DNA staining are shown in panels A, B, and C with blue florescence; panels D, E, and F show the staining of E-cadherin in green fluorescence; panels G, H, and I show the staining of ARID1A in red fluorescence.

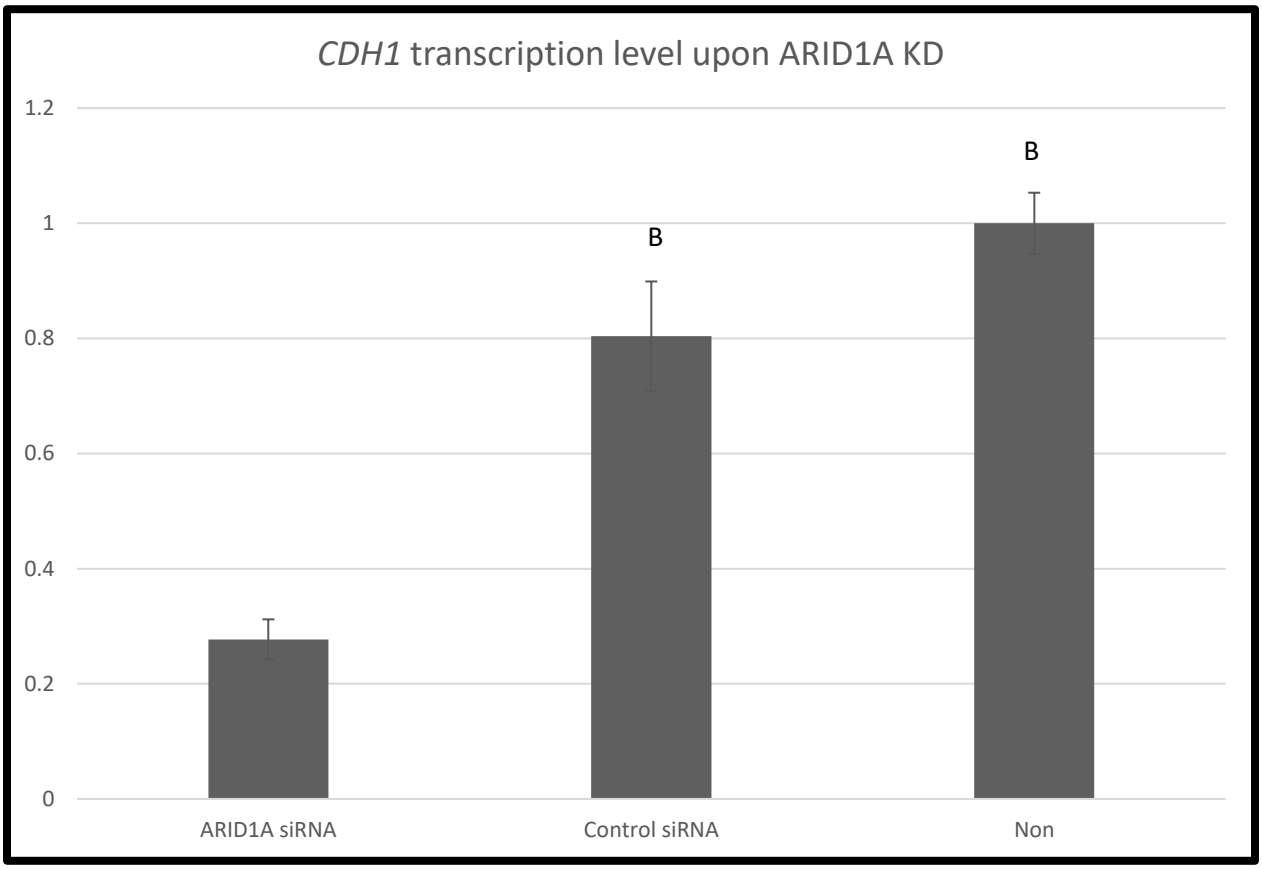

Figure 10. The change of *CDH1* transcript at 4-cell stage embryo in different treatments. Fold expression was calculated by the equation $2^{-\triangle\triangle Ct}$. The average of three independent biological replicates is shown and statistically analysis by SAS using Tukey's multiple comparison post-test; error bars represent standard deviation. a, b superscripts denote statistically significant differences ($p<0.05$).

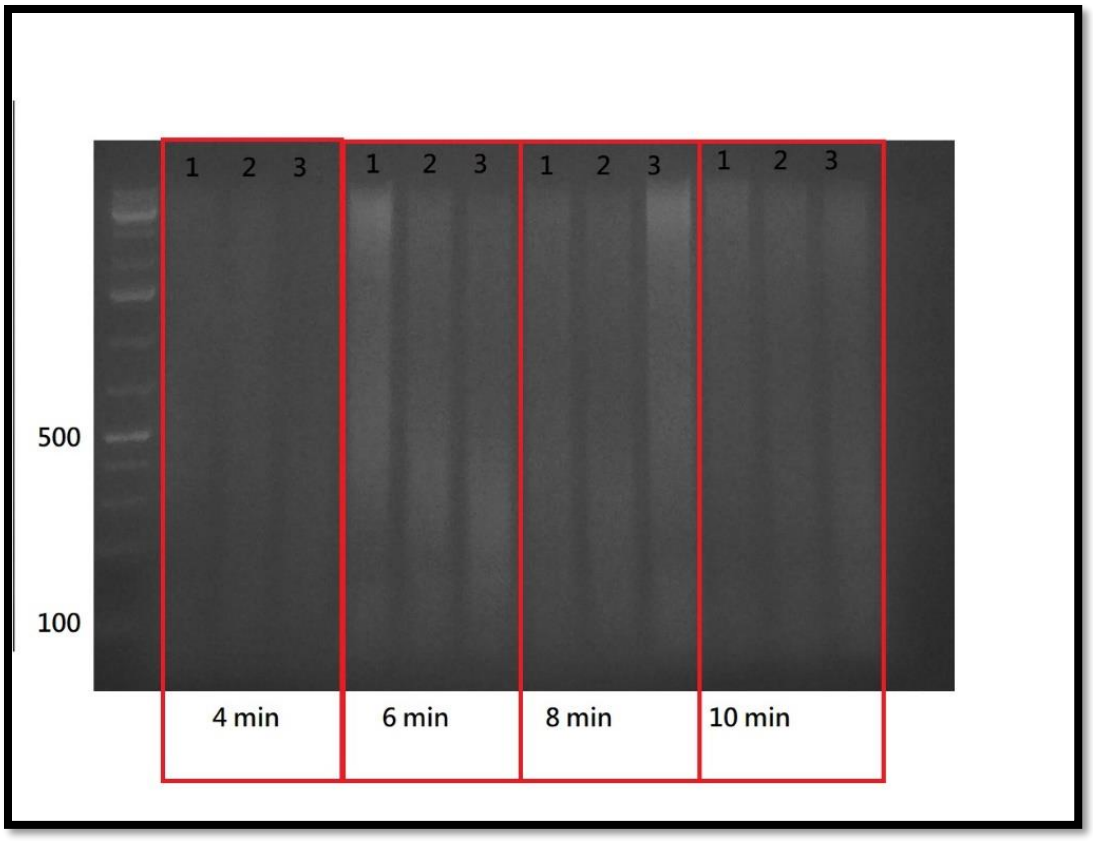

Figure 11. Electrophoresis from sheared PFF nuclear extract in 1% agarose gel. The Y axis is product size (bp); the x axis indicates different crosslink duration, including 4, 6, 8, 10 min of fixation. The numbers on the top of Figure 11. represent the time of sonication (1=2.5, 2=5, 3=7.5 mins of shearing).

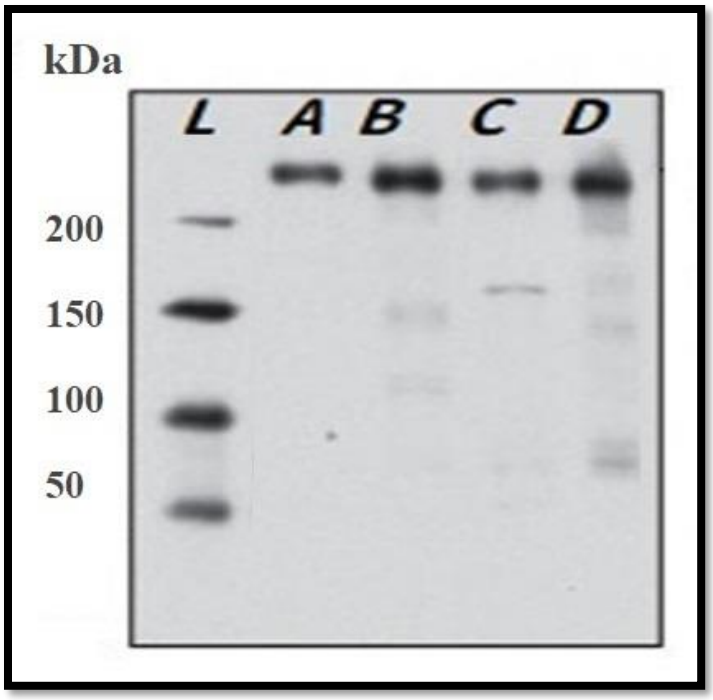

Figure 12. Western blot analysis of output of immunoprecipitation from sheared PFF nuclear proteins. A, B, C, and D represent PFF nuclear extract with different fixation and sonication time (A= HeLa cell nuclear extract; B= 8 min fixation and 6 min shearing; C= PFF nuclear extract; D= 8 min fixation and 7.5 min shearing).

5.5 Discussion

The first few days of mammalian embryo development include major biochemical and morphological changes that prepare the embryo further development within the uterus. Transcription must be precisely regulated to accomplish these tasks. Besides pluripotent genes, such as *NANOG*, *POU5F1* and *SOX2*, a screen of 712 genes in the mouse revealed 59 genes that were crucial for proper early embryo development (Cui *et al*., 2016). RNAi approaches employed in the study reveal that 4 genes are required for morula formation, including *Dck, Itgae, Hist1h2a* and *Hist1h2b,* and 20 more genes are essential for blastocyst formation. Forty of these genes do not have documented role during early development. (Cui *et al*., 2016). Although the knockout and knockdown studies have described the functions of several genes, the dynamic transcriptome and the networking of essential genes during preimplantation development are still unclear.

Transcription is controlled and regulated at many levels. Epigenetic modifications are one mechanism closely linked with gene expression. These modifications are often referred to covalently or non-covalently modifications on DNA and histone structures and allow the transcriptional machinery can proceed. For example, DNA methylation, one of the covalent modifications that transfers methyl groups to DNA structure and generally silence the gene. The methylation can be reversed to activate the corresponding gene. DNA methylation and demethylation have been documented that happen in a global level during gamete formation, fertilization, ZGA and blastocyst formation to maintain proper transcriptome (Bird and Wolffe, 1999; Mayer *et al*., 2000; Jones and Takai, 2001; Santos *et al*., 2002).

SWI/SNF chromatin remodeling complexes are multi-components complexes that reposition nucleosomes and impact transcription. Three types of SWI/SNF chromatin remodeling complexes have been identified: the BAF complex, the PBAF complex and the GBAF complex (Wang *et al*., 1996; Lemon *et al*., 2001; Alpsoy and Dykhuizen, 2018). BAF47, BAF53, BAF57, BAF155, BAF170 are conserved in both the BAF complex and the PBAF complex (Wang *et al*., 1996). ARID2, BAF45D, and BRD7 have only been identified in the PBAF complex, while ARID1, BCL7, and BCL11 have only identified in the BAF complex (Phelan *et al.*, 1999). The newly discovered GBAF complex is unique. Unlike BAF and PBAF complexes, the GBAF complex contains a BAF155 dimer, as well as the proteins GLTSCR1, GLTSCR1L, and BRD9 (Alpsoy and

Dykhuizen, 2018). The distinct domain on each subunit has been reported to guide the SWI/SNF complex to specific region on the chromatin. For example, the hydrophobic bromodomain on BRD7 (Bromodomain-containing protein 7) binds to acetylated lysine residues while the AT rich binding domain on ARID1A binds to AT rich DNA sequences (Kortschak *et al*., 2000; Nagy and Tora, 2007).

ARID1A and ARID1B are unique to the BAF complex. The DNA-binding domain within the ARID proteins can bind to AT-rich DNA sequences and its C-terminus can stimulate glucocorticoid receptor-dependent transcriptional activation (Nie *et al*., 2000). ARID1A is a trithorax group (TrxG) protein which antagonize the polycomb proteins to maintain the activity of many differentiation regulators during early embryo development (Vazquez *et al*., 1999; Grimaud *et al*., 2006). ARID1A has reported to be essential for embryo development. ARID1A depletion in mouse embryos leads to early embryonic lethality, with embryos failing to complete gastrulation and mesoderm cells are missing. (Gao *et al*., 2008; Li *et al*., 2010).

CDH1 has been suggested to be regulated by ARID1A (Sun *et al*., 2018); Cdh1-null mouse embryos lose the cell polarity and cell integrity and results in arrest before compaction at the morula stage (Larue *et al*., 1994). It is possible that the early embryo lethality due to ARID1A knockdown is an indirect result of brough about by ARID1A depletion leading to a loss of *CDH1*. *CDH1* encodes the cell adhesion protein E-cadherin. E-cadherin protein is detectable in GV stage oocytes and become highly expressed on the membrane of blastomeres after the 4-cell stage of porcine embryo development (Figure 8). A mouse study supports our finding; E-cadherin was found to have a uniform intracellular distribution in unfertilized mouse oocytes. E-cadherin increased in regions of contact between mouse blastomeres at the 8-cell stage, the stage when compaction begins (Clayton *et al*., 1993). Our immunocytochemical staining and qPCR results reveal that both *CDH1* transcript and E-cadherin protein are down regulated when ARID1A is depleted (Figure 9 and 10).

ARID1A has been shown to directly interact with *CDH1* promoter region and regulate E-cadherin in gastric cancer cell by chromatin immunoprecipitation technique (Yan *et al*., 2014). It is also reported that there is no correlation between *ARID1A* expression level and E-Cadherin in

esophageal squamous cell (Ozawa *et al*., 2015). This indicates that the gene regulation ability of SWI/SNF chromatin remodeling complexes mediated by ARID1A is tissue specific. Several studies have raised the questions regarding the role of ARID1A in different cell linages (Wu and Roberts, 2013). For example, ARID1A has reported to affect expression and stability of other BAFs in mouse embryonic stem cells while some evidences suggest that BAFs, including BAF155, BAF170, and SNF5, are normally expressed in serum-deprived cells upon ARID1A depletion (Nagl *et al*., 2007; Gao *et al*., 2008).

To test our hypothesis, the data we provided here is not sufficient. A *CDH1* knockdown experiment must be done to reveal the requirement of E-cadherin in preimplantation porcine embryo although the similar experiment has been performed in mouse embryo (Larue *et al*., 1994). Several our BAF knockdown experiments result in earlier embryo arrest compare to mouse embryo study (Gao *et al*., 2008; Tseng *et al*., 2017). The key difference between the ablation approaches used in our study and mouse study is the maternal proteins. The interferon RNA approach we employed does not remove maternal proteins while the knockout mice will lack any zygotic target proteins. The maternal stores of proteins enable embryos to develop to a later stage, especially maternal derived E-cadherin can be detected in GV stage oocyte. The requirement of E-cadherin can also be confirmed by a rescue experiment where E-cadherin protein can be supplied in ARID1A depleted embryo.

Chromatin immunoprecipitation is widely used for DNA-protein interaction studies. It can be direct evidence that ARID1A mediated SWI/SNF chromatin remodeling complexes are associate with *CDH1* gene in porcine embryo. In this study, we use PFFs instead of porcine embryos as our input to optimize the ChIP assay condition. The result encourages us to further invest in this project. Together, we show that E-cadherin are expressed through preimplantation porcine embryo and ARID1A depletion leads reduction of *CDH1* and E-cadherin in 4-cell stage porcine embryo. The data we presented here provides knowledge for better understanding of biological function of ARID1A.

5.6 References

Abeydeera LR, Day BN. 1997. Fertilization and subsequent development in vitro of pig oocytes inseminated in a modified Tris-buffered medium with frozen–thawed ejaculated spermatozoa. Biol Reprod 57:729-734.

Abeydeera LR, Wang WH, Prather RS, Day BN. 1998. Maturation in vitro of pig oocytes in protein-free media: fertilization and subsequent embryo development in vitro. Biol Reprod 58: 1316-1320.

Alpsoy A, Dykhuizen EC. 2018. Glioma tumor suppressor candidate region gene 1 (GLTSCR1) and its paralog GLTSCR1-like form SWI/SNF chromatin remodeling subcomplexes. J Biol Chem 293:3892–3903.

Asturias FJ, Chung WH, Kornberg RD, Lorch Y. 2002. Structural analysis of the RSC chromatin-remodeling complex. Proc Natl Acad Sci USA 99(21):13477-13480.

Bird AP, Wolffe AP. 1999. Methylation-induced repression--belts, braces, and chromatin. Cell 99(5):451-454.

Blomberg L, Hashizume K, Viebahn C. 2008. Blastocyst elongation, trophoblastic differentiation, and embryonic pattern formation. Reprod 135(2):181-195.

Cabot B, Tseng YC, Crodian JS, Cabot RA. 2017. Differential expression of key subunits of SWI/SNF chromatin remodeling complexes in porcine embryos derived in vitro or in vivo. Mol Reprod Dev 84:1238-1249.

Chandler RL, Brennan J, Schisler JC, Serber D, Patterson C, Magnuson T. 2013. ARID1a-DNA interactions are required for promoter occupancy by SWI/SNF. Mol Cell Biol 33:265-280.

Chen A, Beetham H, Black MA. 2014. E-cadherin loss alters cytoskeletal organization and adhesion in non-malignant breast cells but is insufficient to induce an epithelial-mesenchymal transition. BMC Cancer 14:552.

Clayton L, Stinchcombe SV, Johnson MH. 1993. Cell surface localization and stability of uvomorulin during early mouse development. Zygote 1:333–344.

Cosma MP. 2002. Ordered recruitment: gene-specific mechanism of transcription activation. Mol Cell 10:227-236.

Cui W, Dai X, Marcho C. 2016. Towards Functional Annotation of the Preimplantation Transcriptome: An RNAi Screen in Mammalian Embryos. Sci Rep 6:37396.

Gao X, Tate P, Hu P, Tjian R, Skarnes WC, Wang Z. 2008. ES cell pluripotency and germ-layer formation require the SWI/SNF chromatin remodeling component BAF250a. Proc Natl Acad Sci USA 105(18):6656–6661.

Geisert RD, Brookbank JW, Roberts RM, Bazer FW. 1982. Establishment of pregnancy in the pig: II. Cellular remodeling of the porcine blastocyst during elongation on day 12 of pregnancy. Biol Reprod 27:941–955.

Grimaud C, Negre N, Cavalli G. 2006. From genetics to epigenetics: the tale of Polycomb group and trithorax group genes. Chromosome Res 14:363-375.

Guan B, Wang TL, Shih I. 2011. ARID1A, a factor that promotes formation of SWI/SNF-mediated chromatin remodeling, is a tumor suppressor in gynecologic cancers. Cancer research 71(21):6718–6727.

Gumbiner BM. 1996. Cell adhesion: The molecular basis of tissue architecture and morphogenesis. Cell 84:345-357.

Ho PJ, Lloyd SM, Bao X. 2019. Unwinding chromatin at the right places: how BAF is targeted to specific genomic locations during development. Development (Cambridge, England) 146(19): dev178780.

Hota SK, Johnson JR, Verschueren E, Thomas R, Blotnick AM, Zhu Y, Sun X, Pennacchio LA, Krogan NJ, Bruneau BG. 2019. Dynamic BAF chromatin remodeling complex subunit inclusion promotes temporally distinct gene expression programs in cardiogenesis. Development (Cambridge, England) 146(19):dev174086.

Jones PA, Takai D. 2001. The role of DNA methylation in mammalian epigenetics. Science 293(5532):1068-1070.

Kelso TWR, Porter DK, Amaral ML, Shokhirev MN, Benner C, Hargreaves DC. 2017 Chromatin accessibility underlies synthetic lethality of SWI/SNF subunits in ARID1A-mutant cancers. eLife 6:e30506.

Kim Y, Andrés Salazar Hernández M, Herrema H, Delibasi T, Park SW. 2017. The role of BRD7 in embryo development and glucose metabolism. J Cell Mol Med 20(8):1561-1570.

Klochendler-Yeivin A, Fiette L, Barra J, Muchardt C, Babinet C, Yaniv M. 2000. The murine SNF5/INI1 chromatin remodeling factor is essential for embryonic development and tumor suppression. EMBO Rep 1(6):500–506.

Kortschak RD, Tucker PW, Saint R. 2000. ARID proteins come in from the desert. Trends Biochem Sci 25:294-299.

Kühholzer B, Hawley RJ, Lai L, Kolber-Simonds D, Prather RS. 2001. Clonal lines of transgenic fibroblast cells derived from the same fetus result in different development when used for nuclear transfer in pigs. Biol Reprod 64(6):1695-1698.

Larue L, Ohsugi M, Hirchenhain J, Kemler R. 1994. E-cadherin null mutant embryos fail to form a trophectoderm epithelium. Proc Natl Acad Sci USA 91(17):8263-8267.

Lemon B, Inouye C, King DS, Tjian R. 2001. Selectivity of chromatin-remodeling cofactors for ligand-activated transcription. Nature 414(6866):924-928.

Lei I, West J, Yan Z, Gao X, Fang P, Dennis JH, Gnatovskiy L, Wang W, Kingston RE, Wang Z. 2015. BAF250a Protein Regulates Nucleosome Occupancy and Histone Modifications in Priming Embryonic Stem Cell Differentiation. J Biol Chem 290(31):19343–19352.

Li XS, Trojer P, Matsumura T, Treisman JE, Tanese N. 2010. Mammalian SWI/SNF-A subunit BAF250/ARID1 is an E3 ubiquitin ligase that targets histone H2B. Mol Cell Biol 30:1673–1688.

Marikawa Y, Alarcón VB. 2009. Establishment of trophectoderm and inner cell mass lineages in the mouse embryo. Mol Reprod Dev 76(11):1019–1032.

Lonergan P, Rizos D, Gutierrez-Adan A, Fair T, Boland MP. 2003. Effect of culture environment on embryo quality and gene expression-experience from animal studies. Reprod Biomed Online 7:657-663.

Mashtalir N, D'Avino A. R, Michel BC, Luo J, Pan J, Otto JE, Zullow HJ, McKenzie ZM, Kubiak RL, St. Pierre R. 2018. Modular organization and assembly of SWI/SNF family chromatin remodeling complexes. Cell 175:1272-1288.

Mathur R, Alver BH, San Roman AK, Wilson BG, Wang X, Agoston AT, Park PJ, Shivdasani RA, Roberts CW. 2017. ARID1A loss impairs enhancer-mediated gene regulation and drives colon cancer in mice. Nat Genet 49:296–302.

Mayer W, Niveleau A, Walter J, Fundele R, Haaf T. 2000. Demethylation of the zygotic paternal genome. Nature 403(6769):501-502.

Nagl NG Jr, Wang X, Patsialou A, Van Scoy M, Moran E. 2007. Distinct mammalian SWI/SNF chromatin remodeling complexes with opposing roles in cell-cycle control. EMBO J 26:752-763.

Nagy Z, Tora L. 2007. Distinct GCN5/PCAF-containing complexes function as co-activators and are involved in transcription factor and global histone acetylation. Oncogene 26(37):5341-5357.

Nie Z, Xue Y, Yang D, Zhou S, Deroo BJ, Archer TK, Wang W. 2000. A specificity and targeting subunit of a human SWI/SNF family-related chromatin-remodeling complex. Mol Cell Biol 20(23):8879-8888.

Ozawa Y, Nakamura Y, Fujishima F, Felizola SJ, Takeda K, Okamoto H, Ito K, Ishida H, Konno T, Kamei T, Ohuchi N, Sasano H. 2015. Decreased expression of ARID1A contributes to infiltrative growth of esophageal squamous cell carcinoma. Tohoku J Exp Med 235(3):185-191.

Panamarova M, Cox A, Wicher KB, Butler R, Bulgakova N, Jeon S, Rosen B, Seong RH, Skarnes W, Crabtree G, Zernicka-Goetz M. 2016. The BAF chromatin remodelling complex is an epigenetic regulator of lineage specification in the early mouse embryo. Development (Cambridge, England) 143(8):1271-1283.

Phelan ML, Sif S, Narlikar GJ, Kingston RE. 1999. Reconstitution of a core chromatin remodeling complex from SWI/SNF subunits. Mol Cell 3:247–253.

Porter EG, Dykhuizen EC. 2017. Individual Bromodomains of Polybromo-1 Contribute to Chromatin Association and Tumor Suppression in Clear Cell Renal Carcinoma. J Biol Chem 292(7):2601–2610.

Prather RS, Rickords LF. 1992. Developmental regulation of a snRNP core protein epitope during pig embryogenesis and after nuclear transfer for cloning. Mol Reprod Dev 33:119-123.

Santos F, Hendrich B, Reik W, Dean W. 2002. Dynamic reprogramming of DNA methylation in the early mouse embryo. Dev Biol 241(1):172-182.

Smith CL, Horowitz-Scherer R, Flanagan JF, Woodcock CL, Peterson CL. 2003. Structural analysis of the yeast SWI/SNF chromatin remodeling complex. Nat Struct Biol 10(2):141-145.

Sun X, Wang SC, Wei Y, Luo X, Jia Y, Li L, Gopal P, Zhu M, Nassour I, Chuang JC, Maples T, Celen C, Nguyen LH, Wu L, Fu S, Li W, Hui L, Tian F, Ji Y, Zhang S, Zhu H. 2017. Arid1a Has Context-Dependent Oncogenic and Tumor Suppressor Functions in Liver Cancer. Cancer cell 32(5):574-589.

Sun X, Wang SC, Wei Y. 2018. Arid1a Has Context-Dependent Oncogenic and Tumor Suppressor Functions in Liver Cancer. Cancer Cell 32(5):574-589.

Toto PC, Puri PL, Albini S. 2016. SWI/SNF-directed stem cell lineage specification: dynamic composition regulates specific stages of skeletal myogenesis. Cellular and molecular life sciences 73(20):3887–3896.

Tseng YC, Cabot B, Cabot RA. 2017. ARID1A, a component of SWI/SNF chromatin remodeling complexes, is required for porcine embryo development. Mol Reprod 84:1250-1256.

Vazquez M, Moore L, Kennison JA. 1999. The trithorax group gene osa encodes an ARID-domain protein that genetically interacts with the brahma chromatin-remodeling factor to regulate transcription. Development 126:733-742.

Wang W, Côté J, Xue Y, Zhou S, Khavari PA, Biggar SR, Muchardt C, Kalpana GV, Goff SP, Yaniv M, Workman JL, Crabtree GR. 1996. Purification and biochemical heterogeneity of the mammalian SWI-SNF complex. J EMBO 15(19):5370-5382.

Whitworth KM, Agca C, Kim JG, Patel RV, Springer GK, Bivens N. 2005. Transcriptional profiling of pig embryogenesis by using a 15K member unigene set specific for pig reproductive tissues and embryos. Biol Reprod 72:1437-1451.

Wu JN, Roberts CW. 2013. ARID1A mutations in cancer: another epigenetic tumor suppressor? Cancer Discov 3(1):35-43.

Yan HB, Wang XF, Zhang Q, Tang ZQ, Jiang YH, Fan HZ, Sun YH, Yang PY, Liu F. 2014. Reduced expression of the chromatin remodeling gene ARID1A enhances gastric cancer cell migration and invasion via downregulation of E-cadherin transcription. Carcinogenesis 35(4):867-876.

Yan Z, Cui K, Murray DM. 2005. PBAF chromatin-remodeling complex requires a novel specificity subunit, BAF200, to regulate expression of selective interferon-responsive genes. Genes Dev 19(14):1662-1667.

Yoshida-Noro, C, Suzuki N, Takeichi M. 1984. Molecular nature of the calcium-dependent cell-cell adhesion system in mouse teratocarcinoma and embryonic cells studied with a monoclonal antibody. Dev Biol 101:19-27.

Yoshioka K, Suzuki C, Tanaka A, Anas IM, Iwamura S. 2002. Birth of piglets derived from porcine zygotes cultured in a chemically defined medium. Biol Reprod 66:112-119.

Yuan Y, Spate LD, Redel BK, Tian Y, Zhou J, Prather RS. 2017. Quadrupling efficiency in production of genetically modified pigs through improved oocyte maturation. Proc Natl Acad Sci USA 114: 5796-5804.

CHAPTER 6. CONCLUSIONS

Embryogenesis involves a series of events in nature. The combination of two specialized cells (gametes) results in a totipotent embryo that can develop into a functional individual. This event is governed by tremendous number of regulators, including epigenetic modifications, the upstream controllers that modulate gene expression. The first epigenetic event during embryogenesis can be observed immediately after fertilization. DNA contributed by the sperm is incorporated with protamine proteins. The protamine is replaced by maternally derived histone proteins so the highly compacted protamine-DNA complex in the paternal pronucleus can shift from transcriptionally quiescent state to an inducible state. After fertilization, the zygote resumes the cell cycle and utilizes maternal derived mRNA and proteins to complete the first few cell cycles. The zygotic genome stays quiescent until a species-specific time-point (4-cell stage in pigs and humans, 2-cell stage in mice and 8-cell stage in cattle). The maternal-to-zygotic transition (MZT) occurs to remove maternally derived mRNA and zygotic genome activation (ZGA) is triggered to begin the transcription of zygotic genome. Remodeling global epigenetic modifications is observed at this critical stage of embryo development. The true mechanism initiating this transition is still unknown, but studies suggest the ratio of cytoplasm and nuclei in the embryo is crucial. The first cell differentiation event during embryogenesis occurs at the late morula stage when the blastocoel begins to form. Two cell types, the trophectoderm (TE) and the inner cell mass (ICM) can be found in a blastocyst and the ICM will give rise to the fetus.

More differentiation events can be observed after blastocyst formation and cells are destined to specialized tasks. Although cells in an individual share the same genetic contents, different cell types can be identified by their unique gene expression patterns. Several factors influence this commitment of fate, epigenetic modifications are one of these determinants.

Epigenetic modifications can be done by several ways to establish the proper epigenetic status. DNA methylation, histone acetylation and histone methylation are considered as covalent modifications. Repositioning of nucleosomes by chromatin remodeling complexes is an example of a non-covalent epigenetic modification. SWI/SNF chromatin remodeling complexes are large, multi-subunits complexes that include a series of BRG1-associated factors (BAFs). The collection

of BAFs determine the identity of a given SWI/SNF chromatin-remodeling complex and dictate where that complex will act. The focus of this dissertation was to identify the developmental requirements and unique roles of selected BAFs (SNF5, BRD7 and ARID1A) in porcine embryos.

SNF5 is a core component for classical BAF complex and the PBAF complex. We have found transcript levels of *SNF5* remained constant from the immature GV-stage oocyte to the blastocyst stage embryo. This finding indicates a global need for this SWI/SNF subunit during this developmental window. A significant reduction in cell number and a significant reduction in the proportion of embryos that formed morphological blastocyst in our RNAi-mediated knockdown experiments further identify the critical role of SNF5 in embryo development. We then investigated the functional role of SNF5 by analyzing transcript levels of *NANOG*, *SOX2*, and *POU5F1* following *SNF5* knockdown. The 2-fold increase in the relative transcript abundance of both *NANOG* and *POU5F1* detected in the *SNF5*-depleted embryos suggests the disruption of downstream genes regulated by SNF5 can be the potential cause leading to early embryo lethality. Besides pluripotent genes, SNF5 has been shown to regulate other genes that necessary for embryo development, for example, HOX genes and genes involved in the p53 pathway (Wilson *et al*., 2010; Xu *et al*., 2010). An RNA-seq approach could be used to study those genes regulated by SNF5. Briefly, total RNA isolated from *SNF5* knockdown embryo is converted to cDNA and subjects to high throughput sequencing. The RNA-seq reads are trimmed, aligned, quantified, and profiled according to their functions. The differential expression of genes is compared with current data base. The result allows us to identify transcripts and their according functions that affected by *SNF5*, but the change in the transcriptome can be directly or indirectly altered by *SNF5* knockdown.

The early embryo lethality we observed upon *SNF5* knockdown can also result from aberrant SWI/SNF complex formation. SNF5 has been reported to involve in SWI/SNF chromatin remodeling complexes assembly. A crosslinking-mass spectrometry (CX-MS) study has revealed the structure role of SNF5 in SWI/SNF chromatin remodeling complexes. SNF5 has been reported to interact with the ATPase subunit in the complex and forms a submodule to maintain the correct configuration of the complex. The high-resolution crystal structure of SNF5 and BAF155 also indicates that interaction between SNF5 and the SWIRM domain on BAF155 is required for constructing the structure of a SWI/SNF chromatin remodeling complex (Sen *et al*., 2017; Yan *et*

al., 2017). To uncover the structure role of SNF5 in preimplantation embryo, an immunoprecipitation approach can be used. Antibodies against the other core subunits, for example, BAFF155 and BAF170 can be employed to pull out the SWI/SNF complexes from protein extracts derived from wild-type embryos or SNF5 depleted embryos. The limitation here is the amount of protein required for immunoprecipitation approach. Our results indicate that SNF5 depleted embryos arrest before cleavage thereby the sample will be the major concern. PFF or porcine trophectoderm can be alternatives used immunoprecipitation. Although these cells have differentiated but they still share some pluripotent characteristics with embryonic stem cells. In summary, the collective data presented here demonstrate that *SNF5*, one of the core subunits for canonical BAF, is required for porcine embryo development. More experiments can be done to further our understanding of the roles served by SNF5 during porcine embryogenesis.

BRD7 contains a bromodomain that is hydrophobic and has been shown to bind to modified lysine residues found on histone tails. BRD7 is a subunit unique to the PBAF complex. A variety of biological functions carried out by BRD7 have been documented, including tumor suppressor, co-factor for p53 pathway, interacts with the regulatory subunits of PI3K, glucose metabolism, and the most important, directs SWI/SNF chromatin remodeling complex (Lee *et al*., 2019). Results from our RNAi-mediated knockdown assay suggest BRD7 is required for porcine embryo development. BRD7 is also required for proper mouse embryo development. BRD7 null embryos died at E16.5 without proper differentiation (Kim et al., 2016).

Comparing the results from our RNAi-mediated knockdown assays targeting different subunits, *BRD7* siRNA is less toxic than *ARID1A* and *SNF5* siRNA. *BRD7* knockdown embryos have reduced development competence but embryos from two other knockdown assays arrest at earlier stages of development (4-cell stage and before the first cleavage division for *ARID1A* and *SNF5* knockdown, respectively). *Arid1a* and *Snf5* null mouse embryos died around E7, while *Brd7* null embryos died at E16.5. These results indicate that either BRD7-mediated SWI/SNF chromatin remodeling complexes participate in embryo development at a later stage of embryogenesis, or there are some unknown mechanisms that compensate for the loss of BRD7 during preimplantation embryo development.

To uncover the potential mechanisms that compensate for the loss of BRD7 during preimplantation embryo development. Genes upregulated in BRD7 depleted embryos needs to be identified, especially genes encode the BAF subunits due to the functional redundancy found between subunits. It has been reported that the subunits can have redundant biological functions, for example, BRG1 can compensate the loss of BRM in cancer studies. The functional similarity is also observed in complex level. In embryonic stem cell studies, both the esBAF complex and the newly discovered GBAF complex have shown regulating the pluripotent genes. esBAF cooperates with pluripotent regulators NANOG, SOX2, and POU5F1 to suppress cell differentiation in embryonic stem cells. GBAF, meanwhile, is shown to maintain pluripotency in embryonic stem cells by regulating NANOG and halts differentiation to the epiblast. BRD9 another bromodomain containing protein has been reported to have similar bromodomain to BRD7. A recent study indicates BRD7 and BRD9 have similar actions on the vitamin D receptor (VDR) in human β cells (Wei *et al*., 2018). It is also possible that BRD7 participates in embryo development at later stage. Studies done in our lab have identified the presence of BRD9 and GBAF in porcine oocytes and cleavage stage embryos. Previous research published by our colleagues revealed distinct localizations and abundances of PBAF complex specific subunits in early porcine embryo, including BAF180, ARID2, and BRD7. Low abundance of BAF180 and cytoplasmic localized BRD7 at 4-cell and blastocyst stages suggests that the canonical PBAF complexes do not exist in early porcine embryos. It requires further investigation to identify why BRD7 depleted embryos can survive till later stage comparing with *ARID1A* and *SNF5* ablation studies. The extension of this project can help us to reveal the dynamic of subunits and to identify the relationship between SWI/SNF chromatin remodeling sub-complexes.

ARID1A is unique to the BAF complex and binds to AT-rich DNA sequences. ARID1A is also a trithorax group (TrxG) protein, which antagonize the polycomb proteins to maintain the activity of differentiation during early embryo development. Our previous work has indicated that ARID1A is essential for preimplantation embryo development. ARID1A depletion leads to early embryonic lethality. *Arid1a*-null mouse embryo studies reported a similar phenotype. *CDH1,* which encodes E-cadherin, has been shown to be directly regulated by ARID1A in gastric cells (Yan *et al*., 2014), *CDH1* is also require for embryo development (Larue *et al*., 1994). According to our data, E-cadherin is detectable in GV stage oocytes and become highly expressed on the

membrane of blastomeres after the 4-cell stage of development. *CDH1* transcript is significantly reduced in ARID1A depleted 4-cell stage embryos. To identify the direct interaction between ARID1A and *CDH1*, a chromatin immunoprecipitation assay was developed in this project. This physical connection between ARID1A and *CDH1* is hypothesized to be critical. If the physical contact between ARID1A and the promoter (or enhancer) regions on *CDH1* can be detected by our ChIP-PCR assay, a conclusion that activation of *CDH1* is controlled by ARID1A mediated SWI/SNF complex can be made. Unfortunately, due to the genome variance between species, it requires more information to identify the promoter and enhancer region on porcine *CDH1* gene. A ChIP-seq may be a better approach than ChIP-PCR we tried in this project. By sequencing the DNA fragment from immunoprecipitation output, we can acquire the information regarding *CDH1* gene as well as other genes that directly regulated by ARID1A. ChIP-PCR is low-cost and time efficient if the target loci for the protein is known while ChIP-seq allows genome-wide discovery of DNA sequences that physically interact with target protein. Except the higher cost, it takes some training to process the sequencing results as well as to interpret the data. These trainings benefit my future research since ChIP-seq is widely employed in epigenetic studies.

To complete this project, the last piece will be conducting a rescue experiment by introducing E-cadherin or *CDH1* mRNA into ARID1A depleted embryos. Coupling the rescue result with the ChIP-seq data, the major factors that contribute to the early embryo death upon ARID1A knockdown will be easier to be identified.

The studies conducted in this dissertation were focused on discrete SWI/SNF chromatin remodeling complex subunits. In the SNF5 study, we focus on critical genes that have been well-documented to associates with embryo development. This reflects the fundamental role of SWI/SNF complexes during embryo development. The BRD7 study leads us to investigate the dynamics and the interactions between different subunits and, furthermore, different subcomplexes. The newly discovered GBAF complex increases the complexity of the relationship in the SWI/SNF chromatin remodeling complex family. The ChIP assay in the ARID1A and *CDH1* project was designed to study the DNA-SWI/SNF complex interactions. The information gained from the experiments reported in this dissertation identify the developmental requirements of several SWI/SNF subunits, but additional work is required to construct the full map of the epigenetic networking in this critical period.

6.1 References

Kaeser MD, Aslanian A, Dong MQ, Yates JR 3rd, Emerson BM. 2008. BRD7, a novel PBAF-specific SWI/SNF subunit, is required for target gene activation and repression in embryonic stem cells. J Biol Chem 283(47):32254-32263.

Kim Y, Andrés Salazar Hernández M, Herrema H, Delibasi T, Park SW. 2016. The role of BRD7 in embryo development and glucose metabolism. Journal of cellular and molecular medicine 20(8):1561–1570.

Larue L, Ohsugi M, Hirchenhain J, Kemler R. 1994. E-cadherin null mutant embryos fail to form a trophectoderm epithelium. Proc Natl Acad Sci USA 91(17):8263-8267.

Lee JM, Kim Y, Salazar Hernández MA. 2019. BRD7 deficiency leads to the development of obesity and hyperglycemia. Sci Rep 9:5327.

Sen P, Luo J, Hada A. 2017. Loss of Snf5 Induces Formation of an Aberrant SWI/SNF Complex. Cell Rep 18(9):2135-2147.

Wei Z, Yoshihara E, He N, Hah N, Fan W, Pinto AFM, Huddy T, Wang Y, Ross B, Estepa G, Dai Y, Ding N, Sherman MH, Fang S, Zhao X, Liddle C, Atkins AR, Yu RT, Downes M, Evans RM. 2018. Vitamin D Switches BAF Complexes to Protect β Cells. Cell 173(5):1135-1149.

Wilson BG, Wang X, Shen X, McKenna ES, Lemieux ME, Cho YJ, Koellhoffer EC, Pomeroy SL, Orkin SH, Roberts CW. 2010. Epigenetic antagonism between polycomb and SWI/SNF complexes during oncogenic transformation. Cancer Cell 18(4):316-328.

Xu Y, Yan W, Chen X. 2010. SNF5, a core component of the SWI/SNF complex, is necessary for p53 expression and cell survival, in part through eIF4E. Oncogene 29(28):4090-4100.

Yan HB, Wang XF, Zhang Q, Tang ZQ, Jiang YH, Fan HZ, Sun YH, Yang PY, Liu F. 2014. Reduced expression of the chromatin remodeling gene ARID1A enhances gastric cancer cell migration and invasion via downregulation of E-cadherin transcription. Carcinogenesis 35(4):867-876.

Yan L, Xie S, Du Y, Qian C. 2017. Structural Insights into BAF47 and BAF155 Complex Formation. J Mol Biol 429(11):1650-1660.